NUMERICAL AND EXPERIMENTAL ANALYSIS OF MICROMILLING OF INCONEL 718

Gabriel de Paiva Silva

Master's Dissertation

Mechanical Sciences

UNIVERSIDADE DE BRASÍLIA

Faculdade de Tecnologia

Departamento de Engenharia Mecânica

UNIVERSIDADE DE BRASÍLIA
FACULDADE DE TECNOLOGIA
DEPARTAMENTO DE ENGENHARIA MECÂNICA

ANÁLISE EXPERIMENTAL E NUMÉRICA DO MICROFRESAMENTO DE INCONEL 718

Gabriel de Paiva Silva

Orientador: Lucival Malcher, PhD - ENM/FT/UnB
Coorientadora: Déborah de Oliveira, PhD - ENM/FT/UnB

DISSERTAÇÃO DE MESTRADO

PUBLICAÇÃO: ENM.DM - XXX.XXX

BRASÍLIA/DF: 6 de novembro de 2023

UNIVERSIDADE DE BRASÍLIA
FACULDADE DE TECNOLOGIA
DEPARTAMENTO DE ENGENHARIA MECÂNICA

Numerical and Experimental Analysis of Micromilling of Inconel 718

Gabriel de Paiva Silva

REPORT SUBMITTED TO THE DEPARTMENT OF MECHANICAL ENGINEERING OF THE FACULTY OF TECHNOLOGY OF THE UNIVERSITY OF BRASILIA AS A PARTIAL REQUIREMENT FOR OBTAINING THE DEGREE OF MASTER IN MECHANICAL SCIENCES.

APPROVED BY:

Lucival Malcher, PhD - ENM/FT/UnB
(Supervisor)

Déborah de Oliveira, PhD - ENM/FT/UnB
(Co-supervisor)

Alysson Martins Almeida Silva, PhD - ENM/FT/UnB
(Internal examiner)

Tiago Emanuel Fraga da Silva, PhD - INEGI/UP
(External examiner)

Thiago de Carvalho Rodrigues Doca, PhD - ENM/FT/UnB
(Surrogate examiner)

BRASÍLIA/DF, 6 DE NOVEMBRO DE 2023.

FICHA CATALOGRÁFICA

Silva, G. P.
Numerical and Experimental Analysis of Micromilling of Inconel 718
[Distrito Federal] 2023.
xvii, 84p. (ENM/FT/UnB, Mestre, Ciências Mecânicas, 2023.
Dissertação de Mestrado - Universidade de Brasília.
Faculdade de Tecnologia.
Departamento de Engenharia Mecânica.
Palavras-chave:
1. Micromilling 2. Finite Element Method
3. Size Effect 4. Inconel 718
I. ENM/FT/UnB II. Título (série)

REFERÊNCIA BIBLIOGRÁFICA

Silva, G. P.(2023). Numerical and Experimental Analysis of Micromilling of Inconel 718. Dissertação de Mestrado, Publicação ENM.DM, Departamento de Engenharia Mecânica, Universidade de Brasília, Brasília, Distrito Federal, xvii, 84p.

CESSÃO DE DIREITOS

NOME DO AUTOR: Gabriel de Paiva Silva.

TÍTULO DA DISSERTAÇÃO DE MESTRADO: Numerical and Experimental Analysis of Micromilling of Inconel 718.

GRAU / ANO: MESTRE / 2023

Gabriel de Paiva Silva

Agradecimentos

Sou grato

A Deus, pelo dom da vida e por ser fonte inesgotável de amor e justiça.

A toda minha família, em especial à minha mãe Roseli, por sua bondade incondicional e seu sacrifício para garantir uma educação de qualidade aos dois filhos que criou sozinha. À minha irmã Laríssa, por acreditar na minha capacidade e torcer pelo meu sucesso.

À Universidade de Brasília, instituição que eu tanto admiro e que tem me oferecido incontáveis oportunidades de aprendizado e crescimento ao longo desses anos de graduação e de pós-graduação, não apenas no âmbito acadêmico.

À Coordenação de Aperfeiçoamento de Pessoal de Nível Superior (CAPES), pelo suporte financeiro.

Aos meus orientadores, professor Dr. Lucival Malcher e professora Dra. Déborah de Oliveira, por todo apoio e confiança depositados em mim.

À professora Dra. Milla Caroline Gomes, por sua grande ajuda nos ensaios experimentais. Aos professores Dr. Leonel Leonardo Delgado Morales e Dr. Maksym Ziberov, pelo incentivo à carreira científica.

Por fim, sou imensamente grato a todos os vários amigos que fiz na UnB, com os quais tenho compartilhado momentos inesquecíveis e que foram essenciais para tornar minha jornada acadêmica muito menos difícil e desgastante.

"Time doesn't hear if you ask it to wait."

Waves - Imagine Dragons

Abstract

In micro machining processes, theories generally used in conventional machining are not applicable because of size effect, which is a phenomenon due to the similar sizes of the cutting-edge radius of the tool and the minimum chip thickness. Inconel 718 is a nickel superalloy with excellent mechanical properties, however it presents low machinability, especially when micromilled. Computational simulations using the finite element method (FEM) can be used to estimate output parameters in machining processes, provided that the constitutive model that describes the elastoplastic behavior of the workpiece material is known. Therefore, the objective of this contribution is to analyze micromilling of Inconel 718 using two different approaches: a FEM numerical simulation and experimental micromilling trials. The computational simulation was performed on Abaqus CAE and the properties of Inconel 718 were characterized using Johnson-Cook isothermal model. The experimental trials consisted in manufacturing microslots on two Inconel 718 samples using tungsten carbide tools with diameter 400 μm. The quality of the machining performed by the simulations was analyzed and compared to the results obtained experimentally. Some of the most important results from the simulations showed that a worn tool (with cutting edge radius 5 μm) generates worse chip formation, up to 300% higher cutting forces and up to 11.7% higher residual stresses on the machined material than a sharp tool (with cutting edge radius 1 μm). The experimental results showed that high values of feed per tooth (4.0 μm) and depth of cut (40 μm) generate worse surface quality on the microslots, with high cutting forces (higher than 0.75 N) and high wear rates, which can even cause rupture of the tool.

Keywords: Micromilling; Finite Element Method; Size Effect; Inconel 718

Resumo

Em processos de microusinagem, as teorias geralmente utilizadas na usinagem convencional não são aplicáveis por causa do efeito escala, que é um fenômeno devido aos tamanhos semelhantes do raio da aresta de corte da ferramenta e a espessura mínima de cavaco. O Inconel 718 é uma superliga de níquel com excelentes propriedades mecânicas, porém apresenta baixa usinabilidade, principalmente quando microfresado. Simulações computacionais utilizando o método dos elementos finitos (MEF) podem ser utilizadas para estimar parâmetros de saída em processos de usinagem, desde que se conheça o modelo constitutivo que descreve o comportamento elastoplástico do material da peça. Portanto, o objetivo desta contribuição é analisar o microfresamento do Inconel 718 usando duas abordagens diferentes: uma simulação numérica por MEF e ensaios experimentais de microfresamento. A simulação computacional foi realizada no Abaqus CAE e as propriedades do Inconel 718 foram caracterizadas utilizando o modelo isotérmico de Johnson-Cook. Os ensaios experimentais consistiram na fabricação de microcanais em duas amostras de Inconel 718 utilizando ferramentas de metal duro com diâmetro de 400 μm. A qualidade da usinagem realizada pelas simulações foi analisada e comparada com os resultados obtidos experimentalmente. Alguns dos resultados mais importantes das simulações mostraram que uma ferramenta desgastada (com raio de aresta de corte 5 μm) gera pior formação de cavacos, forças de corte até 300% maiores e tensões residuais até 11.7% maiores no material usinado do que uma ferramenta afiada (com raio de aresta de corte 1 μm). Os resultados experimentais mostraram que valores elevados de avanço por dente (4.0 μm) e profundidade de corte (40 μm) geram pior qualidade superficial nos microcanais, com forças de corte elevadas (maiores que 0.75 N) e altas taxas de desgaste, podendo até causar ruptura da ferramenta.

Palavras-chave: Microfresamento; Método dos Elementos Finitos; Efeito Escala; Inconel 718.

Table of Contents

List of Figures

List of Tables

1 Introduction

1.1 Motivation

Over the past few years, microfabrication techniques have become increasingly important, because of the growing requirement to produce smaller, highly precise products and components. This need is particularly pronounced in industries such as biochemistry, biotechnology, aerospace, and electronics. There are great market demands not only for the manufacture of small parts, but also for adding complex, small-scale structural features to large parts to enhance their functionality (CÂMARA et al., 2012). There are applications of miniaturization not only in the technological field, but also on visual arts (ZIBEROV, 2017).

Cutting tools used in traditional mechanical machining have been passing through continuous improvements to allow the manufacture of parts by removing smaller and smaller chips. Chae, Park and Freiheit (2006) comment that cutting tools in microscale machining cannot be considered perfectly sharp, as the tool radius is often greater than the chip thickness. One of the most important types of micro machining is micromilling, due to its versatility in the production of different geometries. There is not one single definition for micromachining; for Câmara et al. (2012), this process can be characterized by the diameter of the microtool, which must be between 1 μm and 1000 μm. Ng et al. (2006) associate this process with the chip thickness, which should be around a few nanometers to a few micrometers.

Micromilling can be used in the most diverse areas. Some examples of its application include the manufacture of micro-electro-mechanical components, parts of wristwatches, micro-holes for cooling turbine blades, injection nozzles of fuel, microsensors, microactuators, surgical devices, among others (VENKATESH et al., 2017). According to Jain (2013), micro milling is generally used for making slots, cavities and concave or convex three-dimensional features. For the development of the technology of micromilling, it is essential to understand the chip formation mechanism in this scale of dimensions, as well as the influence of each parameter inherent to the process. Computational methodologies can be used as a complementary approach to analyze the influence of machining parameters on the quality of the machined workpiece.

In this sense, the finite element method (FEM) is a computational tool that can be used to simulate machining procedures. FEM simulations enable the prediction and analysis of different output variables, reducing experimental costs. In computational simulations of machining, the material that constitutes the machined workpiece needs to be characterized using its isotropic hardening curve. The isotropic hardening curves of several materials have already been characterized in literature, including Inconel 718.

Inconel 718 is a nickel superalloy that has very desirable properties, such as high mechanical strength, resistance to fatigue and corrosion and the ability to operate continuously at elevated temperatures. However, this alloy is known as a low machinability material. In addition, the presence of large burrs is frequent when micromilling Inconel 718 (UCUN; ASLANTAS; BEDIR, 2015). Micromilling is a relatively recent field of research, so published works in this area are still scarce compared to works on macroscale milling. In this way, there is a need for the development of further research on micromilling of low machinability materials such as Inconel 718.

1.2 Objectives

Considering the difficulties associated with micromilling of hard-to-cut materials, the objective of this work is to investigate micromilling of Inconel 718. The analysis proposed is based on two methodologies: a numerical approach, consisting in a FEM simulation of the micromilling process; and an experimental approach, consisting in performing micro-end milling to manufacture microslots on Inconel 718 samples, varying the feed per tooth (f_z). The present work aims at validating the numerical results obtained by the simulation by comparing them with the experimental results.

1.2.1 Specific objectives

For the FEM numerical simulations of micromilling of Inconel 718, the following specific objectives are proposed:

- Determine how the machining parameters and the geometry of the tool affect the morphology of the chips;
- Determine the distribution of von Mises stress and accumulated plastic strain on the workpiece after machining;
- Determine how the machining parameters and the geometry of the tool affect the cutting forces.

As for the experimental machining trials, the specif objectives are:

- Determine how the machining parameters influence the wear of the cutting tool;
- Evaluate the surface and geometrical quality of the microslots by measuring their width, surface roughness and burr heights;
- Establish correlations between the numerical and experimental results in terms of tool wear, cutting forces, burr formation and surface quality.

1.3 Outline

This dissertation is divided into seven chapters. Each chapter is divided into subsections to provide a clear understanding of the distinct processes involved in the development of this work.

Chapter 1 is a brief introduction to the subjects addressed in this work. In this chapter, a motivation is given to justify the study of micromilling on Inconel 718 and the objectives of the dissertation are exposed.

In chapter 2, a literature overview is presented to expose concepts that are fundamental for the understanding of this work. This chapter highlights size effect and the challenges inherent to micromilling, such as tool wear and surface quality of micromachined components. A discussion on the machinability of Inconel 718 is shown. Finally, a literature review about simulation of micromachining through the finite element method is also presented.

Chapter 3 is dedicated to explaining the methodology used in the numerical simulations of micromilling. The modeling of the orthogonal cut and the constitutive model of the material are described. Details about the machining parameters, the boundary conditions and the discretization of the elements are explained in this chapter.

Chapter 4 shows the results that were obtained by the numerical simulations. The influence of machining parameters and tool geometry on chip morphology, residual stresses and cutting forces is discussed.

Chapter 5 describes the methodology used in the experimental trials of micromilling and the microscopy operations performed on the microslots that were manufactured. This chapter evidences the input variables used in the experiments and how the microtools, machine tools and microscopes were used to obtain the output variables.

Chapter 6 presents the results that were obtained by the micromilling trials. A discussion on whether the numerical results could be validated by the experimental results is also presented. The quality of the micromilling procedures is discussed in terms of geometry of the microslots, surface roughness, tool wear, cutting forces and burr formation.

Finally, chapter 7 is dedicated to the conclusions that could be drawn, both by the numerical simulations and by the experimental trials. Some suggestions for future works

are given according to the conclusions obtained.

1.4 Publications associated with the dissertation

Some of the discussions presented in this dissertation have been published in the following papers:

- de Paiva Silva, G., de Oliveira, D., Malcher, L. Numerical study of the minimum uncut chip thickness in micro-machining of Inconel 718 based on Johnson–Cook isothermal model. International Journal of Advanced Manufacturing Technology 127, 2707–2721 (2023). https://doi.org/10.1007/s00170-023-11573-0.
- de Paiva Silva, G., Malcher, L., de Oliveira, D. Review on FEM Numerical Simulation of Micromachining Processes. Annals of COBEF 2023 - 12th Brazilian Congress on Manufacturing Engineering. May 10th - 12th, 2023, Brasília, DF, Brazil. http://abcm.org.br/proceedings/view/COF23/0077.

Besides, the author also published the following article previous to this dissertation:

- de Paiva Silva, G., Bacci da Silva, M., de Oliveira, D. Influence of abrasive deburring in indirect tool wear measurement in micromilling of Inconel 718. Journal of the Brazilian Society of Mechanical Sciences and Engineering, v. 45, n. 262 (2023). https://doi.org/10.1007/s40430-023-04190-1.

2 Literature Overview

2.1 Machining in microscale

In recent years, manufacturing processes have sought higher and higher levels of dimensional and geometric quality due to the growing trends towards miniaturization of mechanical components (OLIVEIRA, 2019). The manufacture of microscopic products is advantageous due to their compactness, small amount of material needed and low energy consumption. Microscopic components are often found in industries such as electronics, automotive, telecommunication, biomedicine, and others. Traditional machining tools such as mills and drills have gone through adaptations for the fabrication of microscopic geometries (JAIN, 2013). Applications of micromachining include, for instance, the fabrication of micro-injection molds (TAKÁCS; VERÖ; MÉSZÁROS, 2003), micro-barbs for medical implants (FILIZ et al., 2008) and micro-fluidic chips capable of mimicking physiological functions of human organs (SUN et al., 2016).

One of the principal micromachining processes is micromilling, which is widely used for fabrication of grooves, cavities and three-dimensional shapes (JAIN, 2013). There is not one single definition of micromilling. It is possible to characterize this process by a depth of cut between 10 nm to 2 μm (NG et al., 2006). However, this technique is more often defined by the diameter of the cutting tool, which should range between 1 μm to 1000 μm (CÂMARA et al., 2012). An important aspect of micromilling operations is that the dimension of the cutting edge radius of the tool is similar to that of the depth of cut and even the microstructure of the machined material, in such a way that the physical principles often applied in macroscale milling are not valid for microscale (CHAE; PARK; FREIHEIT, 2006).

Micromachining operations often impose challenges: the cutting forces must be as small as possible and the machine tool rigidity must be high enough to minimize machining errors. This happens because the performance of micromills is highly influenced by small vibrations and excessive forces, which may be prejudicial to the longevity of the tool and tolerance control of micromachined components (CHAE; PARK; FREIHEIT, 2006). Besides, deburring and surface finishing of microscopic features and components is particularly difficult because they require extra precision that may not be supplied by traditional finishing techniques (KHAN et al., 2019).

Milling in microscale allows the fabrication of three-dimensional features in a wide range of materials, from metallic alloys to ceramics and polymers. In many cases, micromilling procedures in steels are performed with end-mills with two flutes, commonly made of fine-grainded tungsten carbide, although other geometries and materials may be used. The chip thickness and the grain size of the workpiece material must be taken into account for the appropriate choice of the cutting edge radius. Owing to the difficulties associated with micromilling, most research works on this subject often focus on operations in materials with good machinability, such as low-hardness steels and aluminum or copper alloys (CÂMARA et al., 2012).

2.1.1 Size effect and minimum chip thickness

In conventional machining (that is to say, machining in macroscopic scale), the cutting-edge radius of the tool is assumed to be perfectly sharp, because the size of its radius is negligible. In this case, there is no contact between the tool and the workpiece material along the clearance face and the chips are formed by the mechanical shear force due to the interaction between the sharp tool and the piece. In micromachining, on the other hand, the radius of the cutting tool becomes significant compared to the uncut chip thickness. This provokes a plowing effect, in which a large amount of material deforms plastically along the radius of the cutting tool and a small amount of material is effectively removed in the form of chips. This phenomenon is known as size effect and it has direct influence on parameters such as cutting forces, chip formation, tool wear and surface quality of micromachined surfaces (ARAMCHAROEN; MATIVENGA, 2009). Figure 2.1 shows the different geometric configurations of orthogonal cutting in macro-scale and in microscale. In macroscale cutting, figure 2.1 (a), the perfectly sharp tool allows the removal of chips with a positive rake angle α, whereas in micro-scale cutting, figure 2.1 (b), the rake angle is negative because the size of the radius of the cutting-edge, r_e, is comparable to the uncut chip thickness, h.

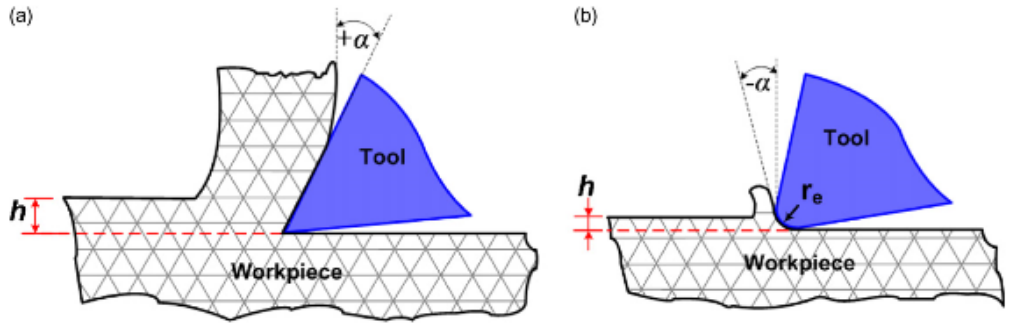

Figure 2.1 – Effect of the size of cutting-edge radius in (a) macromachining and (b) micromachining (ARAMCHAROEN; MATIVENGA, 2009).

As a consequence of size effect, when the chip thickness is below a critical value, chips are not generated in micromachining. This critical value, known as minimum uncut

chip thickness (MUCT), is sometimes referred to as h_{min} or h_m in literature. According to Aramcharoen e Mativenga (2009), when the uncut chip thickness h is less than h_m, figure 2.2 (a), the workpiece material is forced under the tool and suffers elastic recovery after the tool passes, not being eliminated in the form of chips. When h is equal to h_m, figure 2.2 (b), chip formation begins with still a portion of deformation and elastic recovery. Finally, when the chip thickness is larger than the minimum chip thickness, figure 2.2 (c), the material is sheared and removed as a chip.

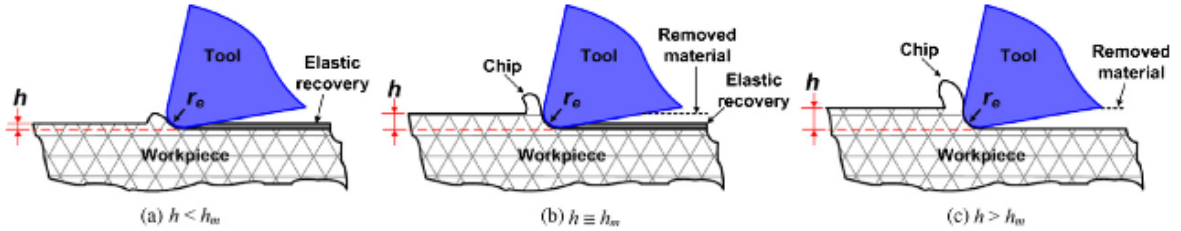

Figure 2.2 – Chip formation mechanism according to chip thickness (ARAMCHAROEN; MATIVENGA, 2009).

The value of the minimum uncut chip thickness is still difficult to predict, although some authors have attempted to determine it for different materials and cutting conditions. Malekian et al. (2012) used analytical models based on identifying the stagnant point of the workpiece material to determine the value of MUCT, which was assumed to be a function of the edge radius and friction coefficient. The authors concluded that MUCT increases for higher values of friction angle, however it was found to be around 0.23 of the cutting-edge radius for an Al6061 workpiece. On the other hand, in their work, Oliveira et al. (2015) used quantitative and qualitative analyses based on surface roughness and cutting forces, determining that MUCT varies from around 1/4 to 1/3 of the cutting-edge radius, regardless of workpiece material, tool geometry or machining process.

Saha, Deb and Bandyopadhyay (2021) used TiAlN-coated WC/6Co end-mills, with diameter 500 μm, to micromill Ti6Al4V. The authors noticed that the presence of lubrication in the machining process, as well as higher cutting velocities, facilitates the chip formation mechanism. Under dry machining, the authors found that MUCT remains within 23-28% of the edge radius, whereas in machining under MQL (minimum quantity of lubrication), it reduces to 11-13% of the edge radius. However, Aslantas and Çiçek (2018), also machining Ti6Al4V alloy, found that MUCT is about 0.3 times the cutting-edge radius, with very little variation with the type of coating of the microtool.

The size effect is related to a non-linear increase of the specific cutting energy as the depth of sheared material decreases (CÂMARA, 2014). It can be observed in figure 2.3 that the smaller the feed value corresponding to the machined thickness, the higher the specific cutting pressure. Therefore, it is generally undesirable to perform micromachining for values excessively close to the minimum uncut chip thickness, because this condition causes high rates of energy expended over small volumes of removed material, meaning

poor productivity.

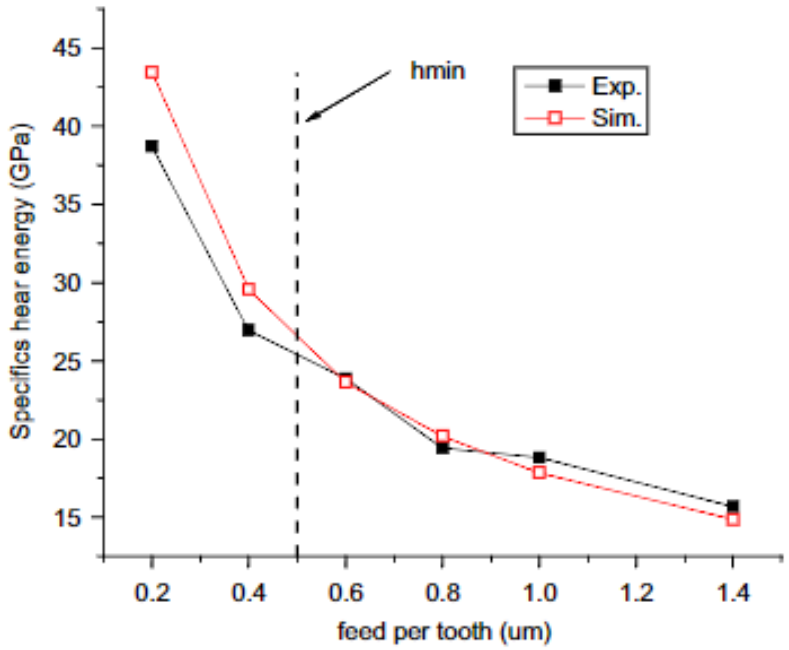

Figure 2.3 – Size effect in shear energy for different values of feed (LAI et al., 2008).

A common problem in micromilling is that the radius of the tool usually have the same scale size as the grains that constitute the microstructure of the workpiece material. Therefore, most metal alloys cannot be considered homogeneous and isotropic in micromilling, because when a microtool passes through different grains, it can encounter interstitial atoms, voids, dislocations and changes in crystallographic orientations that can have substantial effect on the cutting mechanism. Besides, peaks of cutting force tends to appear in the grain boundaries because of the geometrical hardening effects, leading to variations of cutting forces and increase in vibration of the tool. This problem can be aggravated, for example, when there are hard precipitates in the material matrix, which have considerable different hardness than the rest of the material (LIU et al., 2017).

2.1.2 Tool wear in micromachining

All cutting tools used in traditional machining operations naturally become worn out because of continuous use. Understanding how wear develops is essential to avoid machining errors, guarantee the quality of the machined surface and increase tool life. Evaluating wear of micro tools is particularly difficult, since standards used for measuring wear in macro tools are generally not applicable for micro tools. Therefore, adapted tests must be carried out, which do not typically yield traditional wear curves. Besides, micro tools tend to have considerably shorter lives, with a quicker and more unpredictable fracturing process when compared to macro tools (ALHADEFF et al., 2019).

Filiz et al. (2007) performed an experimental investigation of micro machinability of pure copper 101 using tungsten carbide micro end-mills with diameter 254 μm. The

authors conducted a series of experiments in which forty channels were micromilled at three speeds and four feeds, using a new tool for each test. The authors noticed that there was considerable reduction in tool diameter due to wear, however no tool breakage was observed, which the authors attribute to the low hardness of copper. Since the tool diameter could not be directly measured during the process, the authors measured the widths of the microchannels to evaluate tool wear. The highest values of wear were observed at the lowest feed rate, which is the opposite of the results expected from conventional machining, in which higher feeds usually result in more rapid wear progression. According to the authors, lower feed rates, especially those below the cutting edge radius of the tool, produce a basic form of attrition, where the individual tungsten carbide particles are dislodged from the softer matrix, causing the most rapid wear progression (FILIZ et al., 2007).

Santos, Silva and Jackson (2018) analyzed the evolution of wear on TiN coated tungsten carbide micromills with diameter 381 μm, when micromilling UNS S32205 duplex stainless steel. After examining the tools before and after each experiment using a scanning electron microscope, the authors found that the major forms of wear encountered during micromilling are nose and flank face wear, with evidences of adhesion and microchipping, as observed in figure 2.4. The authors also noticed the formation of buit-up edge (BUE) when using low values of cutting speed, which contributed to an increase in tool life.

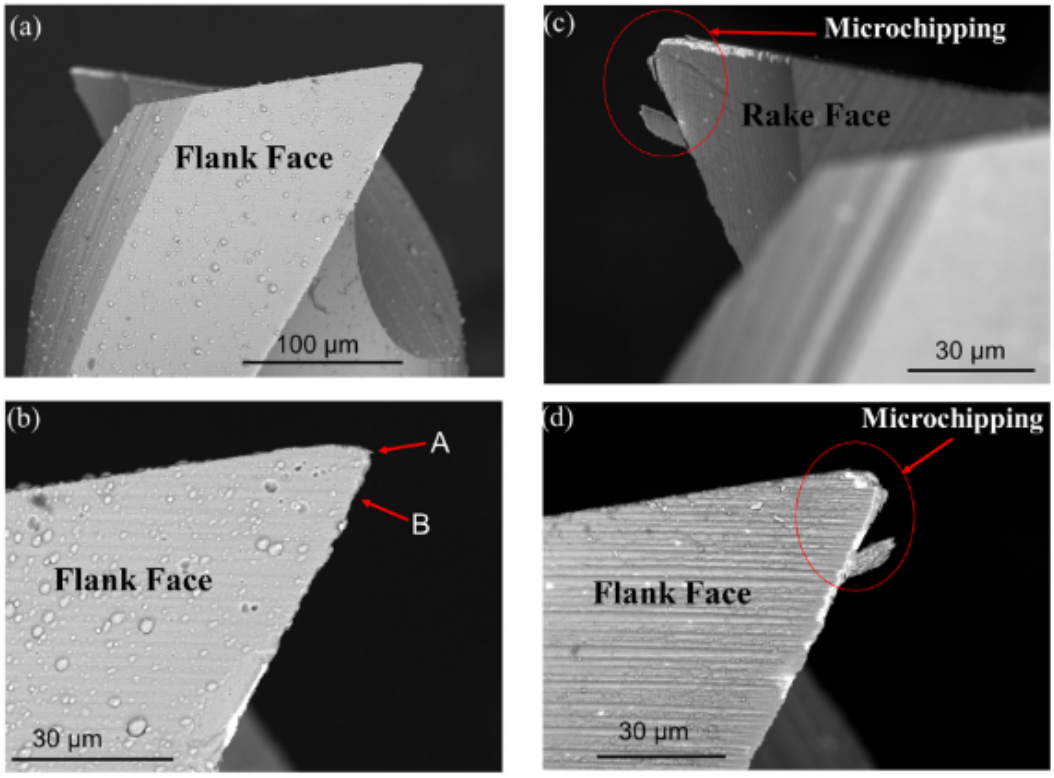

Figure 2.4 – Worn tool (a) and (b): occurrence of microchipping, on rake face (c) and major clearance face (d) after machining a microchannel (SANTOS; SILVA; JACKSON, 2018).

Buit-up edge formation was also observed by Ziberov et al. (2020), who investigated

the micro machinability of Ti-6Al-4V, considered a hard-to-cut material. The authors compared the performance of microtools, with diameter of 152.4 μm, coated with TiAlN or diamond-like carbon (DLC), against uncoated tools. By manufacturing microslots 4.2 mm long at a cutting speed of 9,6 m/min, the authors analyzed tool wear as a function of machining length. It was observed that after the first pass, the edge radius of the microtool becomes blunt and the rounding intensifies, especially in dry micromachining. The authors concluded that dry micromachining improves tool life, because BUE protects the wedge of the microtool, even though the surface quality of the slots deteriorates, since BUE particles are left loose on the machined surface. Besides, the authors found that DLC coating provides the longest tool life under dry condition, despite the appearance of a crack, observed in figure 2.5, which the authors attribute to thermal fatigue or to mechanical impact.

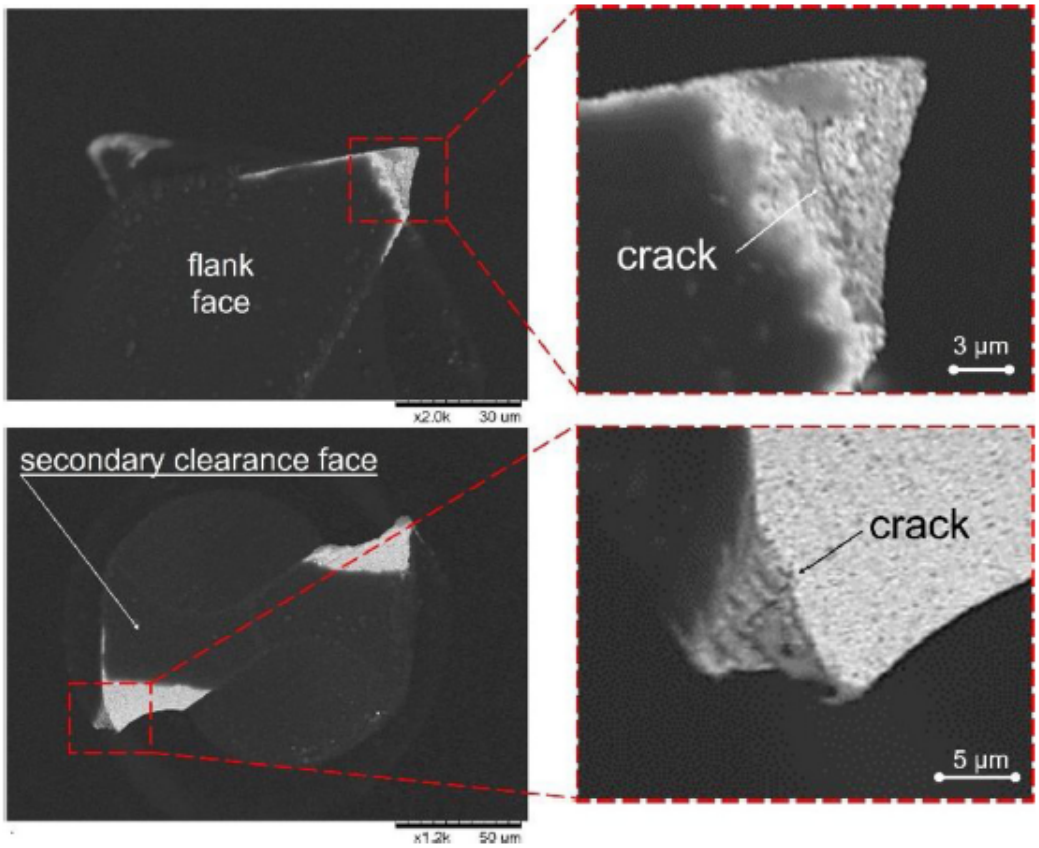

Figure 2.5 – Crack in a DLC coated microtool (ZIBEROV et al., 2020).

Teng et al. (2018) investigated tool wear in micromilling of magnesium-based metal matrix composites (MMC) using 500 μm diameter two-flute WC micro end-mills. Tool wear was characterized both quantitatively and qualitatively by observing tool wear patterns and analyzing the effect of cutting parameters on flank wear, reduction in tool diameter, cutting forces, surface roughness, and burr formation. Flank wear and reduction in tool diameter proved to become more evident with the decrease of feed per tooth. According to the authors, the plowing effect could cause a significant portion of materials to flow underneath the cutting edge and elastically deform, so that the workpiece material

recovers to its original position without proper chip formation after the cutting edge passes. Therefore, the abrasive wear mechanism is induced at small values of feed per tooth, resulting in large flank wear and edge chipping.

Vazquez et al. (2015) characterized the effect of cooling and lubrication conditions in tool wear in micromilling of Ti6Al4V, comparing jet application, MQL and dry machining. The authors noticed that tool wear for jet application increases almost three times in comparison with the other lubrication conditions. This is due to the fact that, in the MQL system, the low rate of the fluid enables small droplets to penetrate the turbulent region created by the tool rotation, whereas in jet application the fluid cannot penetrate the tool turbulence and therefore cannot touch the cutting edge of the micromill.

In general, the wear of tools used in micro cutting operations is a complex parameter to measure, because there is no standardization of the measuring process (ALHADEFF et al., 2019). The small size of the microtool demands thorough and time-consuming microscopy operations, besides the necessity of making multiple interruptions in the machining process in order to analyze tool wear, as performed in the works of Ziberov et al. (2020), Dos Santos et al. (2018) and Gomes et al. (2021). As an alternative, it is also possible to indirectly measure tool wear by measuring the geometry of the microslot produced by the tool. However, the presence of burrs may cause imprecision and it is therefore recommended that the part is deburred before any wear measurement operation (SILVA; SILVA; OLIVEIRA, 2023).

2.1.3 Surface quality in micromachining

The surface quality of machined components exerts significant influence in its performance. One of the most important variables used to analyze the quality of micromachined parts is the surface roughness, in such a way that the greater the surface roughness, the worse the surface quality. It is essential to determine the influence of cutting parameters on the surface roughness of the piece, because this parameter is strongly associated with size effect. Decreasing the depth of cut, in general, tends to generate smaller surface roughness; however, it has been reported that beyond a certain threshold that depends on the minimum chip thickness, further reductions can actually lead to an increase in roughness. This phenomenon was observed by Aslantas et al. (2016). The authors used flat end-mills with diameter 500 μm to machine Ti6Al4V and observed that the critical value of feed was 0.5 μm/tooth for the given conditions, as shown in figure 2.6. For values of feed greater than this threshold, surface roughness increases. However, in the region of smaller values of feed, the cutting process is dominated by the plowing effect.

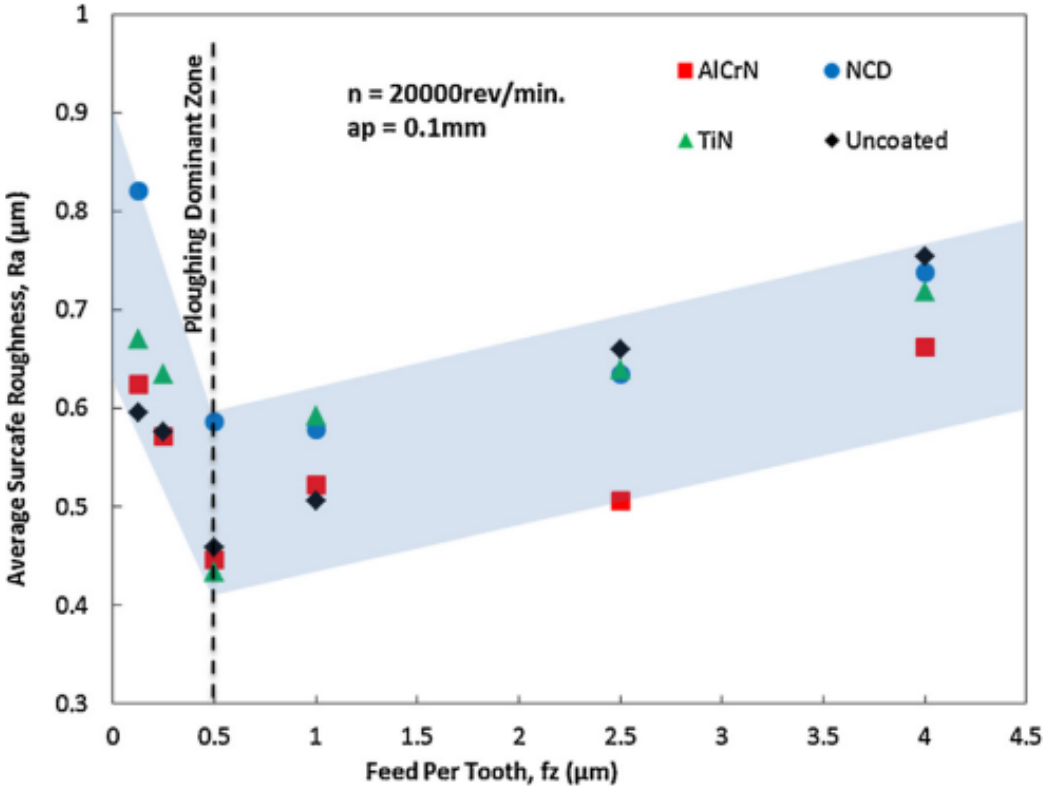

Figure 2.6 – Variation of surface roughness as a function of feed per tooth in micromilling of Ti6Al4V (ASLANTAS et al., 2016).

The friction and heat generated in the interface between the workpiece and the tool can cause the workpiece material to adhere to the tool's surface, which can form a built-up edge (BUE). It is known that the formation of BUE can cause several problems, including poor surface finish, high cutting forces and elevated tool wear rates. The BUE can also detach from the tool and leave a rough surface finish on the machined part, which is a critical problem in micromilling considering that the scale size of the BUE tends to be particularly significant in comparison with the tool diameter. According to Wang et al. (2016), BUE formation is the major determinant of surface finish in micromilling. The fractured segments of the brittle BUE are either swept away as the chip flows up the tool and/or would adhere to the workpiece surface, thereby deteriorating the surface quality, as observed in figure 2.7.

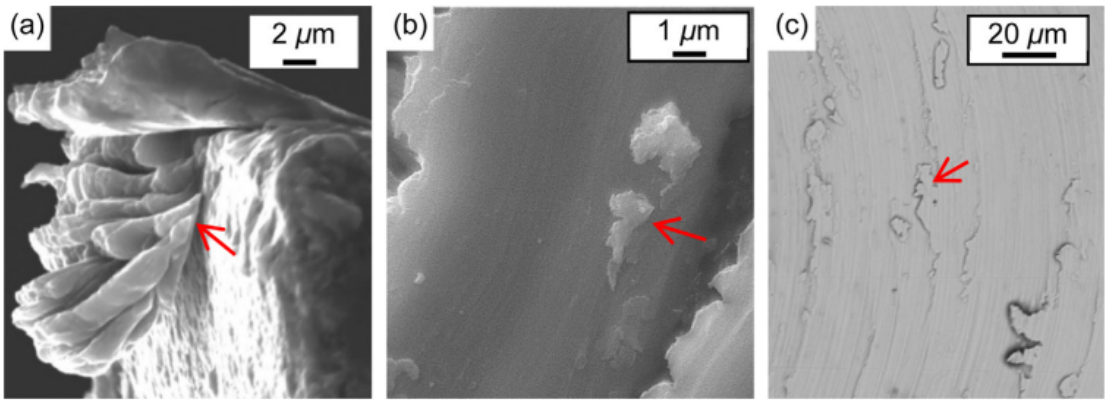

Figure 2.7 – BUE deposits on (a) microtool rake face, (b) chip flank face and (c) micromilled surface (WANG et al., 2016).

The problem of BUE formation can be minimized by the application of cutting fluid during the micromilling process. In the work of Santos, Silva and Jackson (2018), the authors observed that the surface condition of micro slots manufactured under dry condition presented some adhered particles, whereas for micromilling with lubrication, these particles are not present, as observed in figure 2.8. The authors discuss that the particles are fragments of BUE, which is not formed when cutting fluid is used.

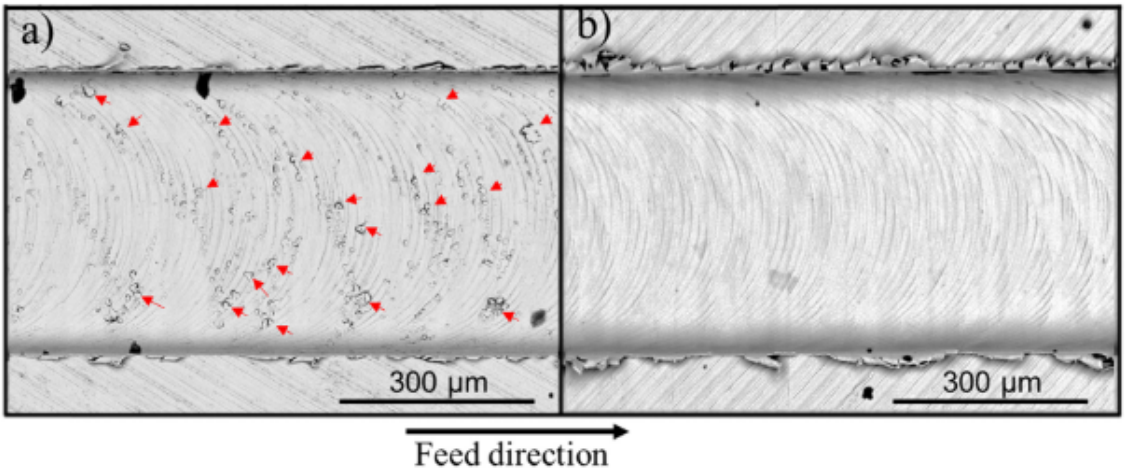

Figure 2.8 – Contrast of micromilled surface quality under a) dry condition and b) wet condition (SANTOS; SILVA; JACKSON, 2018).

Another major factor that affects surface quality in micromachined surfaces is the presence of burrs, which are small ridges obtained from plastic deformation that extend beyond the limits of the workpiece. Burrs can affect the appearance, safety, cost and performance of the product, therefore they are generally undesired and efforts are normally made to avoid, minimize or remove them (GILLESPIE, 1999). Burrs in micromilling have large size compared with the dimensions of the tool and can get even higher than the depth of cut (OLIVEIRA, 2019). Removing burrs from micromilled features is particularly difficult since deburring and edge finishing techniques traditionally used for macro components may not provide the precision levels required in micromilling (KHAN et al., 2019).

There are several deburring methods that can be used to enhance surface finish of micromilled parts. Kienzeler, Deuchert and Schulze (2010) used abrasive peening and ultrasonic wet peening to deburr 30CrMo6 steel steel samples with microslots 5 mm long and 100 μm deep. These deburring techniques consist in accelerating a peening agent, usually beads of microscopic size, at high velocities, toward the workpiece. Thereby, material is removed from the surface of the target upon impact. Although these techniques can reduce burr size, the authors found that the topography of the microcomponents can also be affected, because most burrs are not eliminated but are rather bent over the sample surface due to plastic deformation.

The removal of burrs from micro parts can also be performed by means of lasers. The use of laser deburring is advantageous over traditional mechanical deburring because of its high-precision control. Nevertheless, major concerns in laser processing are its high cost and the heat-affected zone (HAZ), which is the region in the vicinity of the cutting area where the mechanical properties of the workpiece are altered by high temperature. In the HAZ, there is grain size change, which can be detrimental to reduce wear resistance (LEE; DORNFELD, 2001).

Non-conventional finishing techniques, such as micro peening or laser deburring, require specific equipment, skilled labor, and thorough monitoring of the process, which lead to elevated costs. Since burr removal tends to add little or no value to the final product, the most used deburring methods worldwide are manual and abrasive techniques, which stand out for their versatility, easy handling by the operator and low costs (GILLESPIE, 2003). In their works, Mathai and Melkote (2012) and Mathai, Melkote and Rosen (2013) used a rotating nylon bush immerged in an abrasive slurry on micromilled samples of A2 steel and NiTi, respectively, in order to remove burrs. In these studies, the authors reported that abrasive deburring can be an efficient method for removing large burrs and enhance surface quality of slots manufactured by micromilling. Silva, Silva and Oliveira (2023) also used abrasive deburring in slots fabricated by micromilling. The authors used sandpaper sheets to deburr micro slots of Inconel 718, considered a hard-to-cut material, and it was reported that this technique can reduce burr height in around 99.00% without any significant damage to the surface quality of the samples, as observed in figure 2.9.

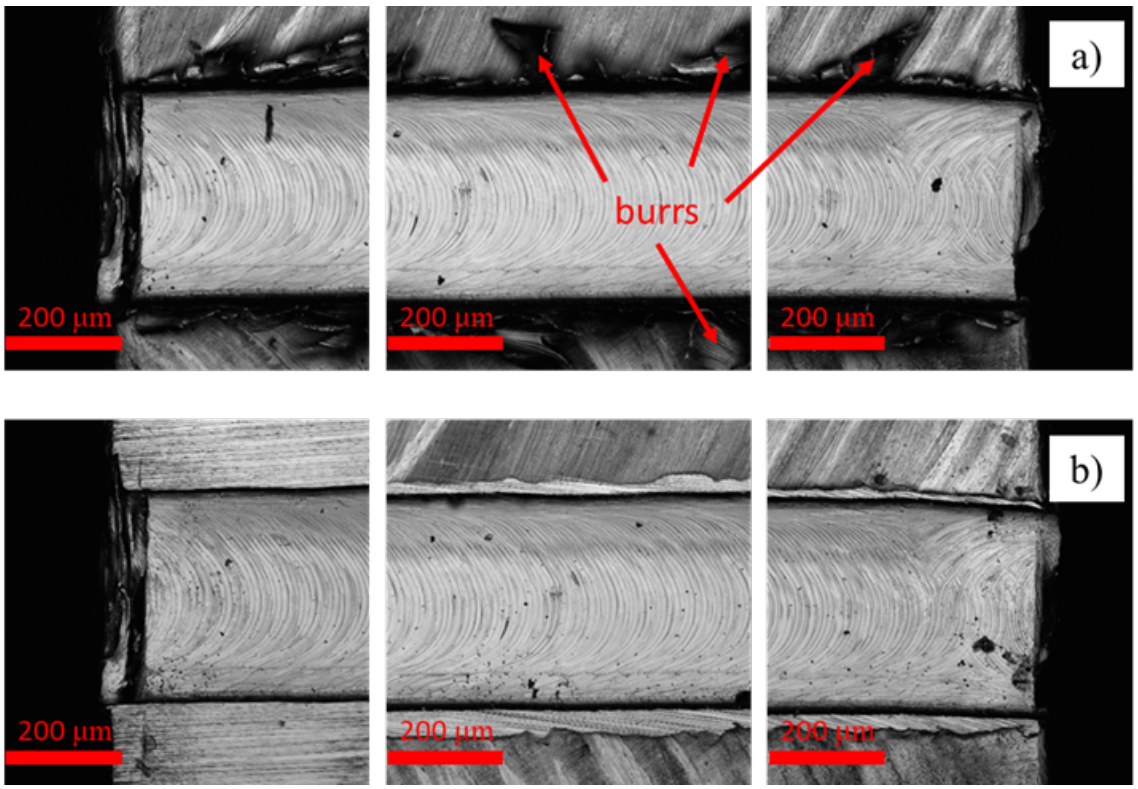

Figure 2.9 – Surface quality of microslots of Inconel 718 a) before deburring and b) after deburring (SILVA; SILVA; OLIVEIRA, 2023).

2.2 Machinability of Inconel 718

Inconel 718 belongs to a group of materials known as superalloys, which are thermo-resistant alloys. These materials have the capacity of maintaining mechanical properties even in elevated temperatures. Besides, superalloys are highly resistant to creep, which is a permanent time-dependent inelastic deformation of materials when they are subjected to constant loads. Another characteristic of these materials is their resistance to corrosion. Since their emergence in the decade of 1950, superalloys have caused great impact in aviation industry, being commonly used, for example, in the fabrication of jet engines. The typical microstructure of nickel superalloys such as Inconel 718 consists in three main phases: the phase γ, which has FCC (face centered cubic) crystal structure and enables the formation of a continuous matrix where other phases remain; the γ' or γ'' phases, which are precipitated phases coherent with the γ matrix; and carbides or borides, which occur because of reactions of carbon or boron with other reactive elements situated in the grain boundaries of the γ phase (REED, 2006).

The desirable properties of Inconel 718, however, result in poor machinability. Since it is remarkable for being a hard-to-cut material, recent studies have focused on enhancing the machinability of this superalloy through different machining conditions. Liu et al. (2021) performed a numerical and experimental investigation on the effect of tool geometry on residual stresses in machining of Inconel 718. The authors observed that friction in the

interface between the tool and the workpiece generates high heat, which is confined in a small region due to the low thermal conductivity of Inconel 718, leading to thermally induced residual stresses.

Bushlya, Zhou and Stahl (2012) performedd turning of Inconel 718 using tools of cubic boron nitride with and without coating of TiN, so as to determine the influence of the presence of coating on tool life, wear mechanisms and surface integrity of the workpiece. The authors verified that the presence of coating on the tool caused an increase of 20% in tool life, although this increase is limited to conditions of low cutting speed. This parameter proved to be highly sensitive to cutting speed, considering that an increase from 250 m/min to 350 m/min caused a fall of 250% on tool life. Liao, Lin and Wang (2008), on the other hand, investigated the behavior of WC tools in top milling operations. It was observed that high amounts of precipitates γ' and γ'' appear when Inconel 718 deforms, hindering dislocation movement and leading to hardening of the material. Below 650°C, the hardness of the material increases with temperature. For very low cutting speeds (lower than 56.6 m/min), the temperature in the cut region is lower than the softening point of phase γ'. As for excessively high speeds (from 124.4 m/min), the output of chip is highly impaired because much of the chip sticks to the edges of the slot in a process similar to welding (figure 2.10).

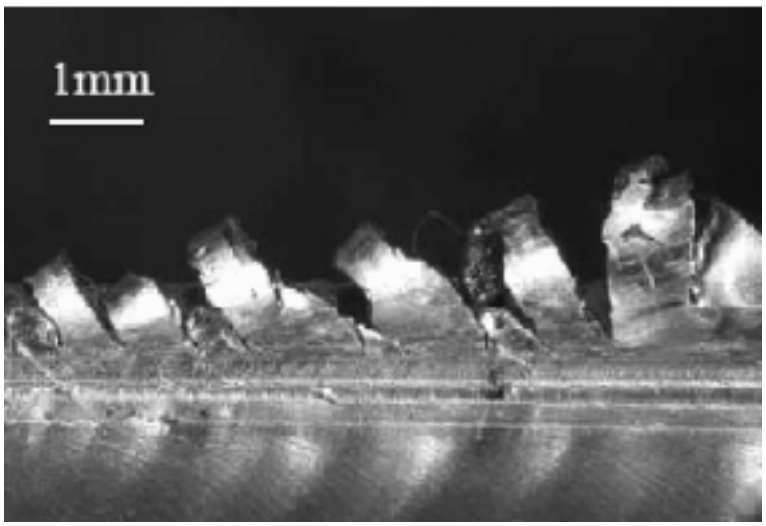

Figure 2.10 – Chip adherence on a slot obtained by top milling of Inconel 718 (LIAO; LIN; WANG, 2008).

Favero Filho et al. (2019) compared the performances of two cemented carbide tools when milling Inconel 718 with an average hardness of 450 HV. The authors observed that the low ability to conduct heat through the machined material causes the heat to be concentrated on the surface of the part and on the cutting tool, generating problems such as adhesion of the alloy to the tool, chemical reactions between the materials, and superficial burning of the part. The authors also observed the presence of adhesion and micro-chipping on the tool, as seen in figure 2.11.

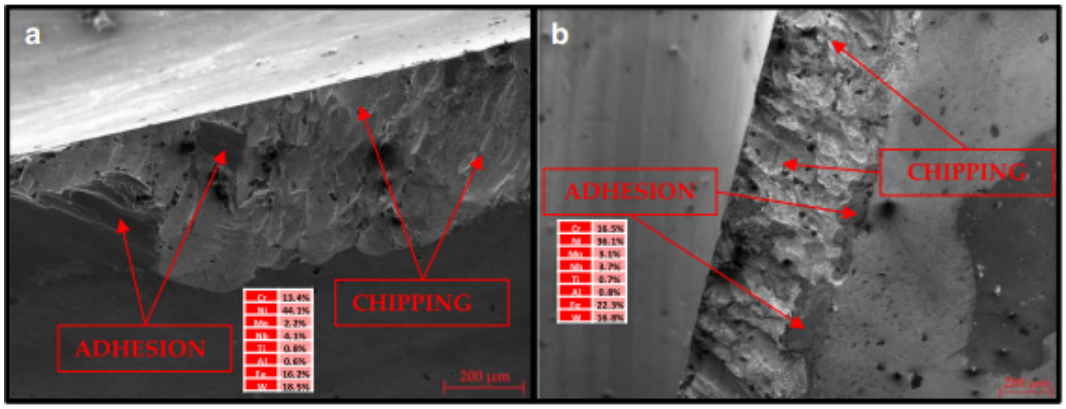

Figure 2.11 – Flank wear of uncoated cemented carbide tools after end milling of Inconel 718 (FILHO et al., 2019).

In general, machining Inconel 718 has proven to be a major challenge. Several studies show that certain characteristics of this material hinder its machinability, for example its high shear strength, the presence of abrasive particles in its microstructure, its low thermal conductivity and its tendency to form burrs and built-up edges.

2.2.1 Micromachining of Inconel 718

In view of the low machinability of Inconel 718 and the difficulties imposed by micromachining processes, micromilling of this material is an arduous task. Fang et al. (2020) conducted a comparative study between two different micromachining methods in Inconel 718: traditional micromilling (TMM) and ultrasonic vibrations assisted micrommilling (UVAMM). The UVAMM method consists of periodically applying ultrasonic vibrations to the part or tool in order to improve the surface quality. The authors observed that, by using TMM method, there was an accumulation of material not removed on the sides of the slot and the formation of undesired protrusions and cavities, so that the size effect had a significant influence on the poor final quality of the surface of the workpiece. With the UVAMM method, however, there was a reduction in surface irregularities. In addition, another observation made by the authors is that, in comparison with TMM, the UVAMM method allowed a certain suppression of burrs. Despite this, the smallest size found for the length of the burrs was 36.57 μm.

Aslantas and Çiçek (2018) performed micromilling in Inconel 718 to investigate the effects of four different cooling conditions: dry machining; ethanol lubrication; oil-water emulsion lubrication; and MQL system. Slots were fabricated through a TiCN micromill with a diameter of 600 μm. Ethanol has proven ineffective for lubricating Inconel 718 in terms of tool wear, burr formation and surface roughness. Ethanol lubrication, despite promoting workpiece cooling, was not able to minimize the effects of abrasive tool wear on the machined material. It was possible to observe significant decrease in the tool diameter and the presence of the largest burrs in the lubrication with ethanol, while the less severe tool wear and the smallest size of burrs occurred with the MQL system. In the

dry machining condition, burrs adhered to the microslot walls. In methods other than MQL, an intense plowing effect was observed, so that the excessive increase in the tool edge radius, caused by wear, intensified the formation of burrs, which reached more than 350 μm, as observed in figure 2.12.

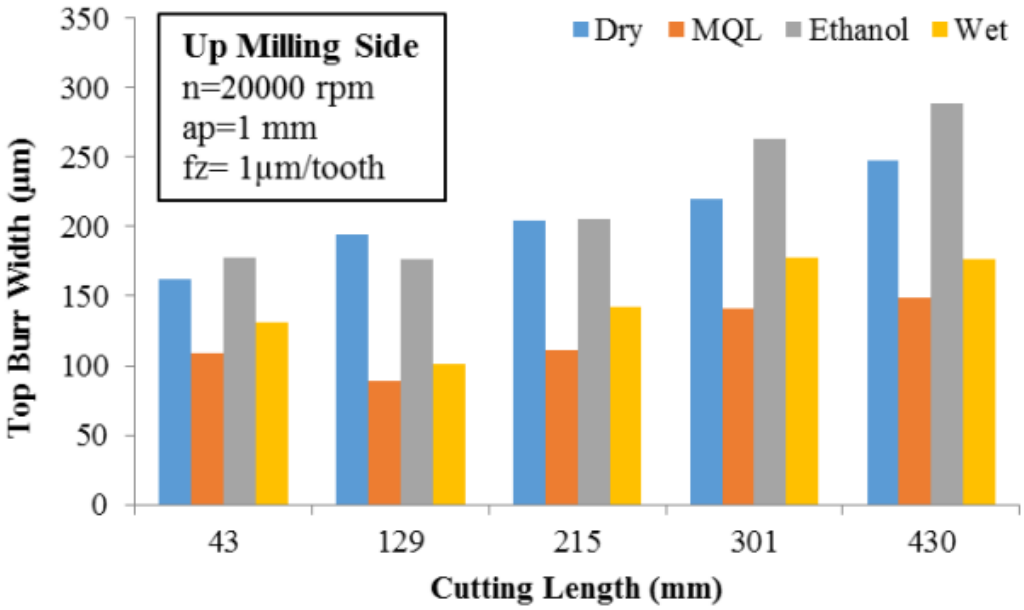

Figure 2.12 – Variation of burr width with cutting length under different lubrication conditions (ASLANTAS; ÇICEK, 2018).

A study of micromilling in Inconel 718 was carried out by Oliveira (2019), who performed experimental tests varying cutting speed, feed per tooth, depth of cut and application of cutting fluid. Titanium and aluminum nitride coated carbide cutters with a diameter of 400 μm, cutting length of 800 μm and two cutting edges of radius (1.1 $\pm$ 0.1) μm were used. The author used as output parameters the quality of the machined surface, the surface roughness, burr height, wear of the micromill, acoustic signals and vibrations, cutting forces and geometry of the chip. The author observed that the presence of cutting fluid can increase the machined length by up to 1000% until the end of tool life, which demonstrates a very high wear in the dry operation, which resulted in rounding of the cutting edge, detachment of the coating and breakage of the cutting edge. As for burr formation, it was found that there is less burr formation in tests with cutting fluid, although the exit burrs are large, up to 50% larger than the depth of the slot, as seen in figure 2.13.

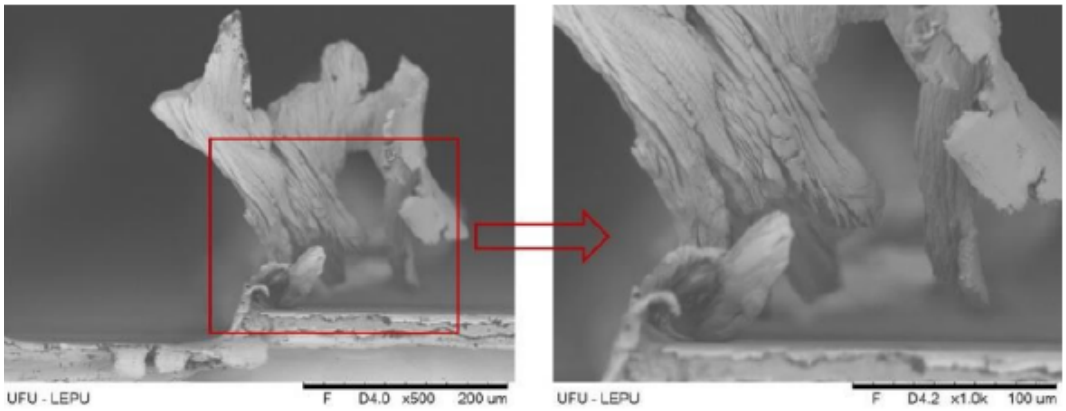

Figure 2.13 – Burrs of large dimensions on a microslot of Inconel 718 (OLIVEIRA, 2019).

2.3 Simulation of micromachining through FEM

Machining processes can be numerically simulated using the finite element method (FEM). Using the orthogonal cut modeling, it is possible to represent in two dimensions any machining process that uses a cutting tool with a defined geometry, such as milling and turning. The orthogonal cut is a simplification of the problem that consists in depicting the two-dimensional tool moving towards the workpiece to analyze chip formation. Different responses can be observed depending on the properties of the workpiece material, the geometry of the instances and machining parameters (WANG et al., 2008). According to Thepsonthi and Özel (2015), physical experiments can be replaced or supplemented by finite element simulation of micromachining, allowing an analysis to be performed at a lower cost. Besides, FEM simulations of micromachining permit the analysis of variables which are hard to be obtained experimentally.

A common methodology to analyze chip formation in FEM simulations is to assign a fracture criterium to the elements that compose the workpiece material (RAO; VIJAYARAGHAVAN, 2013). In order to characterize a material that is submitted to plastic deformation, such as in a machining simulation, its isotropic hardening curve must be determined. Although there are several constitutive models that can be used to mathematically describe the elastoplastic behavior of a material in a FEM simulation, one of the most common is the the Johnson-Cook (JC) constitutive model, which describes the dependency of plastic flow stress on equivalent plastic strain, normalized equivalent plastic strain rate and homologous temperature. According to JC model, it is assumed that damage accumulates linearly in each finite element according to the rate between the increment in plastic strain and the equivalent strain at fracture. The characterization of the material based on the JC model usually requires computational methods to process experimental data from uniaxial tensile tests, however it can also be done using indentation tests (MACHADO; MALCHER, 2019).

2.3.1 Chip formation and morphology

Several authors have used FEM simulations to analyze the plastic flow of the workpiece material and its dissociation in the form of chips during micromachining. Chip formation and morphology in numerical simulations are highly dependent on the constitutive model that describes the material being cut, as well as the cutting parameters. Material constitutive models characterize the deformation behavior during the cutting process and are crucial for the simulation accuracy (CHEN et al., 2019).

Thepsonthi and Özel (2016) conducted a numerical study on the effect of the workpiece constitutive model in 2D micromachining of Ti-6Al-4V. The authors contrasted viscoplastic and elasto-viscoplastic constitutive models. It was possible to conclude that the viscoplastic model has a significant advantage in terms of computational time, requiring approximately 60 hours to complete a single simulation, in contrast to approximately 500 hours for the elasto-viscoplastic model in the same conditions. The authors discuss that, when using the viscoplastic assumption, the elastic deformation is considered negligible in comparison with the plastic deformation, which is a generally valid assumption for macro scale machining. Nevertheless, the degree of elastic deformation may become relevant in micromachining due to size effect. Therefore, the elasto-viscoplastic model, which takes into account the elastic effects, is better to reproduce the physics of the process. This is evidenced by the difference in chip morphology for each assumption, since the viscoplastic model generated continuous chips, whereas the elasto-viscoplastic model generated segmented chip, as observed in figure 2.14.

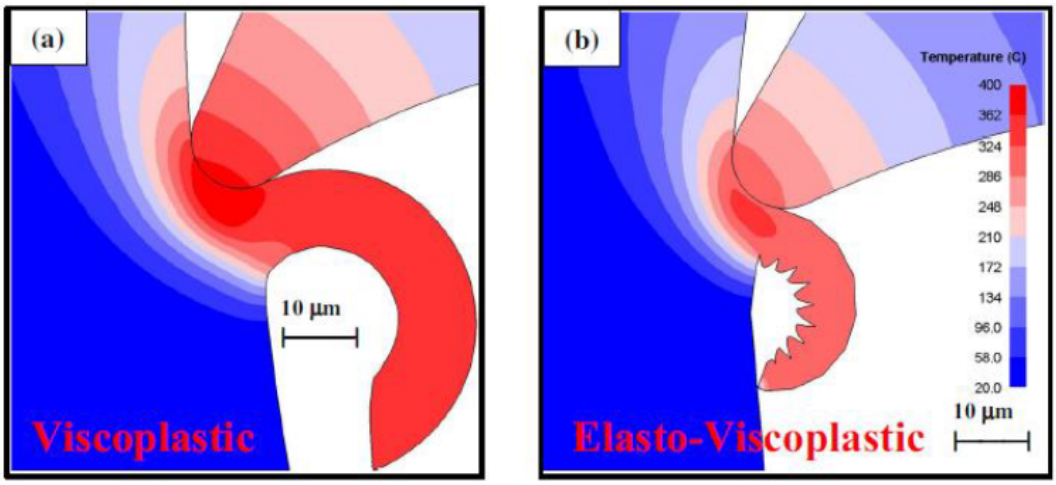

Figure 2.14 – Formation of a) continuous chip and b) segmented chip according to material constitutive assumption (THEPSONTHI; ÖZEL, 2016).

In another work, Thepsonthi and Özel (2015) predicted chip morphology in 3D simulation of micromachining of Ti-6Al-4V. In the simulation, the workpiece was modeled as a viscoplastic material and the tool was considered a rigid body, having the same geometrical feature as the physical micro-end milling tool of 508 μm of diameter and helix angle of 30°. The authors compared the results with experimental chips and obtained

reasonably good agreement, as observed in figure 2.15. The authors' results indicated that tool wear has a significant impact to the cutting force, cutting temperature, tool wear rate, chip flow and burr formation in micromilling.

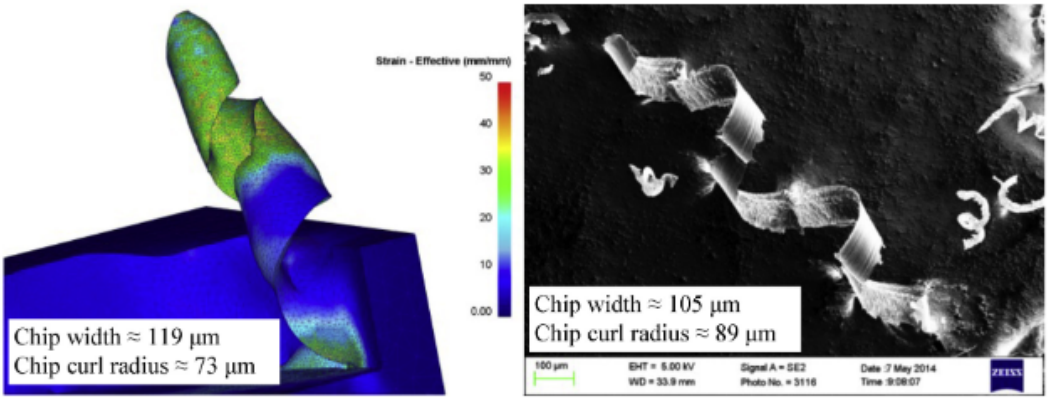

Figure 2.15 – Comparison of predicted and measured 3D chip formation in micromilling (THEPSONTHI; ÖZEL, 2015).

In their work, Liu and Melkote (2007) proposed a strain gradient plasticity-based finite element model of orthogonal micro-cutting of Al5083-H116 alloy, in order to examine fundamentally the influence of tool edge radius on size effect. The authors used cutting tools with two different edge radii, 5 μm and 20 μm, each one operating under different ranges of uncut chip thickness. The authors observed that tool edge radius and the temperature drop in the secondary deformation zone can cause non-linearities in the chip formation simulation. Besides, according to the authors, the edge radius affects the material deformation process and thereby contributes to the size effect by changing the material flow pattern around the tool tip, as well as causing higher energy dissipation due to increased tool–chip contact length at smaller uncut chip thickness values (LIU; MELKOTE, 2007).

Attanasio et al. (2019) performed an experimental and numerical investigation on the effects of tool run-out in chip flow in micromilling of CuZn37 brass. The authors performed 3D FEM simulations of the process by using the visco-plastic workpiece assumption and performing a thermo-mechanical analysis. The qualitative comparison of numerically predicted and experimentally measured chip shapes yielded in reasonably good results, as observed in figure 2.16. The authors observed that the size of the tool run-out deviation does not result in direct connection to the cutting speed, remaining in the magnitude order of few micrometers.

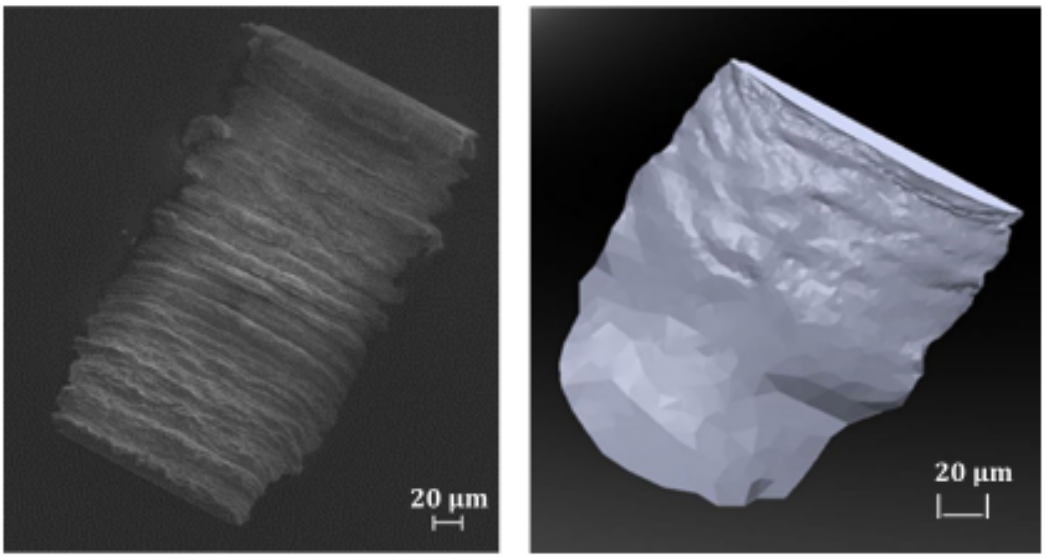

Figure 2.16 – comparison between a) a SEM image of a chip sample and b) a part of the simulated chip (ATTANASIO et al., 2019).

2.3.2 Cutting forces

Cutting forces are one of the most fundamental parameters for controlling and optimizing machining processes. So, the precise determination of cutting forces is a common objective in most research works on machining simulations. Chen et al. (2019), in their study, concluded that different plastic constitutive models result in similar cutting forces, when simulating machining of Ti-6Al-4V. The authors compared the Johnson-Cook model (JC), modified Johnson-Cook model (JCM) and Khan Huang model (KHL), obtaining a maximum error of 8% in comparison with experimental results. However, the authors performed simulations of machining in macro scale, which tend to be more often coherent with experimental results than simulations of micromachining, due to the non-linearities associated with the size effect.

In micro milling, the dimensions of the machined feature are dominated by tool deflection, which is associated with forces in the X and Y directions. Therefore, the component of the cutting force in the Z direction (axial direction) is negligible since it has no significant effect on regenerative chatter. Yuan et al (2018) proposed a mechanics model for precisely predicting cutting forces in X and Y directions in micromilling. The authors took into account several parameters, such as the variation of entry and exit angles for each engaged cutting edge, the instantaneous uncut chip thickness, the trajectory of the cutting tool flute and the elastic recovery of the material. The authors used the finite element method to calculate cutting force coefficients, which were identifies as nonlinear functions of the uncut chip thickness, the edge radii and the cutting velocities. The authors found out that the predicted and experimental cutting forces showed similar variation

patterns and closely matched amplitude levels, with a difference of less than 7%.

In another work, Jing et al. (2020) developed a model for predicting cutting forces in micro end milling, considering the effect of elastic recovery rate (P_e) in different values of feed per tooth, comparing numerical and experimental data. The authors found that P_e has a more obvious effect on predicted cutting forces for lower feed per tooth. Besides, the authors draw attention to the importance of tool run-out calibration, because it was observed that slight changes in tool run-out lead to great variations in cutting forces, as shown in figures 2.17 and 2.18.

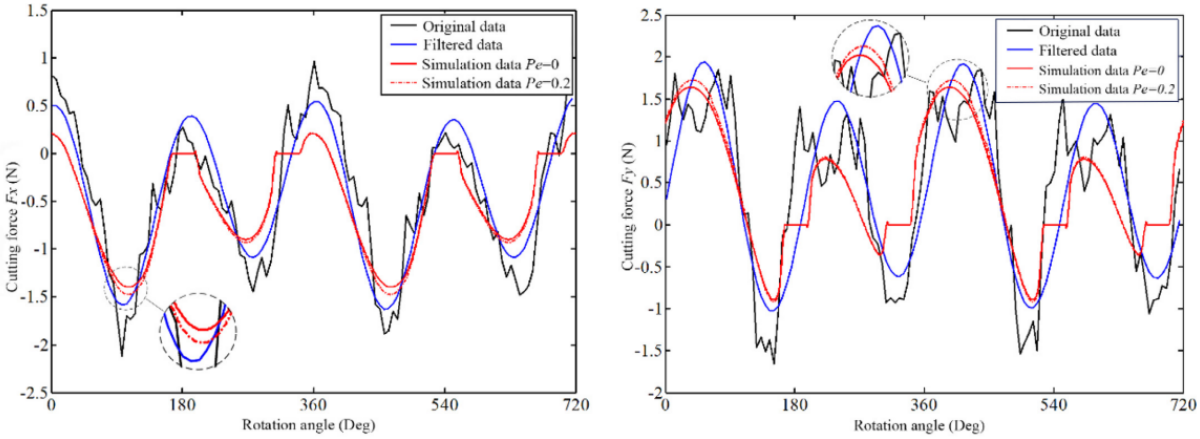

Figure 2.17 – Predicted and experimental cutting forces (feed = 2.0 μm per tooth) (JING et al., 2020).

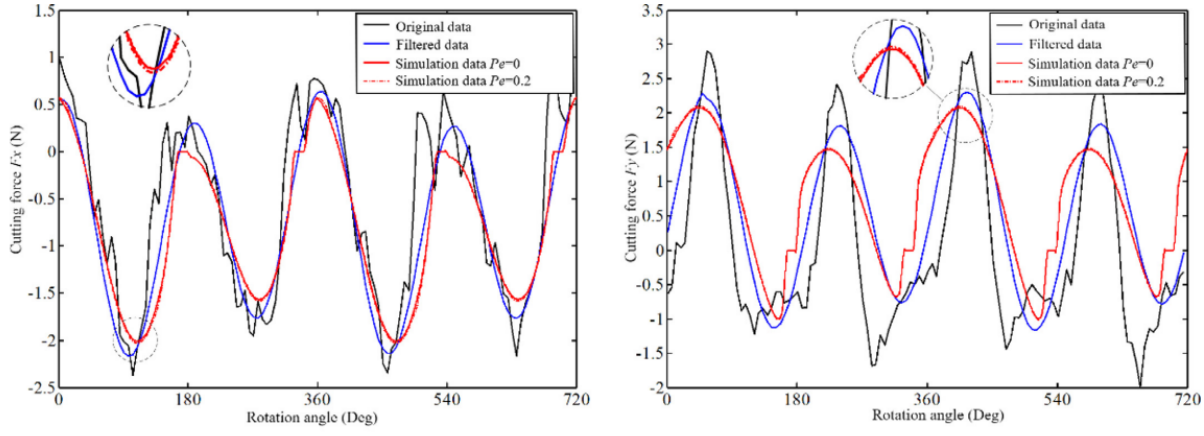

Figure 2.18 – Predicted and experimental cutting forces (feed = 4.0 μm per tooth) (JING et al., 2020).

Zhang et al. (2022) created a finite element model with three phases to explore the machinability of interfacial phases in SiCp/Al composites. This two-dimensional model included an interfacial phase, an Al matrix phase, and a SiC particle reinforced phase. The authors used a cohesive model to investigate the plasticity and failure behavior of the

composite matrix under micro milling conditions. The composite used for the experiment had a 20% volume fraction of SiC particles. As the tool advanced, the Al matrix was extruded by the cutting tool, leading to material being pushed to the upper part of the SiC particles. This caused some of the SiC particles to break and form pits on the machined surface after being pulled out of the Al matrix. The numerical model was capable of predicting cutting forces close to the experimental results. The authors concluded that the cohesive model accurately describes the mechanical properties of interfacial phases in composites.

In the work of Thepsonthi and Özel (2016), the authors found that the material assumption - viscoplastic or elasto-viscoplastic - has a minor effect on cutting forces when simulating micromilling of Ti-6Al-4V. The predicted cutting forces obtained from the two assumptions were compared and both presented similar trends. The difference in the maximum values of force was less than 1%, as observed in figure 2.19. Therefore, the authors concluded that the viscoplastic assumption is enough to predict cutting forces in FEM simulation of micromilling, and the use of elasto-viscoplastic assumption is not justified considering its high computational cost.

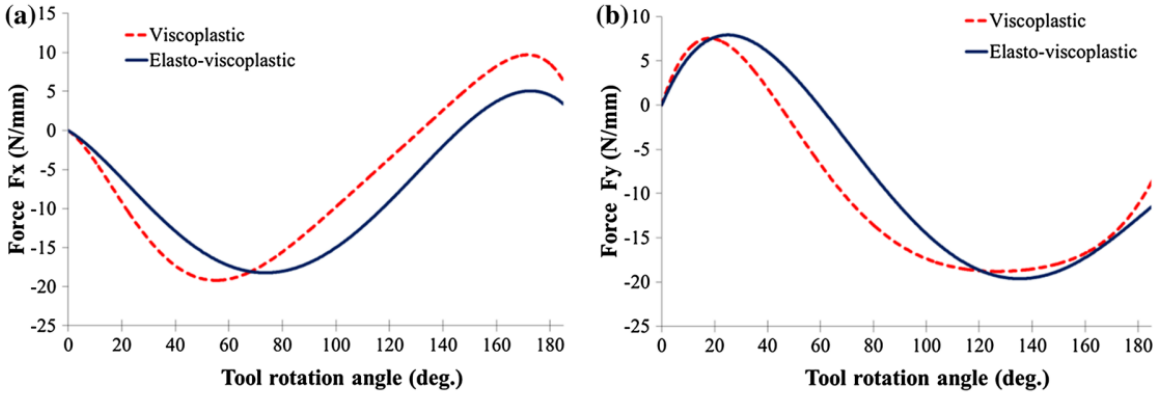

Figure 2.19 – Comparison of cutting forces obtained from a) viscoplastic model and b) elasto-viscoplastic model (THEPSONTHI; ÖZEL, 2016).

Fei et al. (2017) proposed a finite element simulation model to analyze chip formation and cutting forces in micromilling of Inconel 718. The simulation used the Deform-3D software, including modeling, definition of part and tool properties, control and execution of the simulation and analysis. A three-dimensional model of the tool was made, which had two carbide cutting edges, with a diameter of 500 μm and cutting-edge radius of 5 μm. The authors' results showed that, by increasing feed per tooth or radial depth of cut, while other parameters are kept constant, causes a proportional increase in cutting forces, and material removal becomes more pronounced. Carrying out the simulation, the authors obtained a critical advance value of 1.5 μm/tooth. For values lower than this threshold, there was no indication of chip formation, only plastic deformation.

A novel strategy for 2D FEM simulation of micromilling was proposed in the work of Abeni, Cappellini e Attanasio (2023). The authors used an algorithm to modify the

parameters of the Johnson-Cook flow stress law for simulating micromilling of additive manufactured Inconel 625, which is similar to the material studied in the present work. The forces obtained by the authors' simulations were compared with the ones calculated by a previously validated analytic model, resulting in good agreement.

2.3.3 Burr formation

Since the presence of large burrs is a common problem in micromachining, especially in hard-to-cut materials such as Inconel 718, it is important to predict burr formation by means of numerical simulations in order to avoid the deterioration of the tool and the surface quality of the machined part. Özel et al. (2017) performed an experimental and numerical analysis of micro-end milling using three-dimensional simulations. By measuringn the burr heights resulted from the simulations, the authors concluded that burrs become higher with increase of tool edge radius, as observed in figure 2.20.

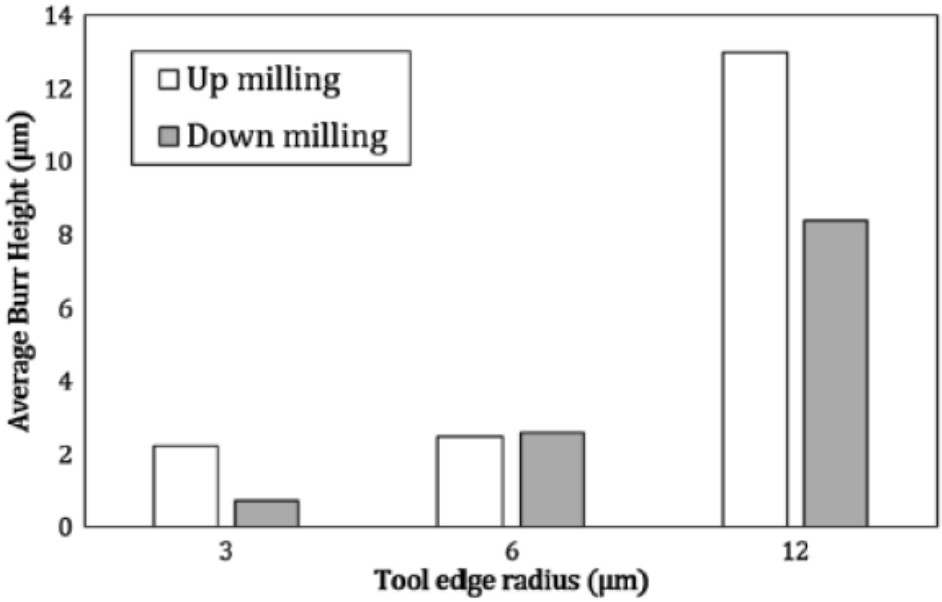

Figure 2.20 – Effect of tool edge roundness on burr height in FEM simulation of micro milling (ÖZEL; OLLEAK; THEPSONTHI, 2017).

Although most research works about burr formation in micro milling focus on milling of conventional rectangular or circular micro slots, Deng et al. (2022) proposed a technique to manufacture Ω-shaped reentrant microchannels. The authors investigated the effects of cutting parameters on side burr size by means of experiments and numerical analysis. The authors used tungsten carbide micro ball end mills with two flutes and a diameter of 0.8 mm to fabricate circular cavities in prefabricated micro slots in samples of copper. The burr area was used to characterize the burr size due to the difficulty in measuring burr height in the circular shaped cavities. The material was characterized by the Johnson-Cook model, the tool was described as a rigid body and both instances were discretized by tetrahedral meshes. By comparing the shapes of the micro channels

obtained by the simulation and the experiment, the authors noticed that the side burrs were formed only on the down milling side, as observed in figure 2.21.

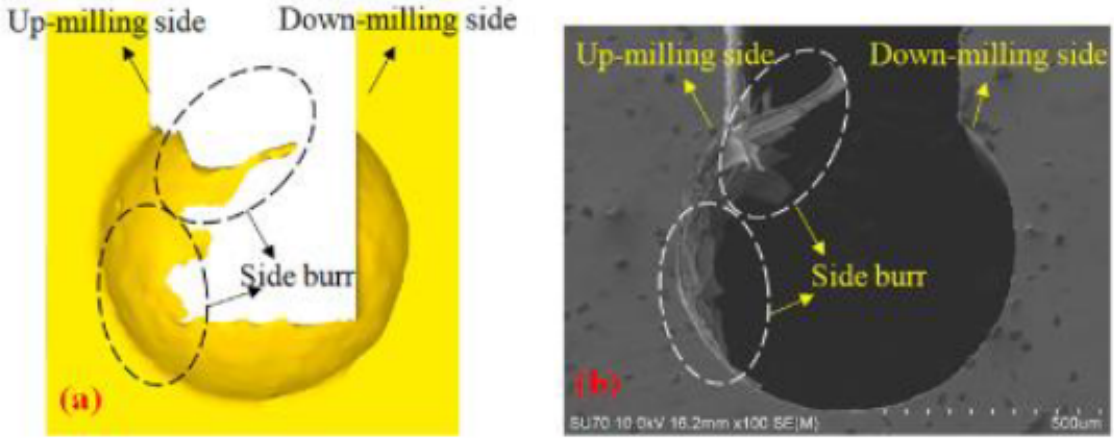

Figure 2.21 – Burr formation in Ω-shaped reentrant microchannels obtained by (a) simulation and (b) experiment (ÖZEL; OLLEAK; THEPSONTHI, 2017).

Considering that burr formation generally depends on the stress state and microstructure of the undeformed workpiece material, it can be hindered by cold working, which leads to grain refinement and the appearance of residual stresses on the material surface. In that regard, Yadav et al (2022) proposed a robust numerical model and experimental verification of burr size control in micro milling of Ti-6Al-4V by introducing compressive residual stresses on the surface of the workpiece. The authors found that the presence of residual stress suppresses the burr generation by up to 63% in terms of width and height. The simulation was performed using a recrystallization and strain gradient flow model accompanied by a user-defined friction algorithm. The critical uncut chip thickness was found to be 24% of the cutting-edge radius and more burrs were seen on the down-milling side rather than on the up-milling side, which is uncommon in micromilling.

3 Simulation methodology

3.1 Modelling of orthogonal cutting

In the present work, the simulations were carried out by creating standard database explicit models on Abaqus CAE, version 6.14-1, which is a commercial software for finite element analysis. In order to simulate micromilling in Inconel 718, an orthogonal cutting model was used. Through this technique, any machining process that uses a cutting tool with defined geometry, such as turning or milling, can be represented in two dimensions, which simplifies the problem. A FEM simulation of an orthogonal cutting process can have considerably less computational cost than a 3D simulation. In the orthogonal cut, the cutting tool and the workpiece are depicted as 2D instances with defined material properties. Some kind of relative movement is then applied to the instances to provoke physical interaction between them, aiming to simulate chip formation and removal. Some of the most important factors affecting an orthogonal cut simulation include tool geometry, cutting parameters, and the macro physical characteristics of the workpiece (WANG et al., 2008).

In micromilling, the cutting-edge radius of the micro-tool is a crucial parameter due to size effect and the non-linear increase in cutting energy. It is well known from literature that the radius of micromills tend to increase rapidly over small values of machined length, owing to high wear rates, as observed in the works of Santos, Silva and Jackson (2018) and Ziberov et al. (2020). In the work of Saha, Deb and Bandyopadhyay (2021), the authors used TiAlN-coated WC/6Co micro end mills with edge radius 1.35 μm to machine Ti-6Al-4V samples and observed that the edge radius increased to 4.27 – 5.21 μm after a length of cut of only 40 mm. Thus, in the present work, in order to analyze the effect of edge radius size in chip morphology in the FEM simulation, two different geometries were proposed for the cutting tool: one configuration representing a novel tool, with edge radius of 1 μm, and another configuration representing a tool which suffered wear and rounding of the tip, with edge radius of 5 μm. The tools were modeled by creating 2D planar, discrete rigid sketches on Abaqus with the dimensions in milimeters shown in figures 3.1 and 3.2. Each tool was created in a different database model. A reference point (RP) was placed on each tool. The RPs were associated to the respective sketches, so that the machining conditions could be set to the reference points rather than the whole instances.

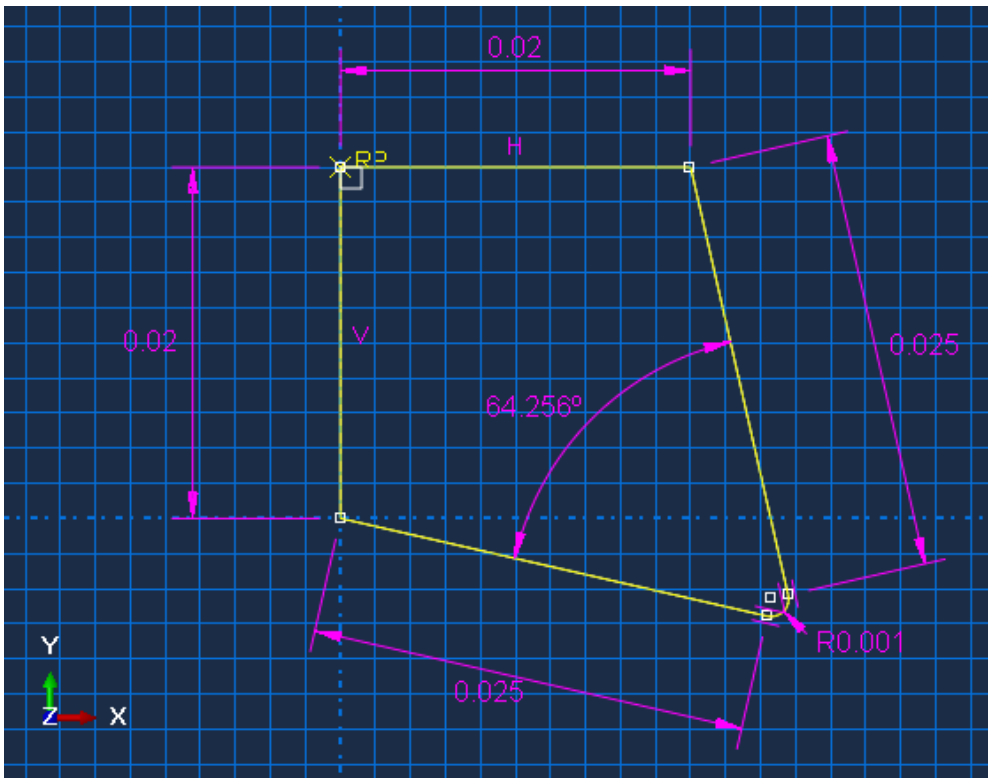

Figure 3.1 – Sketch made on Abaqus of the cutting tool with edge radius 1 μm. The dimensions on the sketch are in millimeters.

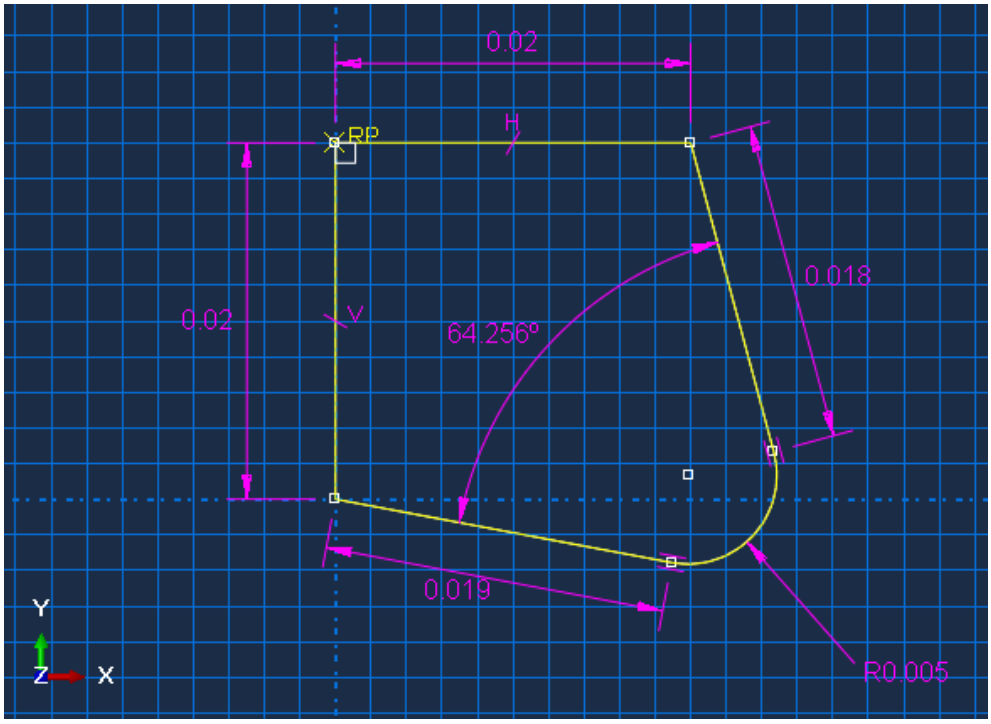

Figure 3.2 – Sketch made on Abaqus of the cutting tool with edge radius 5 μm. The dimensions on the sketch are in millimeters.

After creating the sketch of each tool, another part was created in each database model for the sketch of the workpiece. The workpiece sketches were created as 2D planar deformable shells with the dimensions in millimeters shown in figure 3.3. The workpiece

sketches were partitioned with two horizontal lines distant 2.5 μm and 5 μm from the top edge. The objective of the partition lines is to facilitate discretization later on. In each model, the workpiece was associated to a solid homogeneous section, with plane stress/strain thickness of 0.03 mm. This value represents a depth of cut of 30 μm and is equivalent to the dimension of the workpiece in the Z direction in figure 3.3. Although this dimension cannot be seen in the 2D representation of figure 3.3, its value is crucial for determining the cutting forces. The input of the depth of cut on Abaqus CAE is done in the definition of the section in the model database, as shown in figure 3.4.

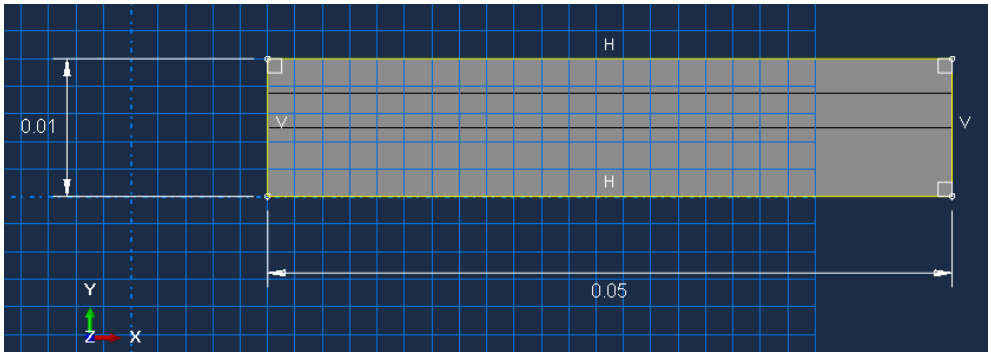

Figure 3.3 – Sketch made on Abaqus of the workpiece. The dimensions are in millimeters.

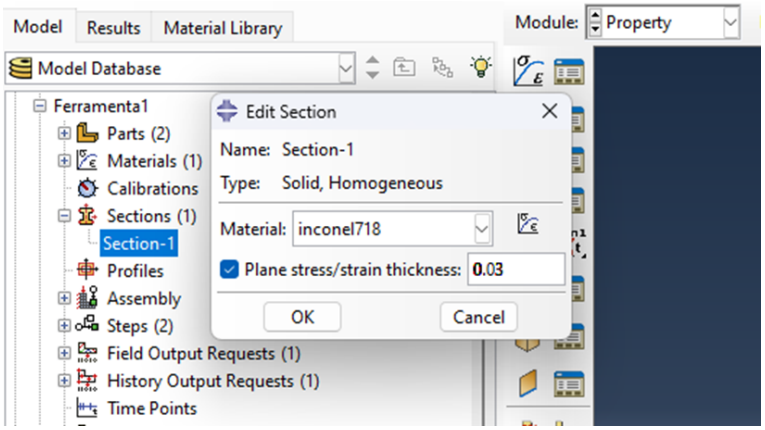

Figure 3.4 – Definition of depth of cut on Abaqus.

Therefore, the two models aimed at comparing chip formation with different values of tool edge radius. In each model, an assembly was made by positioning the tool and the workpiece according to figure 3.5. Afterwards, for simulating the cutting process, each workpiece was kept stationary and a horizontal displacement from left to right was applied to the tool.

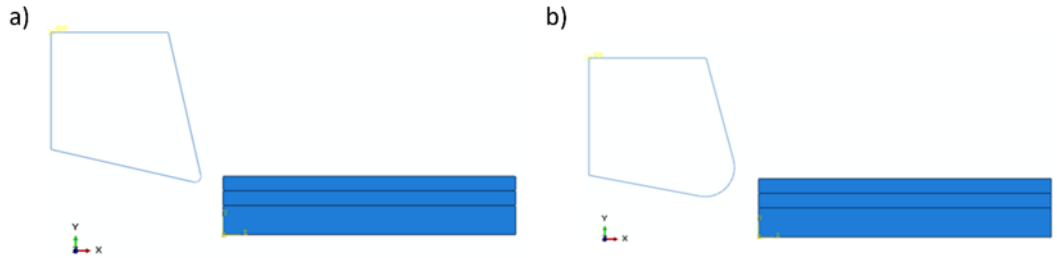

Figure 3.5 – Assembly of the instances for the two models: a) tool with edge radius 1 μm and b) tool with edge radius 5 μm.

3.2 Material characterization

3.2.1 Johnson-Cook model with isothermal approach

Before associating the workpieces to the respective solid homogeneous sections, the material needs to be characterized, in this case the material is Inconel 718. On Abaqus, a constitutive model to describe material behavior is formulated based on the Johnson-Cook (JC) approach (JOHNSON; COOK, 1985). According to the JC model, the hardening rule of the material depends on accumulated plastic strain and its rate, as well as the temperature, as shown in equation 3.1.

$$\sigma_y = \left[A + B\left(\overline{\varepsilon}^p\right)^n\right]\left[1 + C\ln\left(\dot{\overline{\varepsilon}}^{p*}\right)\right]\left(1 - \widehat{\theta}^m\right) \tag{3.1}$$

In equation (3.1), σ_y represents the hardening rule of the material. The term $\overline{\varepsilon}^p$ is the accumulated plastic strain, while $\dot{\overline{\varepsilon}}^p$ is the accumulated plastic strain rate, which describes the change on equivalent plastic strain over time. The term $\widehat{\theta}^m$ is the thermal effect. The terms A, B and n are material constants which represent, respectively, the initial yield stress, the isotropic hardening modulus and the exponent of hardening. The parameter C is the coefficient of strain rate, which describes the mechanical behavior of the material according to the load application rate. Finally, m is the thermal exponent, which specifies the decrease in mechanical resistance according to temperature rise. The term in the logarithm is the dimensionless plastic stress rate, which is calculated by equation 3.2.

$$\dot{\overline{\varepsilon}}^{p*} = \dot{\overline{\varepsilon}}^p / \dot{\overline{\varepsilon}}^p_0 \tag{3.2}$$

In equation 3.2, $\dot{\overline{\varepsilon}}^p_0$ represents the reference accumulated plastic strain rate. Finally, the homologous temperature is represented by the term $\widehat{\theta}$ and is calculated by equation 3.3, where T is the current temperature, T_r is the reference temperature and T_m is the melting temperature:

$$\widehat{\theta} = \frac{T - T_r}{T_m - T_r} \tag{3.3}$$

It is known that nickel super-alloys such as Inconel 718 are able to maintain high strength and hardness even in elevated cutting temperatures due to their low thermal conductivity (LIANG; LIU; WANG, 2019). Considering this, in the present work, isothermal condition was assumed to analyze chip formation, to represent a situation where there is no softening of the material because of temperature rise. This condition is valid to analyze chip geometry, since the small cutting time of the simulation is not enough to generate sufficient temperature rise to cause a considerable change in chip morphology (THEPSONTHI; ÖZEL, 2016). Thus, assuming isothermal behavior of the material, the hardening rule of equation 3.1 can be simplified according to equation 3.4:

$$\sigma_y = \left[A + B\left(\overline{\varepsilon}^p\right)^n\right]\left[1 + C\ln\left(\dot{\overline{\varepsilon}}^{p*}\right)\right] \tag{3.4}$$

3.2.2 Johnson-Cook failure indicator

The failure model based on Johnson-Cook considers fracture of individual elements, assuming that damage is accumulated linearly according to equation 3.5, where I_{JC} is the Johnson-Cook fracture indicator and ε_f is the equivalent plastic strain at fracture:

$$I_{JC} = \int_0^{\varepsilon_f} \frac{\dot{\overline{\varepsilon}}^p}{\varepsilon_f} \tag{3.5}$$

According to JC model, the equivalent plastic strain at fracture is a function of the stress triaxiality η, which is the ratio between hydrostatic pressure and the von Mises equivalent stress, as well as the dimensionless plastic strain rate $\dot{\overline{\varepsilon}}^{p*}$ and the homologous temperature $\hat{\theta}$, according to equation 3.6.

$$\varepsilon_f = \left[D_1 + D_2\exp\left(D_3\eta\right)\right]\left[1 + D_4\ln\left(\dot{\overline{\varepsilon}}^{p*}\right)\right]\left[1 + D_5\hat{\theta}\right] \tag{3.6}$$

In equation 3.6, D_1, D_2, D_3, D_4 and D_5 are material parameters that need to be calibrated by adjusting experimental and numerical data (JOHNSON; COOK, 1985).

3.2.3 Mechanical properties

The mechanical properties that were used in the present work to characterize the workpiece material were obtained from the work of Erice and Galvez (2014). The authors determined the Johnson-Cook parameters from equation 3.1, as well as the damage coefficients from equation 3.6. The elastic properties such as Young modulus and Poisson coefficient were also determined. The parameters obtained from the authors that were

used as input on Abaqus are shown in table 1. Since the cutting tools were modeled as rigid bodies, no material properties were defined to them.

Table 1 – Material parameters for characterization of Inconel 718 (ERICE; GALVEZ, 2014).

Parameter	**Value**
D_1	0.04
D_2	0.75
D_3	-1.45
D_4	0.04
D_5	0.89
T_m	1800 °C
T_r	25°C
A	1200 MPa
B	1284 MPa
C	0.006
m	1.20
n	0.54
$\dot{\bar{\varepsilon}}_0^p$	0.001 s^{-1}
Young modulus	185000 MPa
Density	0.000000819 kg/mm^3
Poisson coefficient	0.33

It is important to point out that Abaqus CAE does not define measurement units, so it is the author's responsibility to supply the input parameters in the correct units according to the desired output units. For this reason, for example, the density was supplied in kg/mm^3 so that the values of reaction force could be given in newtons, considering that the sketches of the instances were created in millimeters. All the parameters shown in table 1 were supplied in the "edit material" section on Abaqus CAE, as exemplified in figures 3.6 and 3.7.

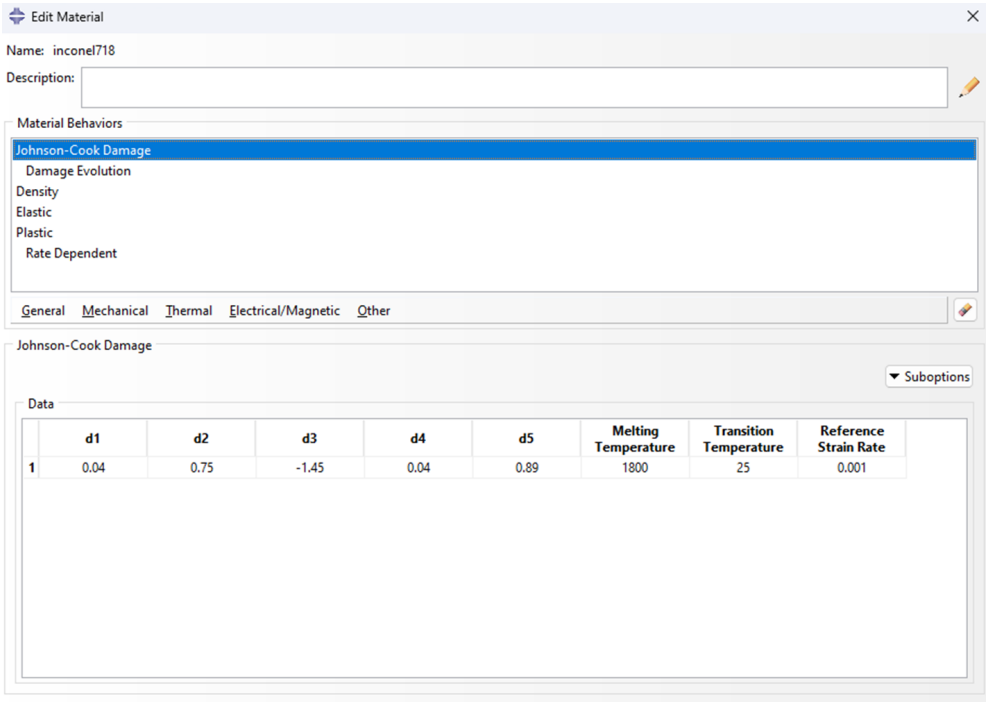

Figure 3.6 – Definition of material properties on Abaqus CAE: JC damage parameters.

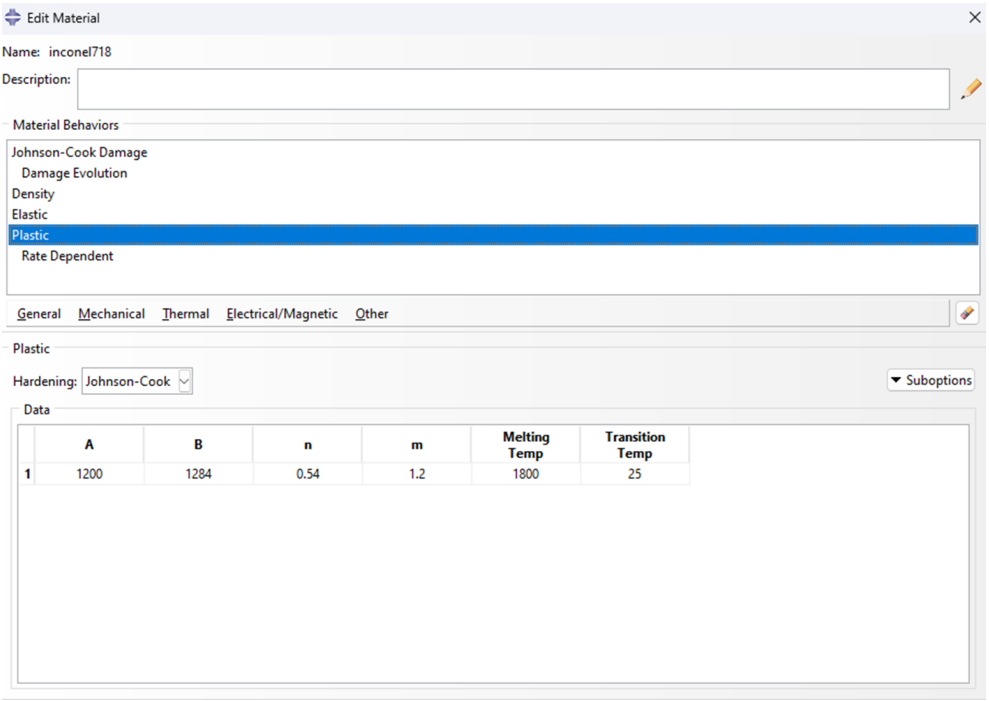

Figure 3.7 – Definition of material properties on Abaqus CAE: JC hardening rule parameters.

3.3 Interaction of the instances

3.3.1 Boundary condition 1

After creating the sketches and the assembly of the instances, with the defined workpiece material parameters, it is necessary to define the boundary conditions and interaction properties. The first boundary condition consists in restricting the movement of the inferior edge of the workpiece, so that it stays stationary throughout the simulation. The implementation of this boundary condition on Abaqus is shown in figure 3.8. It was applied in the initial step of the simulations and propagated to the following steps.

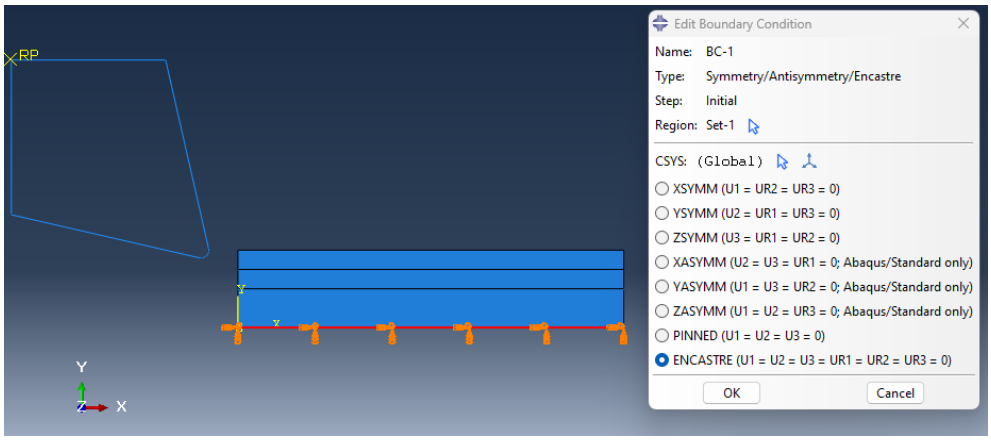

Figure 3.8 – Boundary condition 1: restriction of movement of inferior edge of the workpiece.

3.3.2 Boundary condition 2

The second boundary condition was to apply the cutting speed of the tool, which was done in the step 1, or one step after the initial step. Since the tool was modeled as a rigid body with a reference point associated to it, this boundary condition consisted in applying a displacement to the reference point. The displacement chosen was 0.07 mm, or 70 μm, because it is enough for the tool to sweep the whole range of the workpiece length. The displacement of the tool was applied with a linear amplitude, which means that the tool would move with constant velocity throughout the simulation. To model this linear constant motion, the tabular amplitude and the displacement of the reference point were assigned so as to define a cutting speed of 100 mm/s, or 6 m/min, as shown in figure 3.9. The total simulation time is 7×10^{-4} s, so the tool was set up to cover the complete distance of 0.07 mm by the end of the simulation. This value of 6 m/min corresponds to the approximate cutting speed of a micro end-mill with diameter 400 μm spinning at 5000 rpm. This value was chosen because the effect of depth of cut in the minimum uncut chip thickness is supposed to be more intense for low cutting velocities (RAMOS et al., 2012).

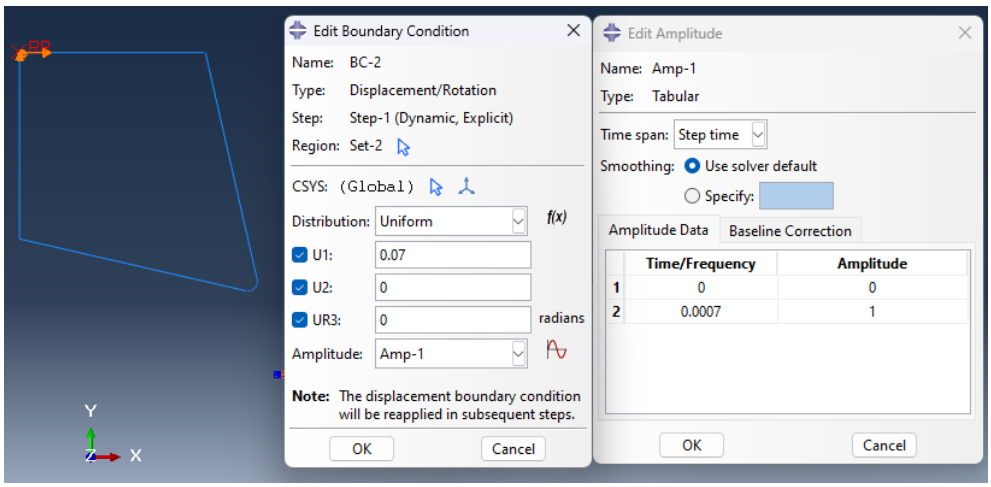

Figure 3.9 – Boundary condition 2: application of the cutting velocity of 100 mm/s to the cutting tool.

3.3.3 Contact properties

As for the interaction of the instances, the contact properties need to be defined. As exemplified in figure 3.10, the flank face of the tool (red) was considered the first surface and the node region of the whole workpiece (purple) was set as the second surface. The vertical distance between the upper edge of the workpiece and the lowest point of the cutting tool corresponds to the feed per tooth (f_z) in a micro-milling process. The plane stress state thickness, on the other hand, corresponds to the depth of cut (a_p). The horizontal velocity of the tool in the simulations corresponds to the cutting velocity in a real machining process, which, in the case of micro-end milling, depends on the spindle speed and diameter of the micromill. In a real micro-end milling process, the tool rotates around a center with angle Φ and the cutting-edge attempts to cut a continuously varying chip thickness, figure 3.11(a), and plowing occurs if the undeformed chip thickness is less than the minimum chip thickness, figure 3.11(b).

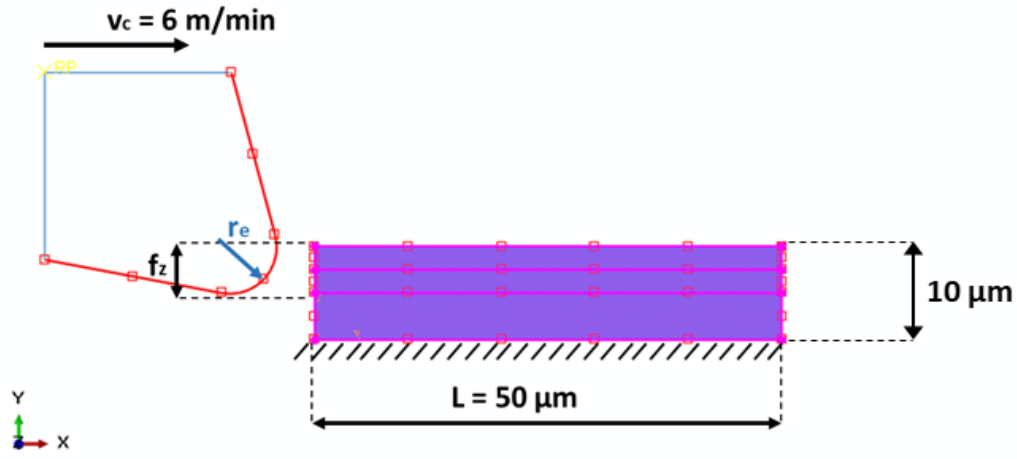

Figure 3.10 – Modeling of the contact between the workpiece and the tool.

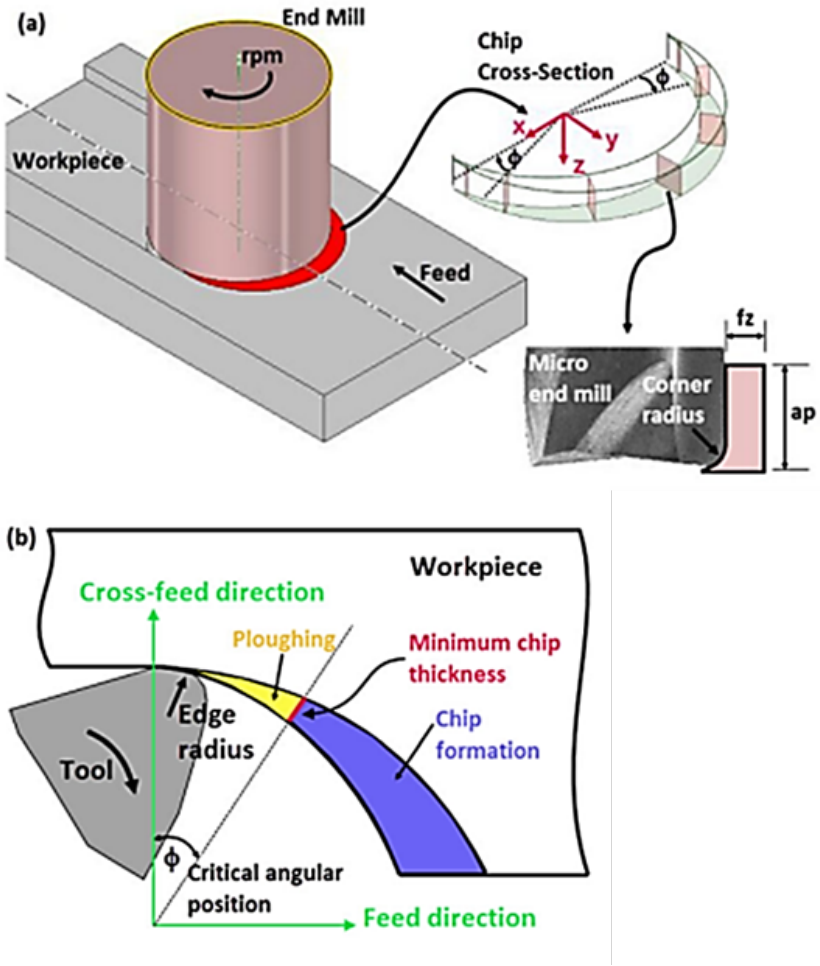

Figure 3.11 – (a) Change of chip cross-section in micro milling process; (b) Schematic diagram of the effect of the minimum chip thickness. Adapted from Erçetin, Aslantas and Özgün (2020).

The interaction considered normal behavior and tangential behavior with penalty friction formulation, with a friction coefficient of 0.2. This value is a valid estimation since most research works on micromilling of Inconel 718 recommend the use of cutting fluid to decrease friction, so the use of higher friction coefficient would be closer to a dry cutting condition, which is known to cause very rapid tool wear rates (THEPSONTHI; ÖZEL, 2016). The definition of the friction coefficient is shown in figure 3.12.

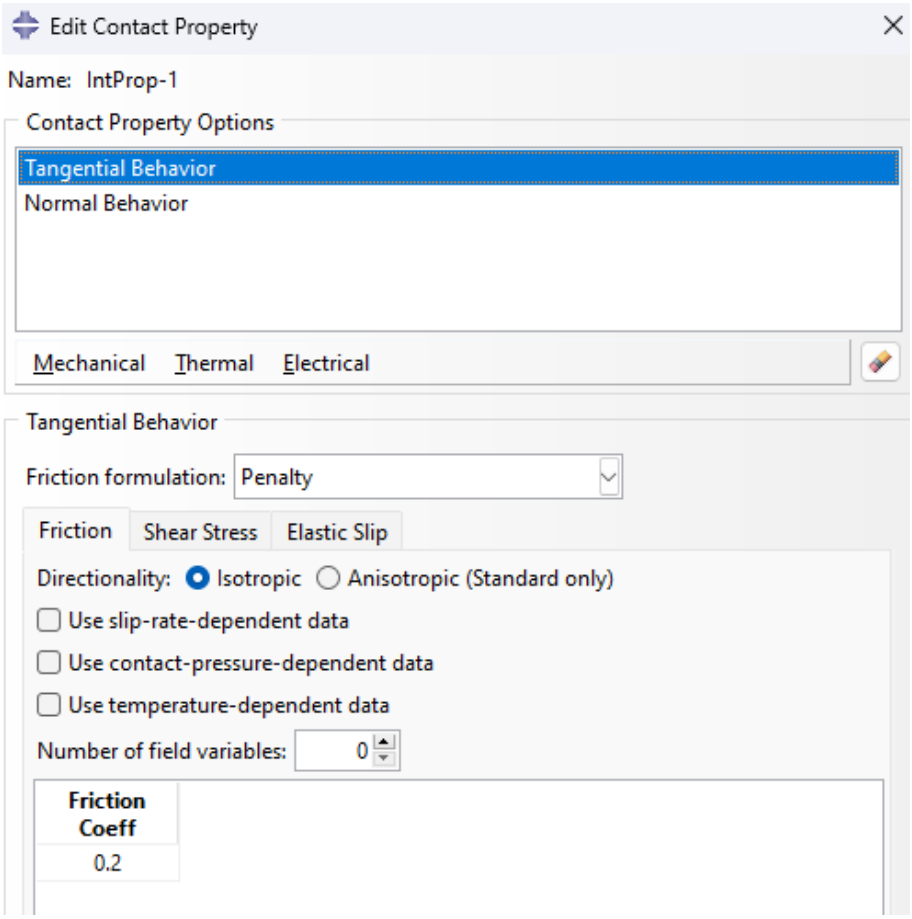

Figure 3.12 – Definition of contact properties.

3.4 Field output requests

Each simulation was carried out at a frequency of 20 evenly spaced time intervals. Since the total displacement of the tool is 70 μm, it means that the tool moves $70 \div 20 = 3.5$ μm per frame. Considering the constant velocity of 100 mm/s, each frame corresponds to an advance of 0.035 ms in machining time, so that the total simulated machining time is 0.7 ms. In each frame, the software calculates the requested output parameters. Seeing that isothermal condition is assumed, the temperature of the elements was not requested as an output, as observed in figure 3.13. The most important parameters that were requested as outputs were the von Mises stress and the reaction force, which can be compared to the cutting force in a real micro-milling operation.

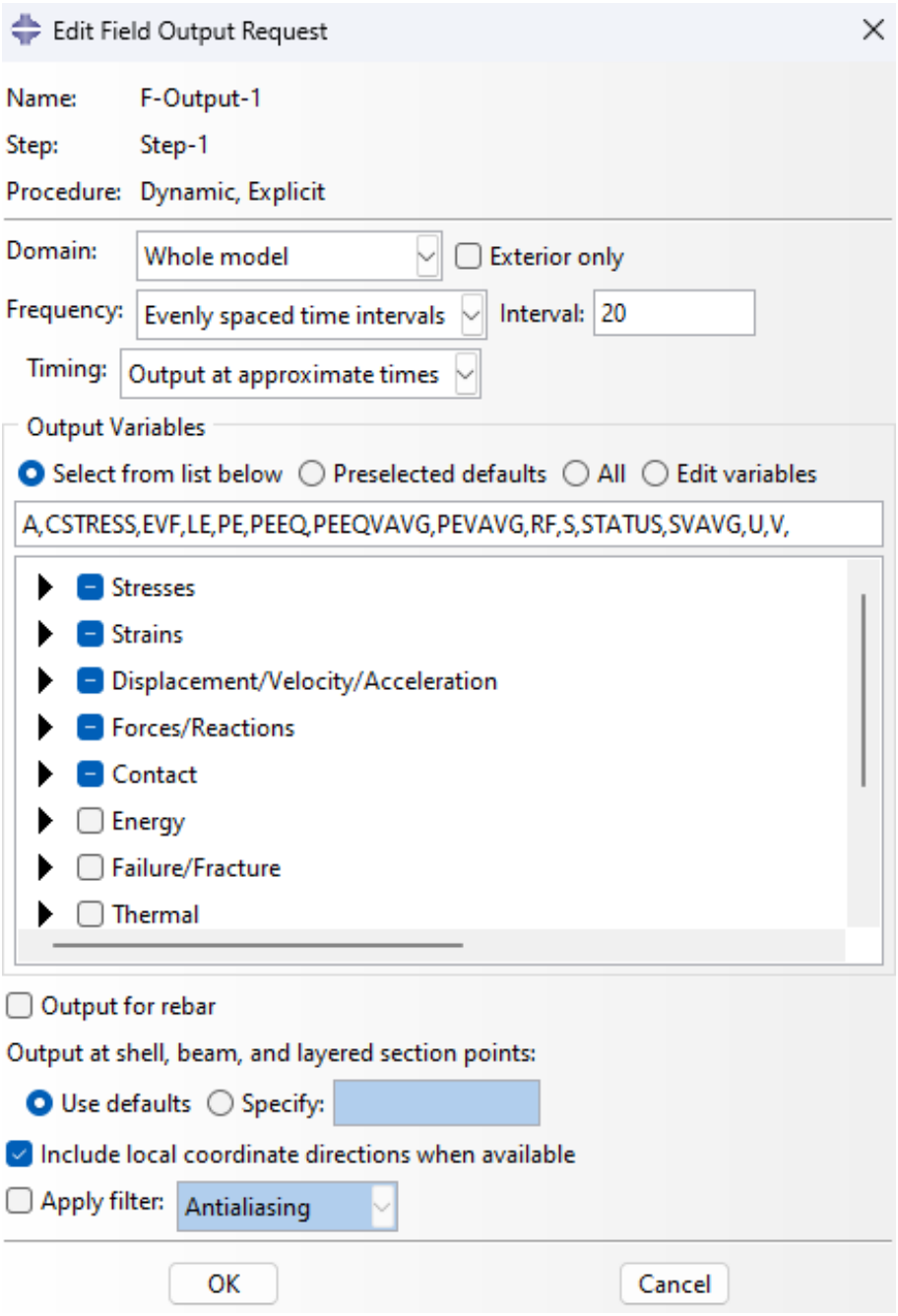

Figure 3.13 – Definition of field output requests.

3.5 Discretization

With all the interaction properties and output requests defined, the next step is to discretize the tool and the workpiece into finite elements. The discretization of the workpiece was facilitated by the partition lines, which permit the top of the instance to be more refined than the bottom. Different configurations of meshes for the workpiece were considered depending on the radius of the cutting tool. The most suitable mesh varies with the tool because the sharper tool needs to be more refined in a very small area (which is the region closest to the edge), whereas the worn tool has a larger area to be refined, so the tool with larger radius has more elements than the sharp tool. Examples of discretization

of the workpiece and the tools are shown in figures 3.14 and 3.15, respectively. All the discretization processes for the workpiece were done with quadrilateral dominated element shape, whereas the tools were discretized with linear standard elements since they are 2D rigid bodies. The size and number of elements is variable for each simulation and the most suitable meshes that were used are discussed in the mesh convergence analysis.

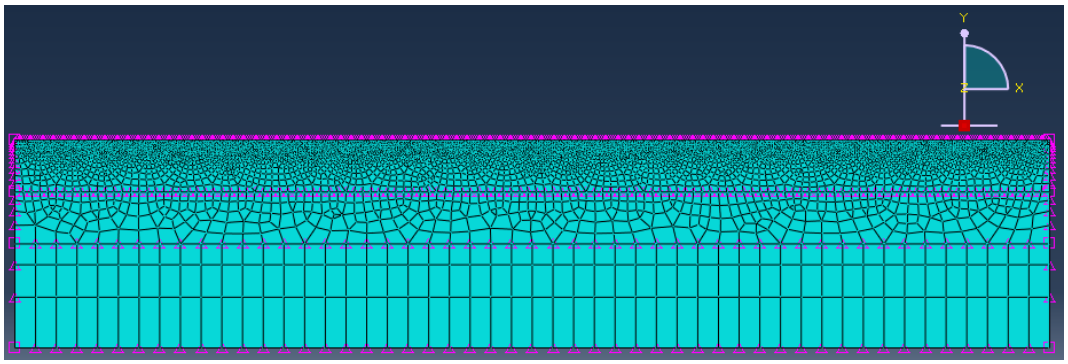

Figure 3.14 – Example of discretization of the workpiece.

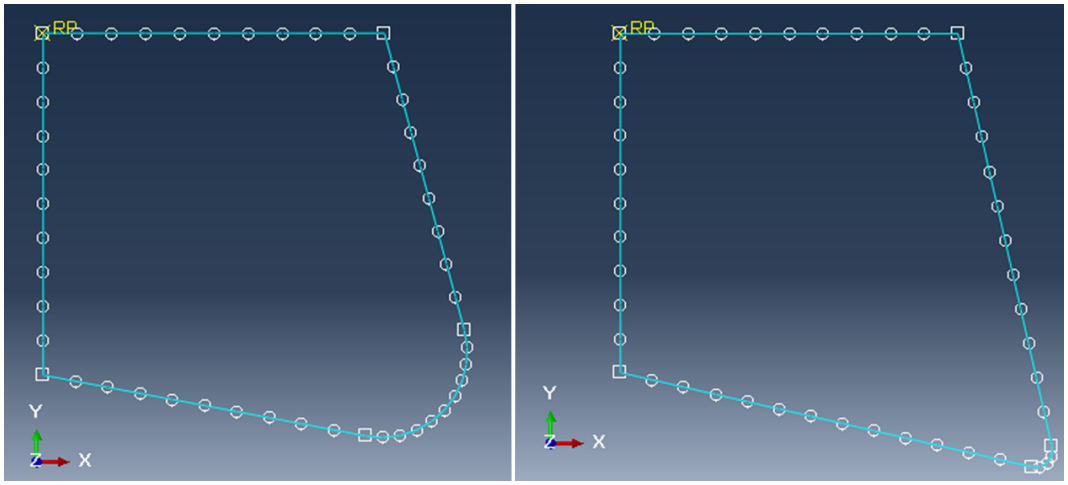

Figure 3.15 – Examples of discretization of the two cutting tools.

The simulation of failure of the workpiece material on Abaqus occurs by element deletion. When each individual finite element suffers deformation beyond a specified limit, the element is deleted. For the correct functioning of this feature in the simulations, the element deletion must be activated in the "Element Type" menu, after selecting the workpiece mesh, as shown in figure 3.16. The determination of the deformation limit is done in the properties of the material, in the damage evolution menu. The values of the displacement at fracture used for the tools with edge radius 1 μm and 5 μm were 10^{-5} and 10^{-3}, respectively. These values were different according to the radius of the tool because the two tools had different element sizes, which could lead to simulation errors caused by excessive element deformation if the same value was used.

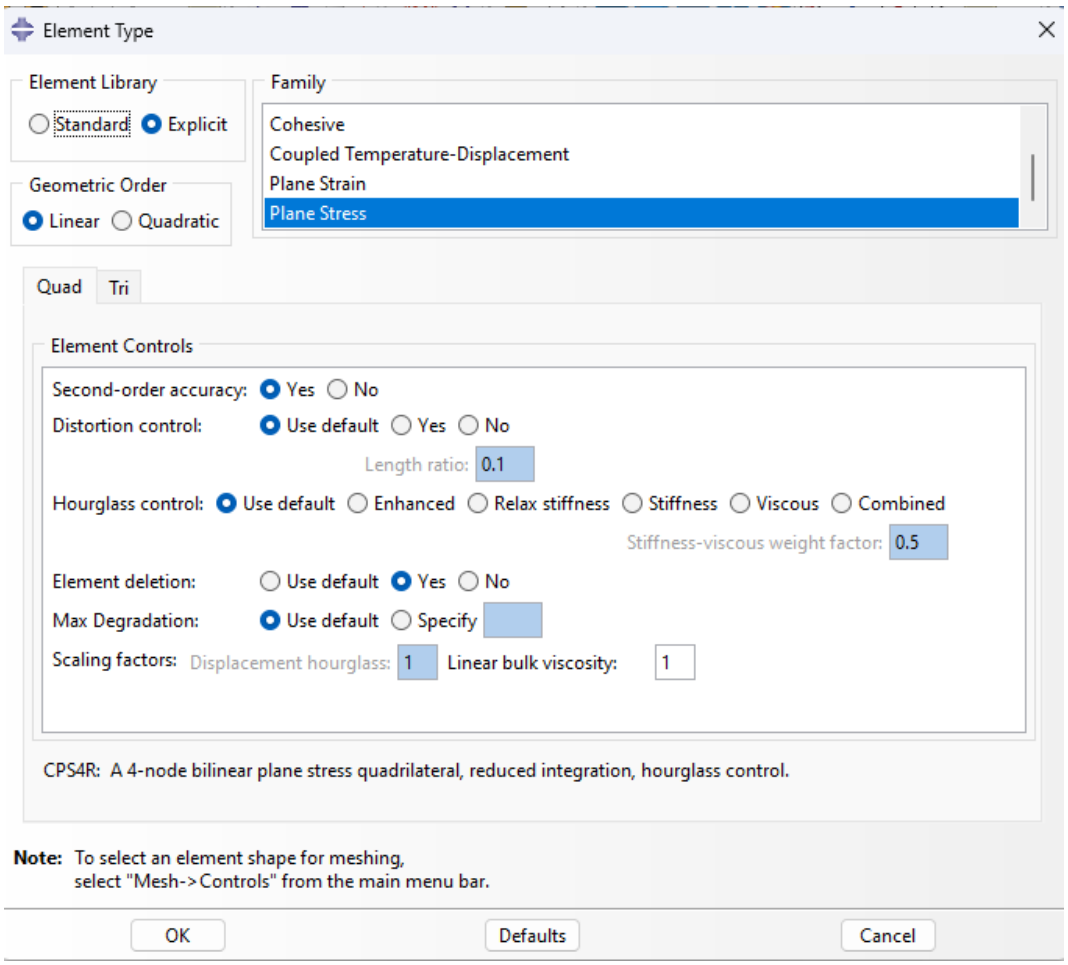

Figure 3.16 – Setup of element type for the workpiece mesh.

3.5.1 Mesh convergence

The values of output parameters supplied by the software can vary depending on the level of discretization, especially the discretization of the workpiece rather than the tool. However, if the number of elements is too elevated, the solution can become highly time-consuming, with high computational cost, which can cause the solution to diverge. Therefore, a mesh convergence analysis was conducted so as to determine the mesh that provides the most accurate results within a relatively short CPU time. Thus, this analysis aims at finding the roughest mesh which leads to stabilization of one or more parameters. For the tool with radius of 1 μm and a feed per tooth of 2.5 μm, the simulation was conducted with five different meshes. The maximum value of von Mises stress at the third frame was used as stabilization indicator. As shown in figure 3.17, the values of stress tend to converge to values close to each other as the number of elements increase.

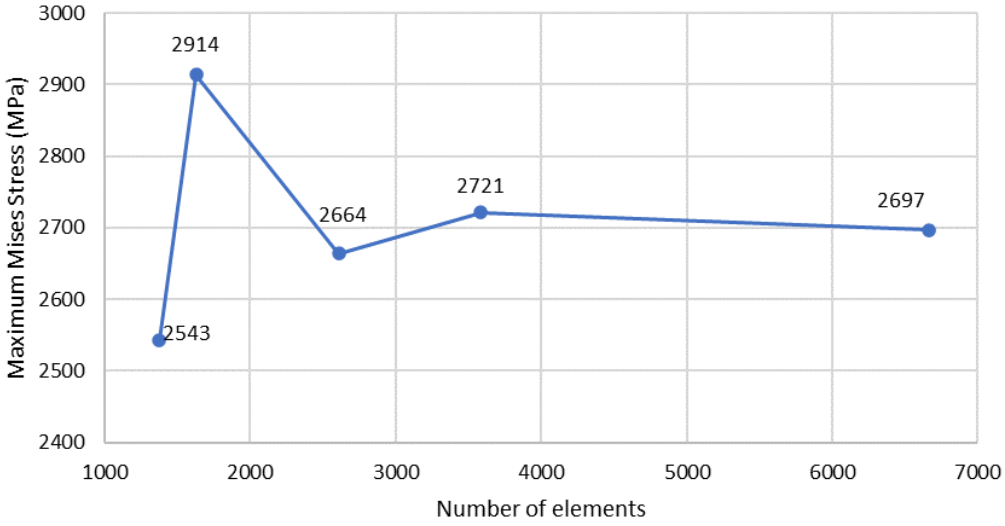

Figure 3.17 – Maximum von Mises stress as a function of number of nodes.

For the tool with radius 1 μm, for example, the mesh that was chosen as the standard for the other simulations is the fifth mesh from figure 3.17, which has 6662 elements and provided 2697 MPa as the maximum von Mises stress at the third frame. With this mesh, the total simulation time taken by the CPU was approximately 100 minutes. A mesh with more elements than that would probably have taken too much unnecessary CPU time, without considerable difference in the output values. Another similar study was carried out for the tool with edge radius 5 μm. The number of elements for the meshes of tool and workpiece used in the final analysis are shown in table 2. The use of other meshes would probably have led to similar values of output parameters, as far as the order of magnitude of the number of elements is similar to the ones presented in table 2.

Table 2 – Discretization parameters.

Instance		**Number of elements**
Edge radius 1 μm	Workpiece	6662
	Cutting tool	49
Edge radius 5 μm	Workpiece	6667
	Cutting tool	56

3.6 Modeling of precipitates in the material matrix

As an extra analysis, a model to simulate the heterogeneity of the workpiece has been proposed. This model was created based on the problem of cutting force variations induced by the high hardness of precipitates of Inconel 718, considering that the small precipitates have a similar size scale as the edge radius of the microtool. In their work,

Filho et al. (2019) identified the presence of precipitates in the matrix of Inconel 718 using SEM electron mapping. It is possible to observe the precipitates (green) in a matrix of chromium (blue) with nickel (red) in the microscopy image obtained by the authors, as shown in figure 3.18. The authors observed that the micro-hardness of the precipitates was 897 HV, whereas the matrix hardness was 513 HV.

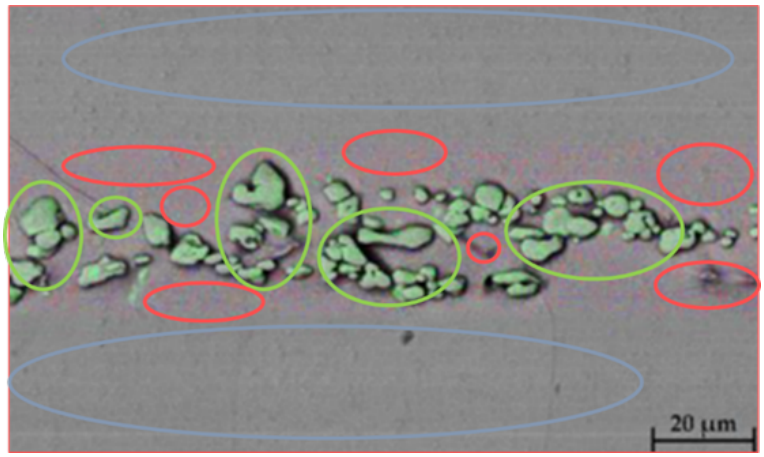

Figure 3.18 – SEM backscattered electron mapping identifying niobium (green) in the precipitates and chromium (blue) and nickel (red) in the matrix. Adapted from Filho et al. (2019).

In this sense, the proposed model to represent a heterogeneous material on Abaqus CAE consists in depicting "precipitates" as enclosed regions of the workpiece with higher Young modulus than the matrix. The workpiece was represented as red precipitates randomly distributed in the gray matrix, as shown in figure 3.19. To create this model, an extra material was created to be associated to the precipitates, with a Young modulus of 300000 MPa, as an attempt to represent the higher hardness, as observed experimentally by Filho et al. (2019). The only parameter of the properties of the precipitates that differ from the matrix is the Young modulus; all the other material parameters remained the same as shown in table 1. Simulations with the presence of precipitates were conducted after the other simulations were completed on the homogeneous workpiece material (without precipitates), with the objective of analyzing if there would be any considerable difference in chip morphology and cutting forces. All the other steps for developing the heterogeneous model were analogous to those presented in subsections 3.3 to 3.5.

Figure 3.19 – Modeling of precipitates (red, Young modulus 300 GPa) in the workpiece matrix (gray, Young modulus 185 GPa).

3.7 Jobs

On Abaqus CAE, the simulation of the machining process itself and calculation of the output parameters is done in different "jobs". Each job represents one simulation with one set of machining parameters. The parameter that was varied for each job was the feed per tooth, aside from the cutting edge radius of the tools. Therefore, for each job, the position of the tool in the assembly was modified so as to simulate different values of f_z. The values of f_z were measured using the vertical distance between the top edge of the workpiece and the lowest point of the tool, which were used as references, as shown in figure 3.20.

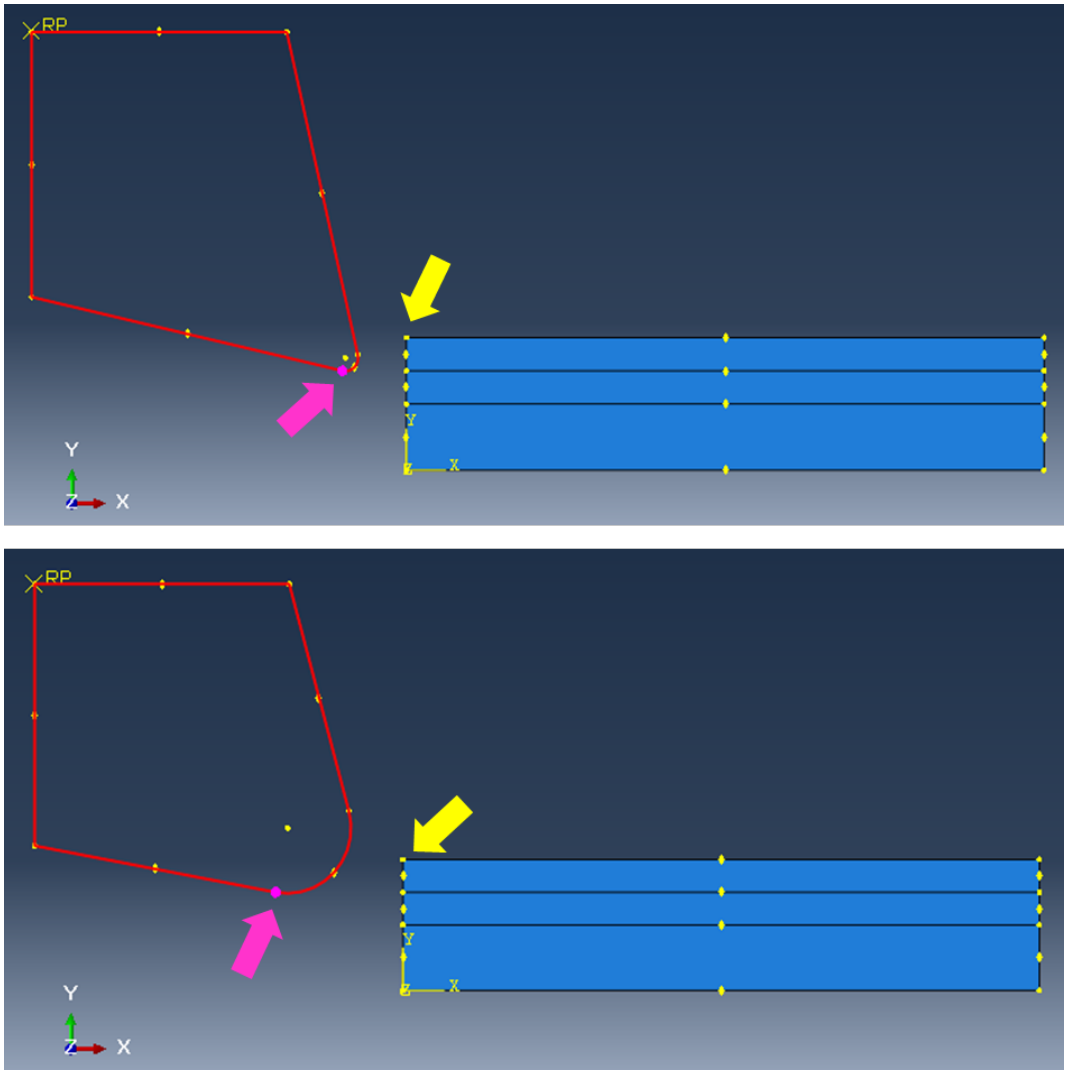

Figure 3.20 – Methodology for varying f_z: the Y coordinates of the points indicated by the pink and yellow arrows were used as references.

Finally, the machining parameters used in all the simulations carried out are shown in table 3, considering the homogeneous workpiece (without hard precipitates) and heterogeneous workpiece (with hard precipitates).

Table 3 – Machining parameters used in the numerical simulations.

Parameter	**Value**	**Symbol**
Cutting speed	6 m/min	v_c
Depth of cut	30 μm	a_p
Cutting length	50 μm	L
Feed per tooth ($r_e = 1$ μm, homogeneous workpiece)	0.5 μm	f_z
	1.0 μm	
	2.5 μm	
Feed per tooth ($r_e = 5$ μm, homogeneous workpiece)	1.0 μm	
	2.5 μm	
	4.0 μm	
Feed per tooth ($r_e = 1$ μm, heterogeneous workpiece)	2.5 μm	
Feed per tooth ($r_e = 5$ μm, heterogeneous workpiece)	7.0 μm	

4 Numerical results

4.1 Homogeneous workpiece

4.1.1 Chip formation and Mises stress concentration

For each job of the simulation, images of the tool-workpiece interface were taken at different instants of the machining process. Figures 4.1, 4.2 and 4.3 show the numerical results for machining times of 7×10^{-5} s, 3.15×10^{-4} s and 7×10^{-4} s, respectively. The distributions of von Mises stress in MPa are highlighted through the color gradients. It is possible to observe that the response of the workpiece differs according to the feed per tooth and the radius of the cutting tool.

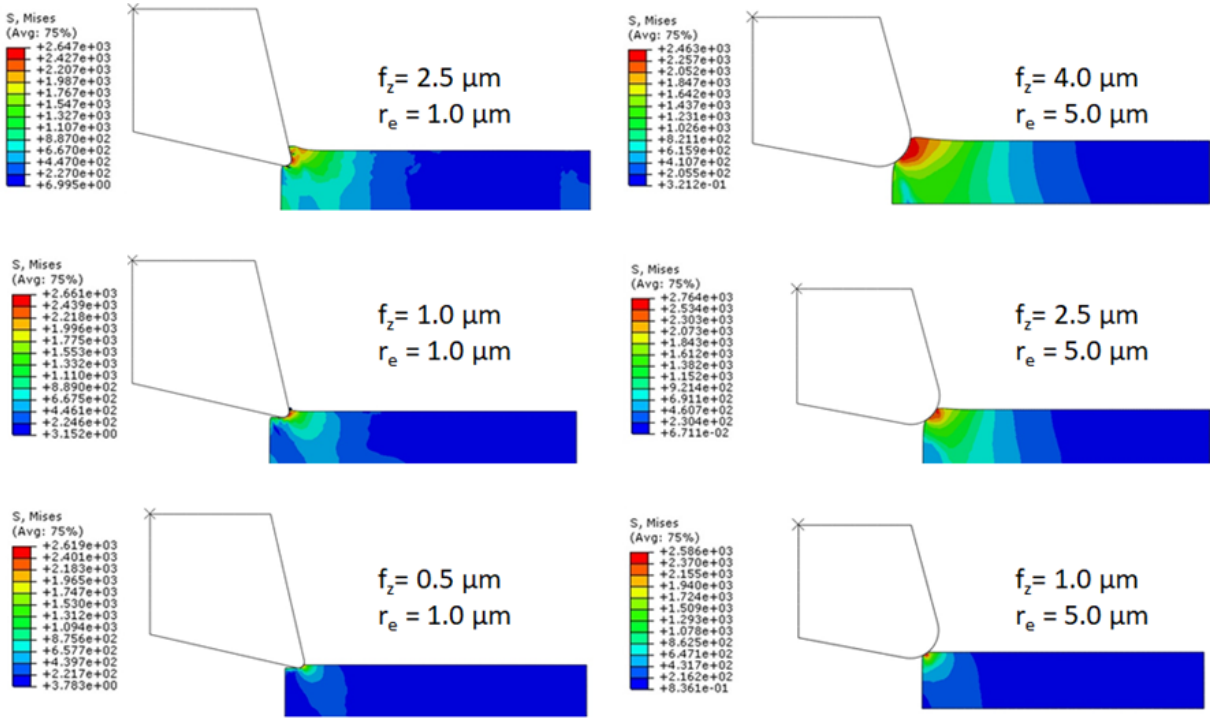

Figure 4.1 – Von Mises stress distribution (machining time: 7×10^{-5} s).

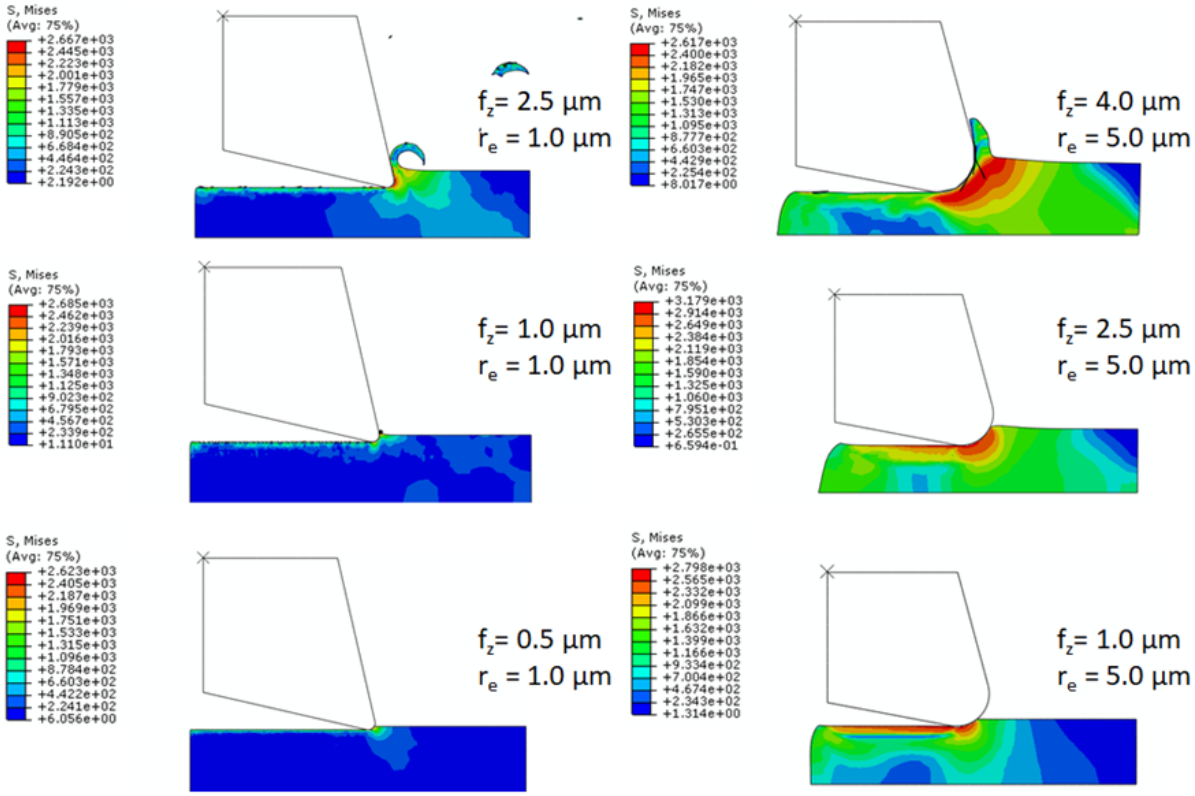

Figure 4.2 – Von Mises stress distribution (machining time: 3.15×10^{-4} s).

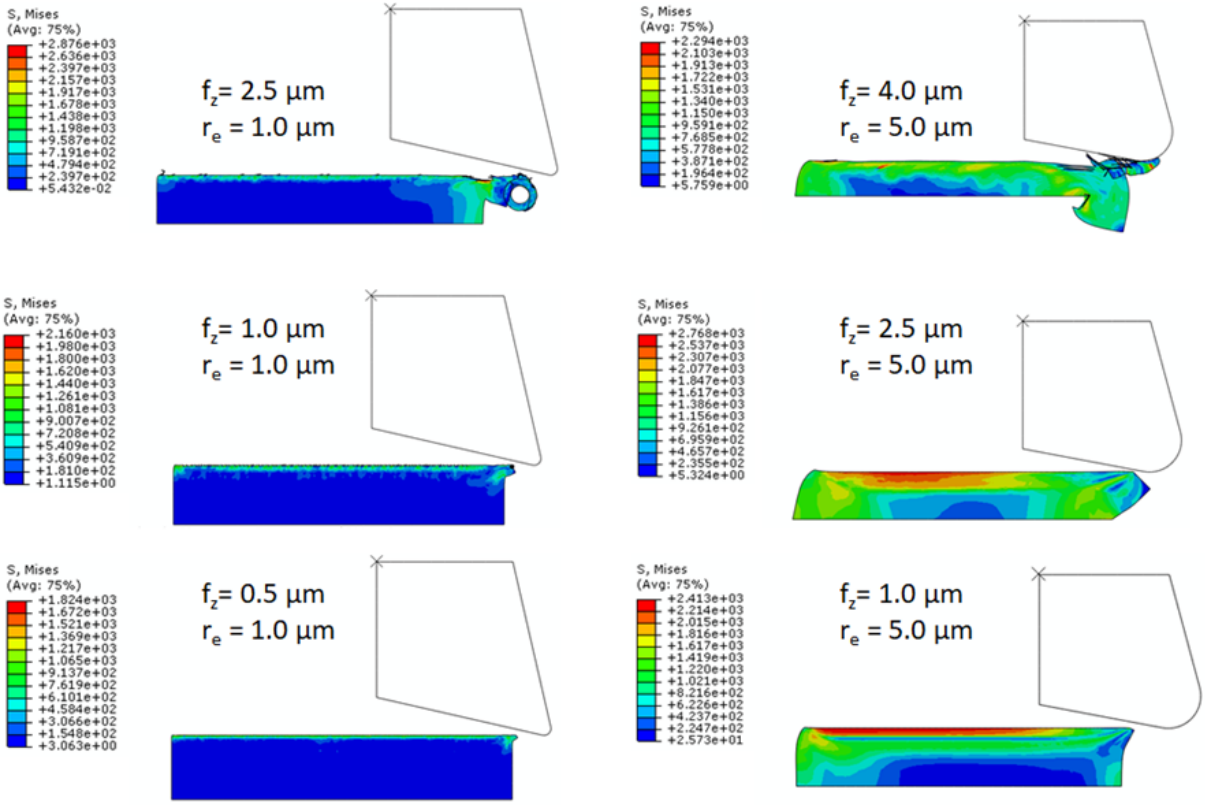

Figure 4.3 – Von Mises stress distribution (machining time: 7×10^{-4} s).

From figures 4.1 to 4.3, considering the tool with $r_e = 1$ μm, a chip begins to be formed for $f_z = 2.5$ μm, however, as the tool advances towards the right extremity of the

workpiece, the chip is not completely sheared and it remains accumulated as a spiral burr. For $f_z = 1$ μm - the same value as the cutting-edge radius - there is a thin layer of finite elements that are deleted in the region of immediate contact with the tool, meaning that the failure criterion was triggered because of excessive deformation of these elements. As for $f_z = 0.5$ μm, the tool barely touches the surface of the workpiece because the feed per tooth is roughly the same size as the elements of the piece, so the layer of elements in the interface zone is distinctly thin. Therefore, most of the elements closest to the surface are deleted.

Considering the rounded tool, with edge radius 5 μm, it is remarkable how much chip formation is hindered by size effect. For $f_z = 4$ μm, there is a initial stage of chip formation, however there is intense accumulation of plastic strain and a large amount of material is bent over the fixed edge at the right corner of the workpiece, in such a way that no material at all is sheared and removed in the form of chip. Finally, both simulations with $f_z = 2.5$ μm and $f_z = 1$ μm presented similar behavior: there is no element deletion and the elements closest to the surface of the workpiece are compressed beneath the cutting-edge. So, these elements remain as a thick layer of plastically deformed material with high residual stresses.

In general, the residual stresses generated by the rounded tool were higher than those produced by the sharper tool. For example, for $f_z = 1$ μm, at the end of the simulation, the rounded tool caused a maximum von Mises stress of 2413 MPa, which is 11.7% higher than the equivalent value on the workpiece produced by the sharper tool, 2160 MPa. This tendency of Inconel 718 to deform during micromilling has been reported in different experimental works. De Oliveira et al. (2021) performed micromilling in this superalloy with a 400 μm diameter microtool, coated with N(Ti, Al), with feed per tooth of 5 μm. The authors used a cutting speed of 25 m/min, which is still considered a low cutting velocity even though it is higher than the value used in the present study. For machining in dry condition, the authors identified portions of plastically deformed material that were not removed as chips and remained attached in the machined surface. In another work of micromilling of Inconel 718, De Oliveira et al. (2020) also noticed the presence of material adhered to the bottom of the micro slots. The authors varied the fluid rate application within the machined slots, identifying a clear contrast between the regions machined with different cutting fluid rates. The authors applied the cutting fluid by pulses, so the use of lower fluid rates led to a smaller amount of fluid and a fewer number of pulses per minute, resulting in some regions of the slot being machined with less lubrication than others. The regions fabricated with less lubrication, which are the machined length between pulses of fluid, are easily identified by the presence of adhered material, which are absent in the regions with abundant lubrication.

An important aspect that has been found to affect chip formation in the FEM simulations is the discretization of the instances. The tool with smaller edge radius requires a finer discretization so as to avoid excessive element distortion on the workpiece elements.

In other words, there might be an element that is big enough to remain attached on the workpiece during machining with the rounded tool; however this same element may be deleted when the sharp tool is used instead. This phenomenon is also influenced by the limit of deformation at fracture that activates the deletion criterion, which is the reason why this value of displacement at fracture should be changed in the properties of the workpiece material according to the edge radius of the tool. If the displacement at fracture is too small, all the elements may simply vanish when the tool touches them, making it impossible to visualize any chip at all. If the displacement at fracture is too large, on the other hand, the elements may remain exaggeratedly distorted, which can cause errors and lead to abortion of the simulation.

Different responses could be observed in the simulations regarding the minimum chip thickness (MUCT), depending on the cutting edge radius. For the sharp tool, even with a feed per tooth of 0.5 μm, no chip formation was detected. Since most of the elements simply disappeared because of the deletion criterion, it is not clear from the simulation whether these cutting parameters would result in chip formation or not in a real machining experiment. This indicates that the value of MUCT for these machining parameters may be equal or smaller than 0.5 μm. This value is within an expected range, considering that it corresponds to one half of the radius of the cutting tool and this ratio is supposed to be at least one third, according to Oliveira et al. (2015). A simulation with a feed per tooth smaller than 0.5 μm would be unrealistic and difficult to implement, for two main reasons: firstly, it would require an extremely refined discretization of the workpiece, which would drastically increase computational cost; and the use of this value would represent a very low productivity rate, increasing the machining time and the production costs. On the other hand, for the rounded tool, it is plausible to conclude that the value of MUCT found in the simulations is between 2.5 μm and 4 μm. This is greater than the ratio of the cutting-edge radius expected for a novel tool, however a radius of 5 μm can represent considerable tool wear, which is often reported to cause deterioration of surface quality.

4.1.2 Accumulated plastic strain

As the cutting tool advances, some elements of the workpiece are subjected to high levels of plastic strain, even when this strain is not high enough to activate the deletion criterion. So, some parts of the elements of the workpiece remain with a layer of elements that suffered accumulated plastic strain. This layer is considerably thicker when the cutting edge radius is greater, as observed in figure 4.4. For $f_z = 2.5$ μm, the rounded tool generated a maximum accumulated plastic strain of 2.853, whereas the sharp tool generated 2.003, representing an increase of 42.4%.

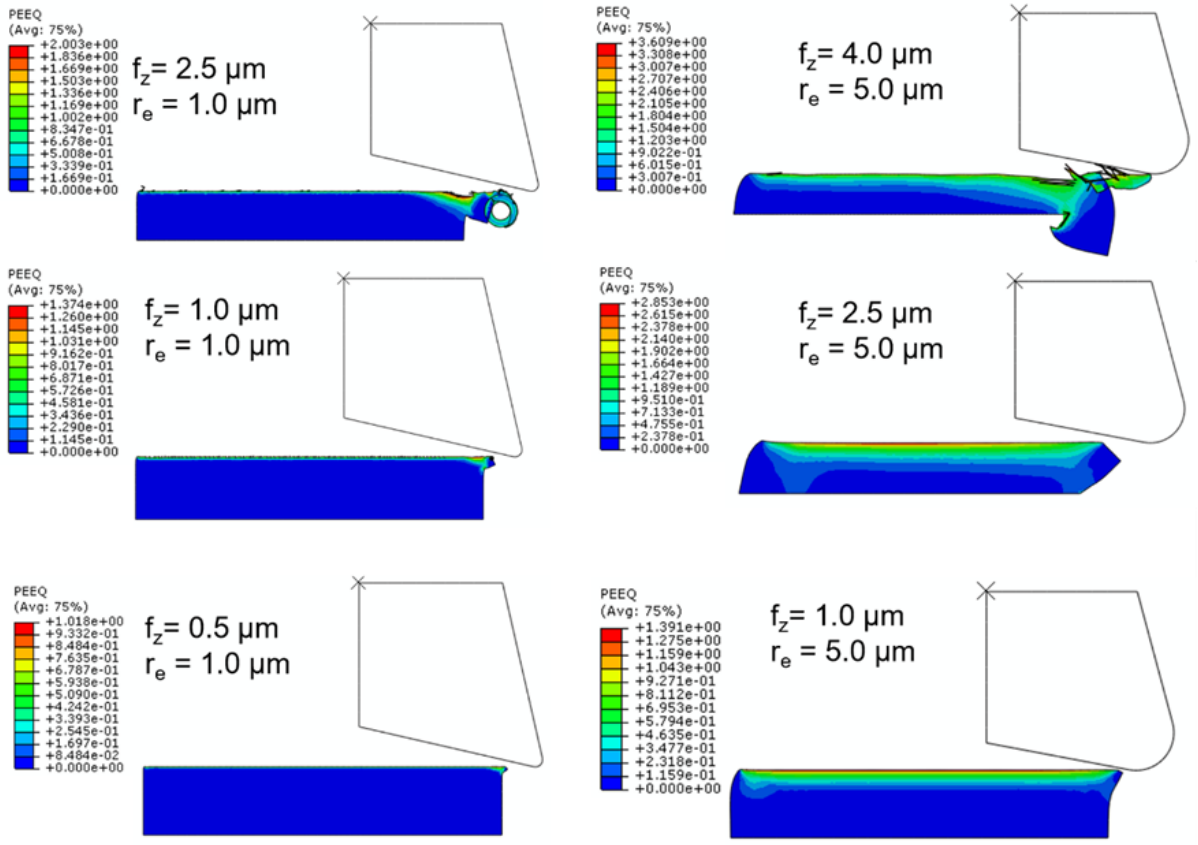

Figure 4.4 – Equivalent plastic strain distribution.

The layer of plastically deformed elements is an indication of poor surface quality, with portions of uncut material remaining in the machined surface, as observed in experimental works (OLIVEIRA; GOMES; SILVA, 2020); (OLIVEIRA et al., 2021). This evidences that the tool with radius of 5 μm causes more plowing, and consequently, worse surface quality than the sharper tool. The plastically deformed material remaining on the machined surface presents degradation of its mechanical properties, which is due to the elongation of microscopic voids in the material (MALCHER; PIRES; SÁ, 2012). The deformed material is more fragile and therefore more likely to present cracks and other defects, because of the work hardening effect.

Figure 4.4 also shows that the accumulated plastic strain increases for higher values of feed per tooth. For the rounded tool, the maximum value of accumulated plastic strain varied from 3.609 to 1.391 when the feed per tooth varied from 4.0 μm to 1.0 μm, representing an increase of 259.2%. Performing a similar analysis for the sharp tool, the increase in feed per tooth caused an increase of 196.8% in accumulated plastic strain. This indicates that surface quality tends to become worse with increase in feed per tooth. This is in accordance to what is expected from literature. Lu et al. (2017) analyzed the surface quality of micro slots of Inconel 718 under different sets of machining parameters. The highest values of surface roughness R_a obtained by the authors (0.225 $\pm$ 0.006 μm) were obtained for the highest feed per tooth (1.1 μm). Feng et al. (2019) proposed an analytical model for the prediction of surface roughness under laser assisted end milling of Inconel

718. The authors also concluded that feed rate has critical influence on surface roughness, while axial depth of milling has a minor effect.

In their work, Meijer et al. (2022) used analytical methods to determine process forces and residual stresses on specimens obtained by micromilling of high speed steel (HSS). The authors' results indicate that micromilling allows the induction of high residual compressive stresses, which increase the component's service life. Higher residual stresses were induced by low values of depth of cut and feed per tooth, as well as the use of lubrication.

4.1.3 Cutting forces

The forces in the X direction, which is the same direction as the movement of the cutting tool, were monitored for all the simulations. For comparison reasons, the forces were plotted for $f_z = 2.5$ μm and $f_z = 1.0$ μm, because these were the values of feed per tooth common to both the sharp tool and the rounded tool. The results are shown in figures 4.5 and 4.6.

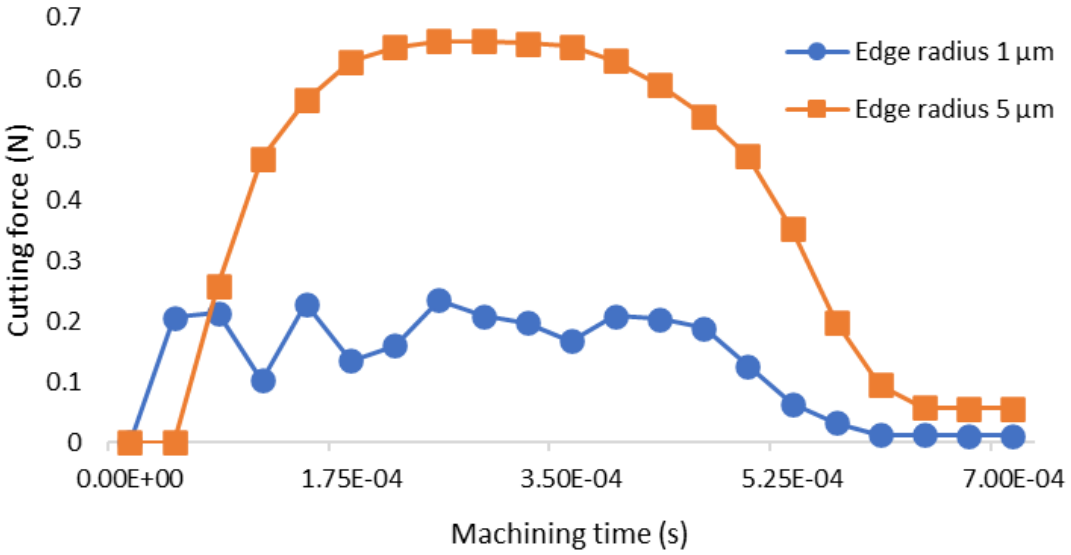

Figure 4.5 – Cutting forces for $f_z = 2.5$ μm.

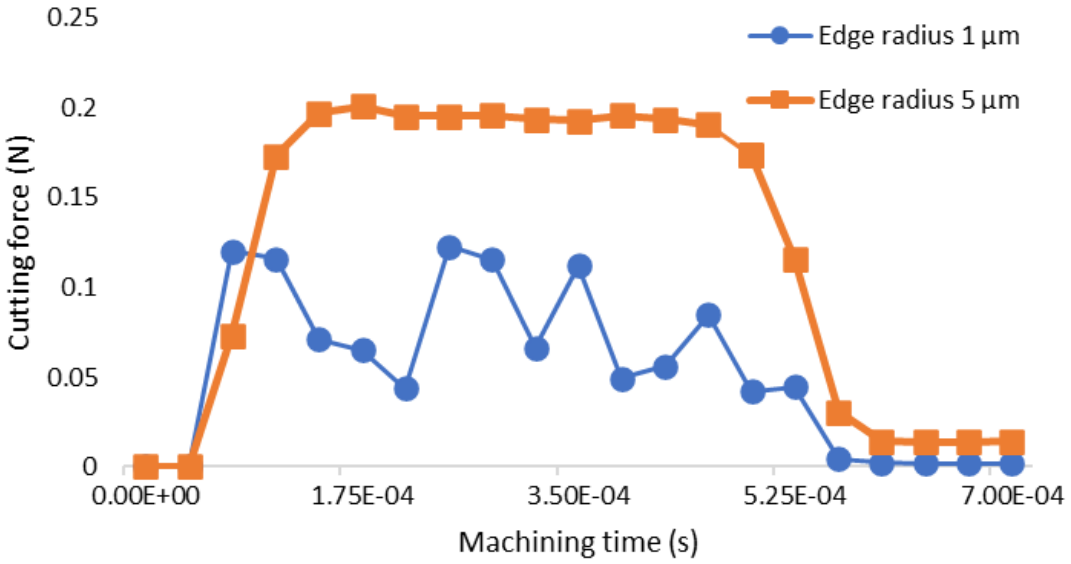

Figure 4.6 – Cutting forces for $f_z = 1.0$ μm.

Monitoring the forces that act on the flank face of cutting tools is of great importance in machining operations, because is allows the estimation of the necessary power consumption of the cutting machine (SILVA; OLIVEIRA; MALCHER, 2023). Figure 4.5 shows that, for $f_z = 2.5$ μm, the maximum values of cutting force for the rounded tool are roughly three times bigger than the equivalent values for the sharp tool. For $f_z = 1.0$ μm, the difference between the peaks of force for both tools is also remarkable. So, it is perceptible that the tool with larger cutting-edge radius causes a significant increase in the cutting forces in comparison with the sharp tool. This phenomenon is owing to size effect, which increases the specific cutting energy. In micromachining, a large amount of energy is wasted deforming the material rather than shearing it, so that the rate of energy per volume of removed material is higher than in conventional machining (LIU; MELKOTE, 2007). Therefore, the numerical simulations show that the use of the rounded tool leads to more energy consumption than the sharp tool.

4.2 Heterogeneous workpiece

The workpieces depicted with hard precipitates were used to analyze the effects of heterogeneity of the material in chip formation, as discussed in section 3.6. The results of chip formation and von Mises stress distribution for the heterogeneous workpieces are shown in figure 4.7.

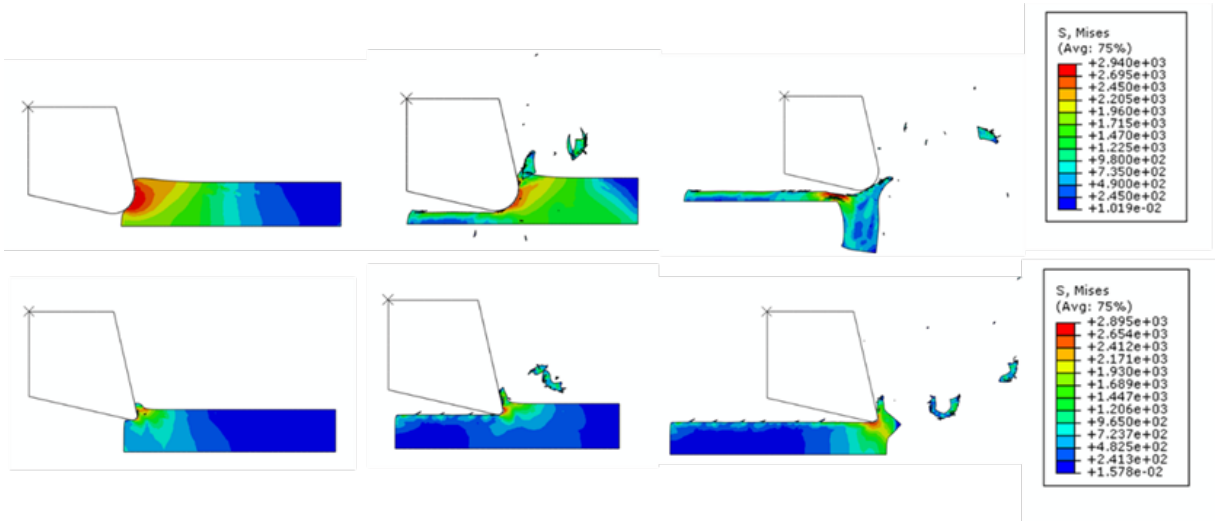

Figure 4.7 – Chip formation for the workpieces with hard precipitates.

Figure 4.7 shows that the presence of hard precipitates led to the formation of brittle chips that were segmented into multiple smaller pieces, which contrasts with the continuous chips obtained from the previous simulations with homogeneous material. Some fragments of the brittle chips were even swept away from the field of view. This patter is expected due to the higher value of Young modulus of the precipitates, which causes the material to become less ductile than the matrix. In the lower section of the workpiece, located further away from the precipitates, there is a greater inclination for the material to bend over and create burrs, which can be interpreted as less ductility. Thepsonthi and Özel (2016) also observed the presence of segmented chip in contrast with continuous chips in FEM simulation of micromachining, attributing the segmented chips to the use of elasto-viscoplastic material assumption.

The cutting forces obtained for the heterogeneous workpiece are shown in figure 4.8. When the cutting tool happens to pass through precipitates with considerably different hardness than the matrix, it may encounter peaks of force that can increase tool vibration. This problem is a particular concern when the radius of the tool has the same size scale as the grains of the workpiece material, leading dislocations to continually nucleate and pile up at grain boundaries, creating repetitive regions of work hardened material (LIU et al., 2017). It is possible to observe from figure 4.8 that the presence of hard precipitates caused higher variations in cutting force through the machined length, with the occurring of irregular peaks. Besides, for the radius of 1 μm, the average forces exerted on the tool throughout the entire machined length are greater than for the radius of 5 μm. This occurs because the material underneath the cutting edge is more prone to being compressed rather than flowing along the flank face. This observation further indicates that chip formation is negatively affected by the rounded tool.

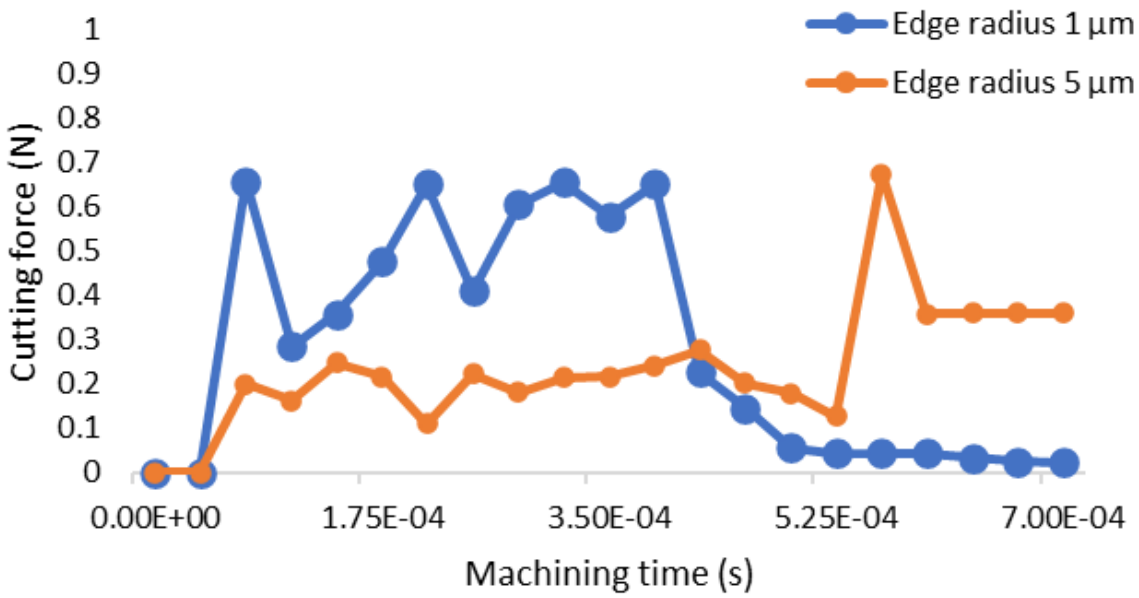

Figure 4.8 – Cutting forces for the heterogeneous workpiece.

5 Experimental methodology

5.1 Material characterization

The micromilling experiments were performed on two samples, sample 1 and sample 2, of age-hardened Inconel 718. The composition of the material was obtained by Oliveira (2019) and compared to the composition provided in the literature by Reed (2006), as observed in table 4. The mechanical properties of the material are shown in table 5. Both samples consisted in blocks of Inconel 718 with dimensions 15 mm × 15 mm × 20 mm.

Table 4 – Chemical composition of Inconel 718. Adapted from Oliveira (2019).

Element	**Mass percentage obtained by Oliveira (2019)**	**Mass percentage according to Reed (2006)**
Carbon	5.588%	0.040%
Aluminum	0.497%	0.500%
Titanium	0.860%	0.900%
Chrome	16.899%	19.000%
Iron	19.079%	18.500%
Nickel	49.000%	50.660%
Niobium	4.582%	5.100%
Molybdenum	3.495%	5.300%

Table 5 – Mechanical properties of Inconel 718 (OLIVEIRA, 2019).

Tensile Strength (MPa)	1275
Yiel Strength (MPa)	1034
Young's Modulus (GPa)	200
Hardness (HRC)	40
Density at room temperature (g/cm^3)	8.22
Melting range (ºC)	1260 - 1336
Thermal conductivity (W/mK)	11.4

5.2 Microtool

In both samples, the trials consisted in manufacturing slots on the upper surface using micro-end mills. The micromills were fabricated with tungsten carbide and coated with (Al,Ti)N, with two flutes, diameter of 400 μm and cutting-edge radius 1.1 $\pm$ 0.1 μm. The dimensions of the cutting tool, in mm, are shown in figure 5.1. One microtool was used for each sample.

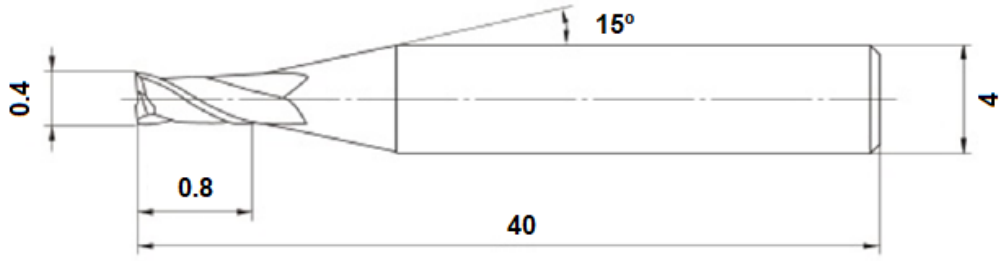

Figure 5.1 – Dimensions in mm of the microtool used in the machining trials.

5.3 Machine tools

The trials were conducted in two different machine tools, one for each sample. The main objective was to compare the performance of the machine tools through the surface quality of the slots produced by them.

The slots on sample 1 were manufactured using the micromilling machine CNC Mini-mill/GX by Minitech Machinery Corporation, shown in figure 5.2. This machine has maximum feed speed of 1000 mm/min, maximum rotation of 60,000 rpm and positioning resolution of 0.1 μm for each axis. The micromilling table has a length of 490 mm and a width of 154 mm. This machine has reduced dimensions, which are appropriate for micromachining, with the X, Y and Z axes having maximum offsets of 300 mm, 228 mm and 228 mm, respectively. To guarantee rigidity to the system, the machine was installed on a granite base. The trials of sample 1 were conducted at the Laboratory of Research in Machining (*Laboratório de Ensino e Pesquisa em Usinagem* - LEPU) of the Federal University of Uberlândia, Brazil.

Figure 5.2 – Machine tool used in sample 1: CNC Mini-mill/GX.

The machine tool used in sample 2 was the CNC machine VEGA XH7132 by McLane, at the Machining Laboratory of the University of Brasília, figure 5.3. This machine can be used for conventional milling as well as micromilling, so its dimensions are considerably bigger than the machine used in sample 1. The maximum offsets are 620 mm, 350 mm and 500 mm for axis X, Y and Z, respectively. The maximum spindle rotation is 6,000 rpm and the maximum feed speed is 3000 mm/min.

Figure 5.3 – Machine tool used in sample 2: CNC VEGA XH7132.

5.4 Experimental configuration and machining parameters

5.4.1 Sample 1

On sample 1, twelve microslots were fabricated. The spindle speed of the tool was 5,000 rpm and the depth of cut a_p was 10 μm, both these parameters were kept constant for all slots. All slots were fabricated without lubrication (dry machining). The only parameter that was varied was the feed per tooth f_z. Four values of f_z were used: 4.0 μm, 2.0 μm, 1.0 μm and 0.5 μm. These values were used, respectively, in slots 1 through 4 (test 1), slots 5 through 8 (test 2) and, finally, slots 9 through 12 (test 3). The machining parameters are shown in table 6.

Table 6 – Machining parameters used in sample 1.

n (rpm)	Lubrication condition	a_p (μm)	**test 1**		**test 2**		**test 3**	
			slot	f_z (μm)	slot	f_z (μm)	slot	f_z (μm)
5,000	Dry machining	10	1	4.0	5	4.0	9	4.0
			2	2.5	6	2.5	10	2.0
			3	1.0	7	1.0	11	1.0
			4	0.5	8	0.5	12	0.5

5.4.1.1 Cutting forces acquisition

The cutting forces of sample 1 were acquired using a Kistler dynamometer, model 9257b. This dynamometer has an operating range of -5 kN to +10 kN and its sensitivity is adjustable, being recommended to 0.02 N. The forces were measured in the X direction, which is the most significant component that acts on the tool.

After the signals were generated, they passed through a Kistler 5405A distribution box, later through a Kistler conditioner/amplifier, model 504E, and then converted (analogue to digital) by a National Instruments board, NI USB-66221, with 16 bits. The signals were acquired using the LabVIEW software with a frequency of 10 kHz, to achieve an adequate trade-off between the quality of the signal and its intensity. Subsequently, the signals were treated and analyzed using the MATLAB software.

In order to guarantee rigidity to the system, the sample was fixed on a clamping vise, on a fixing plate. The experimental configuration of sample 1 was the same as in the work of Gomes (2022), as shown in figure 5.4.

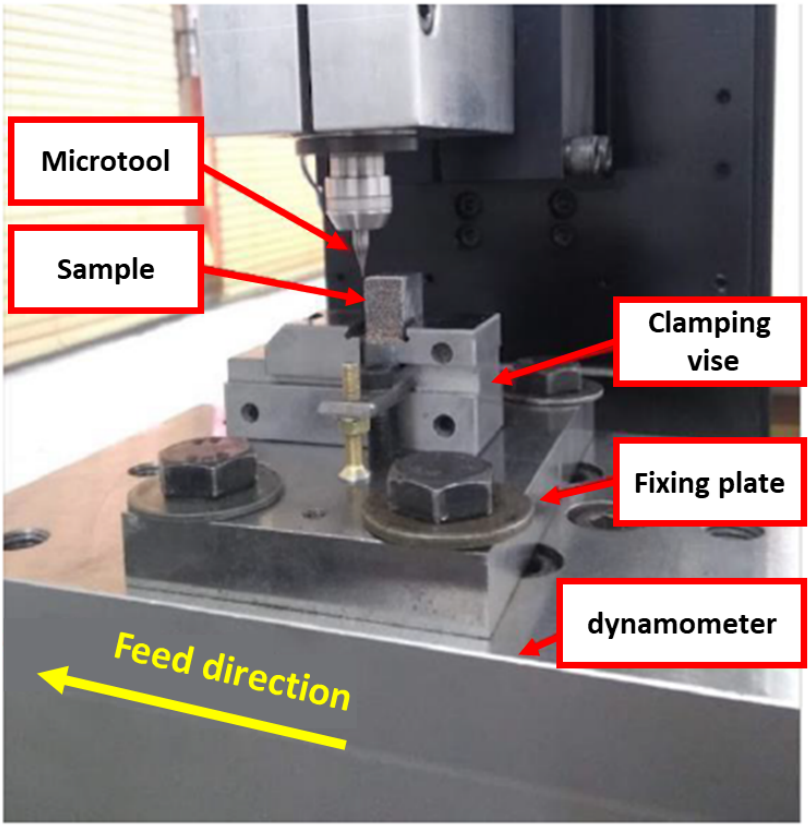

Figure 5.4 – Configuration of sample 1. Adapted from Gomes (2022).

5.4.2 Sample 2

For sample 2, the machining parameters were slightly different from sample 1. The values of f_z, once again, varied between 4.0 μm, 2.0 μm, 1.0 μm and 0.5 μm. The first 12 slots were fabricated under flood lubrication. The depth of cut also varied, it was set

initially at 40 μm and it decreased 10 μm every four slots. Finally, from slot 13 on, the same parameters were repeated, without lubrication this time. Higher values of depth of cut were used in sample 2 to contrast with the fixed value of 10 μm used in sample 1. Besides, it is expected that the variation of a_p results in different levels of surface quality on the machined piece (SILVA; SILVA; OLIVEIRA, 2023). The machining parameters used in sample 2 are shown in table 7.

Table 7 – Machining parameters used in sample 2.

Slot	f_z (μm)	a_p (μm)	Lubrication condition	n (rpm)
1	4.0	40	Flood (5.88 l/min)	5,000
2	2.5			
3	1.0			
4	0.5			
5	4.0	30		
6	2.5			
7	1.0			
8	0.5			
9	4.0	20		
10	2.5			
11	1.0			
12	0.5			
13	4.0	40	Dry machining	
14	2.5			
15	1.0			
16	0.5			
17	4.0	30		

5.4.2.1 Cutting fluid application

For sample 2, lubricated condition was used in the first 12 slots in order to avoid excessive cutting forces, considering that the depth of cut was higher than in sample 1. It was reported in the work of Oliveira (2019) that the depth of cut of 40 μm in dry micromilling of Inconel 718 generates excessive tool wear rates, so the use of cutting fluid is recommended. From slot 13 on, it was intended to replicate the machining conditions of the first slots without lubrication, in order to validate this theory.

The cutting fluid used in the machining tests with lubrication was the biodegradable synthetic soluble fluid BIO100E from Biolub. It is a synthetic soluble oil that has excellent durability, excellent washing and anti-corrosive potential. The fluid must be diluted in water in a proportion of 5%. The fluid was applied at a flow rate of 5.88 l/min, which is the standard of the machine tool and is considered flood lubrication for the micromilling operations. The sample was fixed on a clamping vise, which was attached to the machine tool

with bolts and nuts. The fluid was injected on by means of two nozzles. The experimental configuration of sample 2 is shown in figure 5.5.

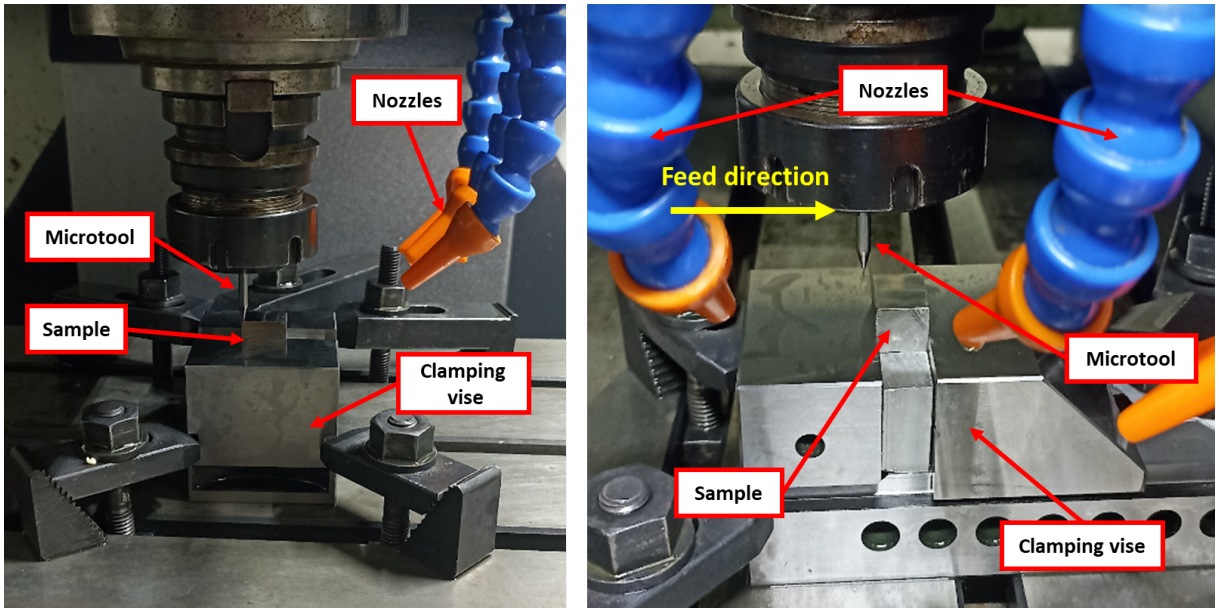

Figure 5.5 – Configuration of sample 2: frontal view (left) and side view (right).

5.5 Microscopy analysis

After the manufacture of the microslots, the samples were observed using two different microscopes. Through the microscopy operations, a qualitative analysis of the slots was performed and output variables were obtained. Before submitting the workpieces to the microscopy operations, they were cleaned in an ultrasonic device with ethanol (C_2H_6O) to avoid contamination.

5.5.1 Laser scanning confocal microscope

Microscopy images were obtained using the laser scanning confocal microscope Olympus Lext OLS4100 (figure 5.6). Besides, this microscope was used to measure the surface roughness and the topography of the samples, so as to obtain values of burr height, depth and width of the microslots.

Figure 5.6 – Laser scanning confocal microscope Olympus Lext OLS4100.

The width and depth of the slots, as well as the burr heights, were measured using reference lines that could be manually controlled on the microscopy images, as indicated by the red arrows in figure 5.7. It is important to highlight that this methodology, which is the same used in the work of Silva, Silva and Oliveira (2023), was used in the present work because there is no standardization for measuring features obtained by micromilling. All measurements were taken at a controlled room temperature of 24.0 ± 1.0 ºC. The instruments and workpiece had been kept at this temperature prior to the measurements. Each of the values of width, depth and burr height was calculated as the arithmetic mean value of three measurements obtained at different inspection planes in each slot. The standard deviations of these values were shown as error bars when representing the data graphically. The laser microscope was also used to measure the surface roughness of the bottom of the slots, using Gauss filter with cut-off 800 μm and sampling length n = 5. The values of surface roughness were measured three times on each slot. The mean values and standard deviations were registered. All mean values and standard deviations were calculated with a confident interval of 95.45%. both for the dimensions of the slots and the surface roughness.

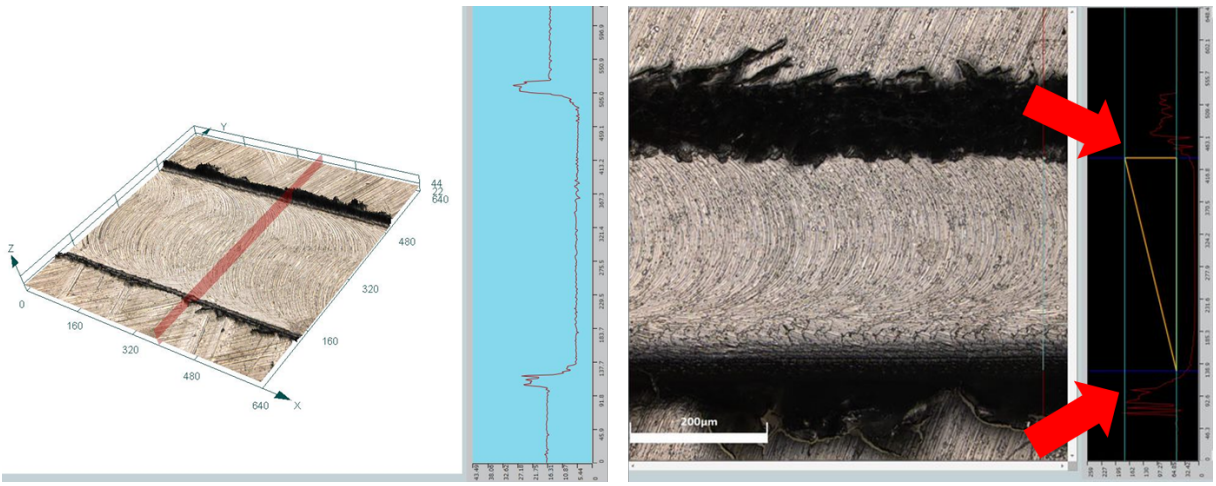

Figure 5.7 – Methodology for measuring the topography of the microslots.

5.5.2 Scanning electron microscope

Microscopy images of the microslots were also obtained using a field emission scanning electron microscope (SEM), model JSM-7100F, shown in figure 5.8. The main justification for the use of a second microscope is that the SEM images tend to be clearer than the images obtained by laser microscopy, allowing the observation of the quality of the slots in further detail.

Figure 5.8 – Field emission scanning electron microscope JSM-7100F.

6 Experimental results

6.1 Surface roughness

The graphs of surface roughness R_a obtained in both samples are shown in figures 6.1 and 6.2. The surface roughness was measured three times on each slot, so that the mean values were displayed on the graphs, using confidence interval of 95.45%, using the standard deviations as error bars.

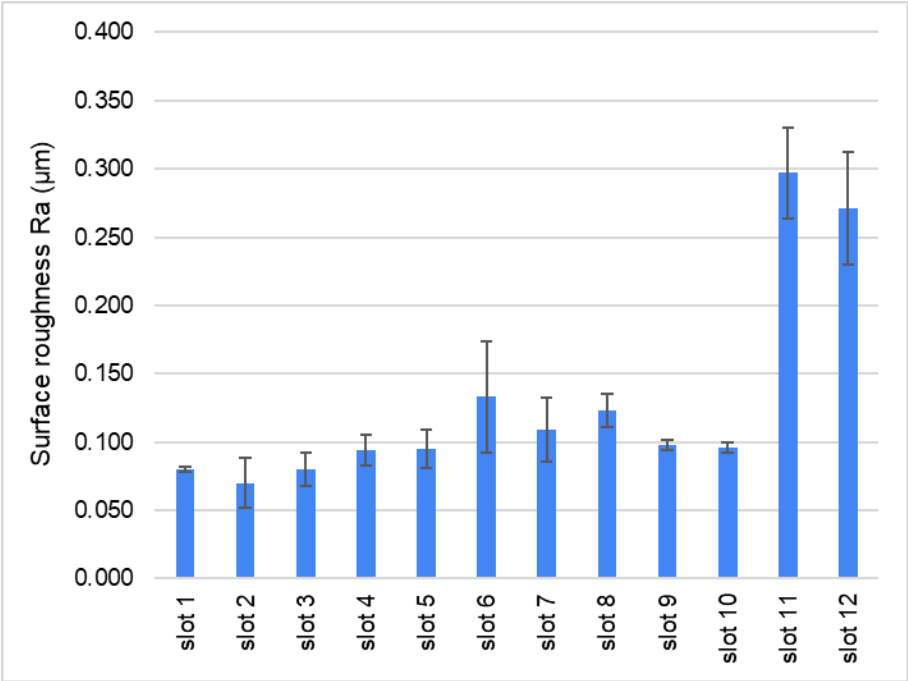

Figure 6.1 – Surface roughness of the microslots of sample 1.

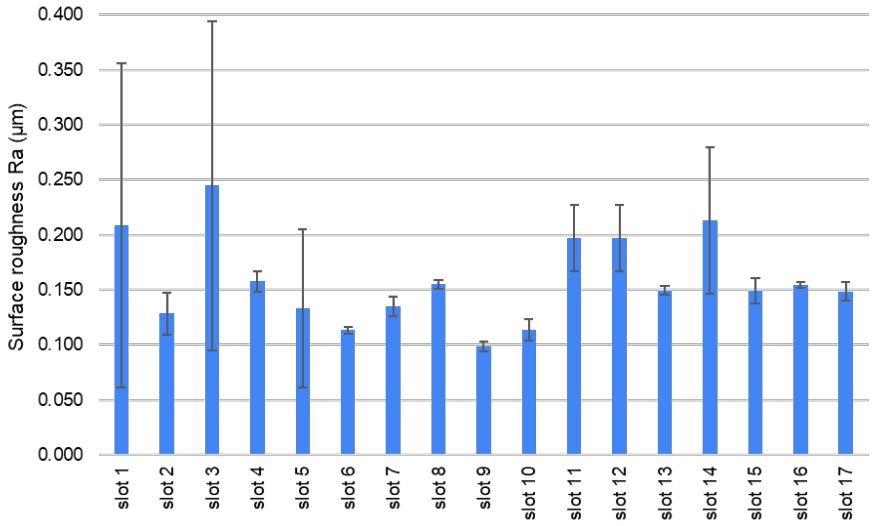

Figure 6.2 – Surface roughness of the microslots of sample 2.

It is possible to observe from figure 6.1 that, on sample 1, slots 1 through 10 presented relatively small values of R_a, all below 0.150 μm. However, this tendency changes abruptly in the last two slots, which presented R_a above 0.250 μm. This possibly indicates that there was some significant deterioration on the microtool when it passed from slot 10 to slot 11. The minimum value of R_a was 0.070 μm on slot 2 and the maximum was that of slot 11, with 0.297 μm. The abrupt change in the general surface condition from slot 10 to slot 11 can also be observed in figure 6.3, which shows that slot 11 has a great number of marks caused by chip adhesion, as highlighted by the red arrows, which are absent in slot 10.

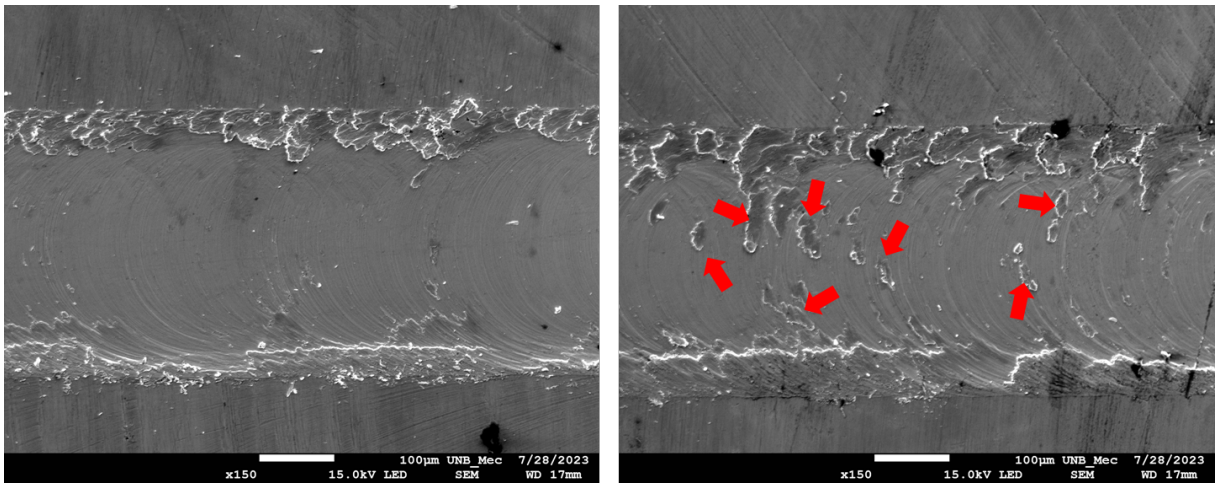

Figure 6.3 – Comparison of surface condition of slot 10 (left) and slot 11 (right) of sample 1.

As for sample 2, figure 6.2, the values of R_a are higher and more irregular, varying from 0.099 μm on slot 9 to 0.245 μm on slot 3. This result is not intuitive, considering that all slots on sample 1 were fabricated under dry machining while most slots of sample 2 was manufactured with lubrication, which should, in theory, generate less tool wear and better

surface quality. The standard deviations were also more remarkable in sample 2 than in sample 1, which indicates that, in general, the microslots on sample 1 were fabricated with more precision. However, it is important to highlight that the machine tool used in sample 1 has smaller dimensions and therefore provides more rigidity to the system, which explains the higher values of R_a and the higher standard deviations. Finally, the variation in the machining parameters between the slots, apparently, did not cause any detectable trend in the values of R_a in neither of the samples.

In general, the surface roughness obtained in the present work were low compared to those obtained by Aslantas and Çicek (2018). The authors, who micromilled Inconel 718 using TiCN-coated 600 μm tools, obtained mean values of R_a all greater than 0.200 μm, both for dry micromilling and MQL system. For flooding lubrication condition, the surface roughness values obtained by the authors were even higher, exceeding 0.400 μm. The authors argument that surface roughness tend to be lower when MQL system is used, because the oil and air spray in the cutting zone at a certain pressure causes rapid chip removal, while in the dry micromilling, chips are easily adhered to the freshly machined surface.

Another factor that can have led to the smaller values of surface roughness obtained in sample 1 is the depth of cut (a_p). All slots of sample 1 were fabricated with $a_p = 10$ μm, whereas in sample 2 a_p varied from 40 μm to 10 μm. This difference in the values of R_a according to the depth of cut can be observed, for example, by comparing the works of Aslantas and Çicek (2018), who used $a_p = 100$ μm, with Ziberov (2018), who used a_p of only 10 μm. This author obtained average R_a of 0.0145 μm for dry micromilling and 0.0099 μm for MQL micromilling of Ti-6Al-4V. Thus, smaller depth of cut can lead to smaller surface roughness of micromilled components. In the work of Brito et al. (2023), the authors compared machinability of austenitic stainless steel and Inconel 718, monitoring micromilling of these materials by means of vibration signals. By analyzing the vibration signals from each experiment, the authors observed that surface roughness is related to microtool wear, and its value increases with wear evolution and with higher cutting speed values.

From figures 6.1 and 6.2, the influence of the variation of the feed per tooth f_z on surface roughness is not completely clear. On sample 1, the highest values of R_a were obtained on slots 11, 12 and 6, which were machined with $f_z = 1.0$ μm, 0.5 μm and 2.5 μm, respectively. On sample 2, slots 1, 3 and 14 presented the highest values of R_a, having been fabricated with $f_z = 4.0$ μm, 1.0 μm and 2.5 μm, respectively. Although there are great variations on the values of R_a depending on f_z, all slots manufactured with $f_z = 0.5$ μm presented smaller values of R_a. Therefore, it is possible to conclude that, in general, the use of higher values of f_z led to worse surface quality. This result was also observed in the work of Gomes (2022). The author, who performed micromilling on stainless steel, obtained the following values of R_a: 0.150 μm for the microslots fabricated with $f_z =$ 5 μm; and 0.04 μm for the microslots fabricated with $f_z = 0.5$ μm. According to the

author, when higher values of f_z are used, there is higher tendency of formation of built-up edge, generating small burrs on the machined surface and consequently increasing surface roughness.

6.1.1 Chip adherence

The surface quality of the slots was deteriorated because of chip adherence, which was observed on the microslots of sample 1. The presence of chips adhered to the slots is more noticeable in the slots fabricated after higher machined length, for example slot 12, shown in figure 6.4. The phenomenon of chip adherence in machining of Inconel 718 using cemented carbide tools was also observed in the work of Liao, Lin and Wang (2008). According to these authors, an optimum cutting velocity should be reached for Inconel 718 to soften just enough so that the carbide tool maintains its cutting capacity.

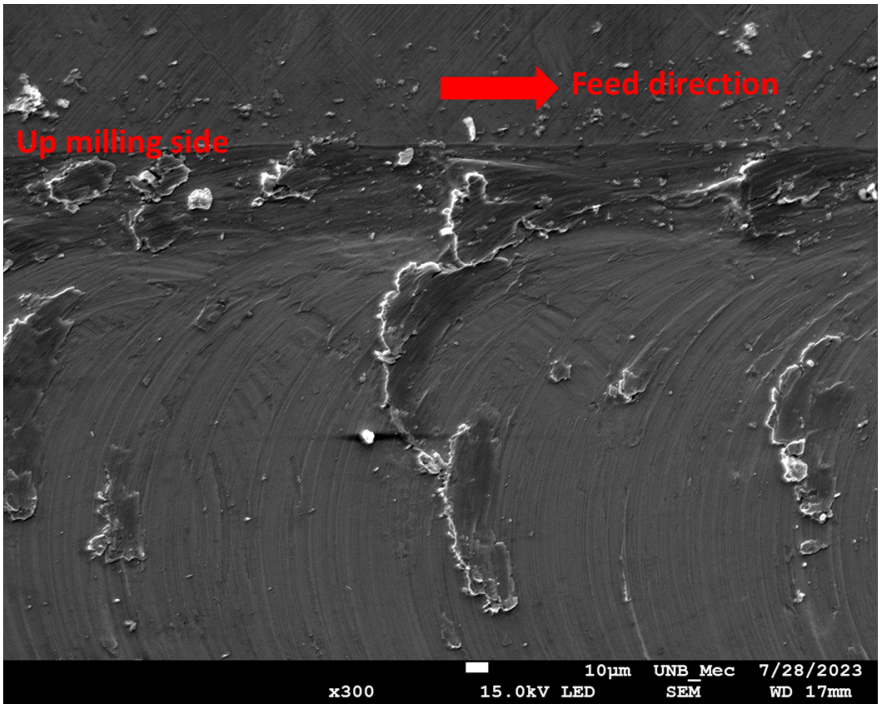

Figure 6.4 – Chip adherence on the bottom of slot 12 of sample 1.

Figure 6.5 shows a comparison of the frontal view of two slots at different machined lengths. It is important to highlight that lubrication was used in the 12 first slots of sample 2, which can explain why this sample has less chip adherence. In the work of Oliveira (2019), the author also noticed that lubrication can avoid chip adherence and improve surface quality on microslots of Inconel 718 in comparison with dry machining. The use of cutting fluid can also avoid deterioration caused by the plowing effect, which causes deformed material to accumulate on the machined surface, as a result of inefficient chip formation.

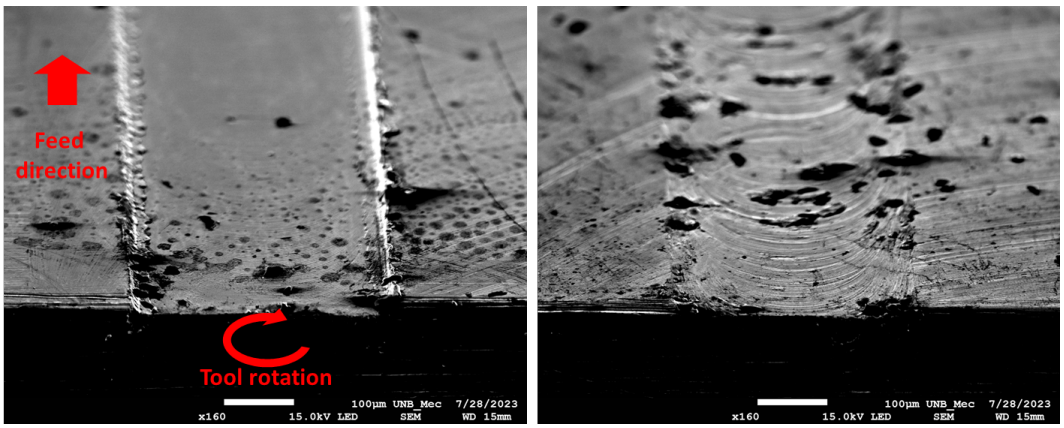

Figure 6.5 – Frontal view of slot 2 (left) and slot 12 (right) of sample 1.

6.2 Burr heights

The presence of large burrs was observed on the microslots, especially on sample 2. The size of burrs is considerably more significant in micro scale machining than conventional machining. Because of size effect, burrs in micromilling have similar size scales than the manufactured features, whereas in conventional machining, burrs size are often small and negligible (SILVA; SILVA; OLIVEIRA, 2023). In figure 6.6, a color gradient was used to indicate the height of the burrs on a representative slot of sample 2. Top burrs in micromilling of Inconel 718 can reach heights more than three times greater than the depth of cut. Because of that, it is normally desired or recommended that pieces should pass through some deburring or edge finishing procedure after machining (GILLESPIE, 1999).

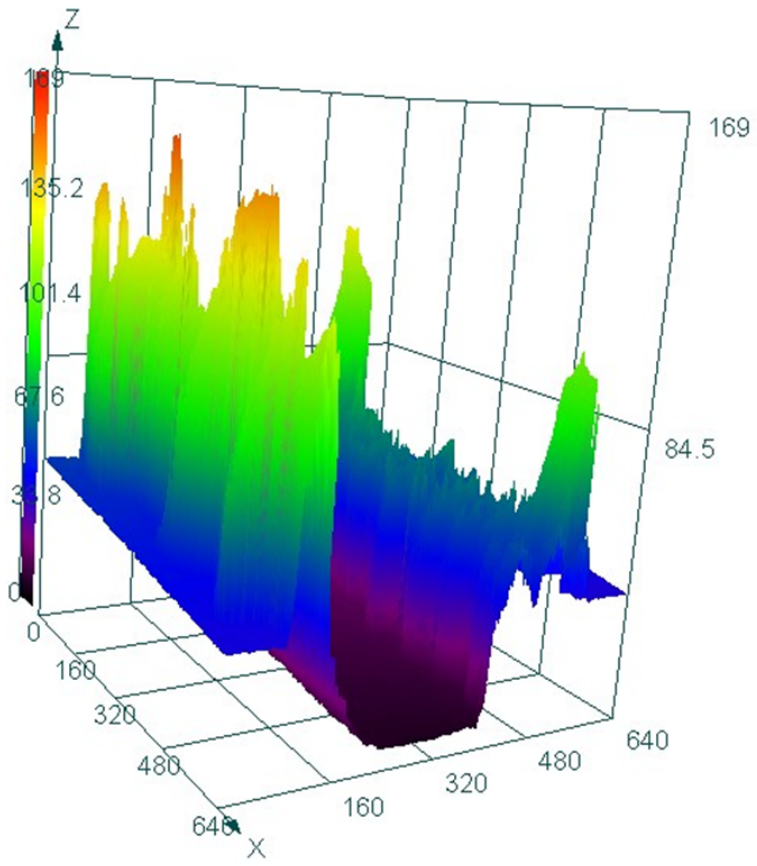

Figure 6.6 – Topography of slot 16 from sample 2 highlighting the burr heights.

The mean values of burr height on the two samples are shown in figures 6.7 and 6.8.

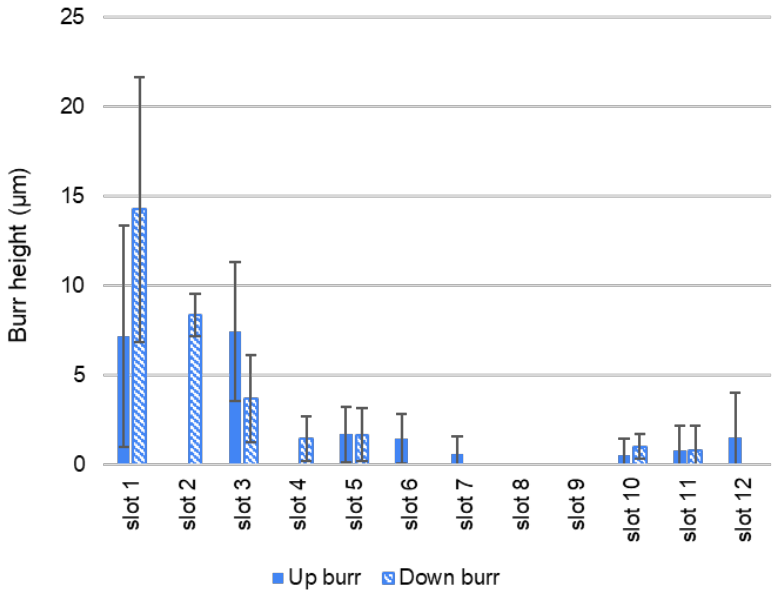

Figure 6.7 – Burr heights of the microslots of sample 1.

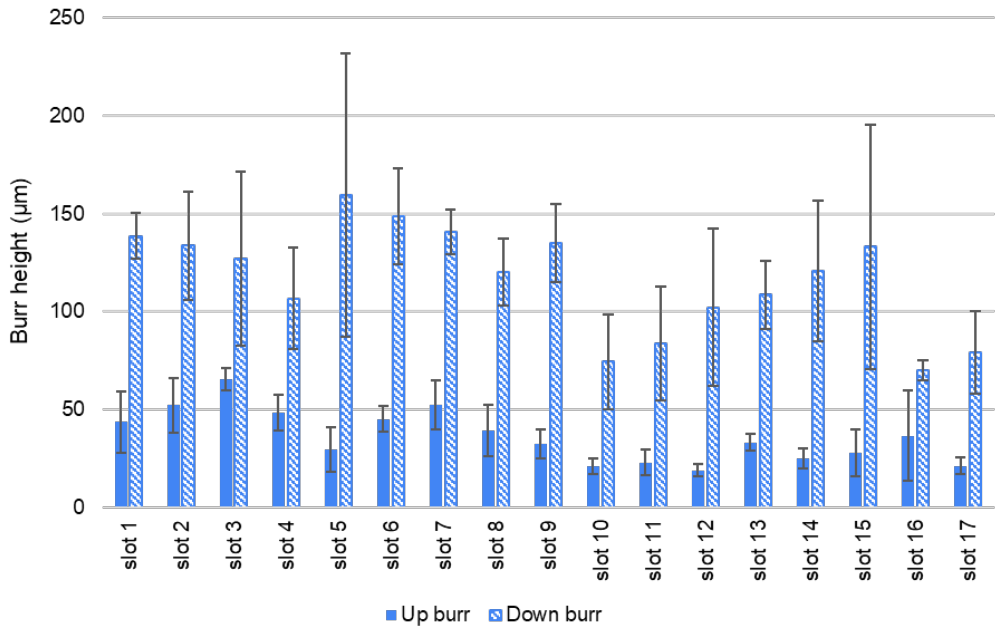

Figure 6.8 – Burr heights of the microslots of sample 2.

It is perceptible, from figures 6.7 and 6.8, that the up and down burrs of sample 2 were substantially higher than those of sample 1. All burrs on sample 1 were less than 15 μm high, and some of the slots did not even present any measurable burr at all, which is the case of slots 8 and 9. The slots of sample 2, on the other hand, all presented down burrs higher than 50 μm, most of them even higher than 100 μm. There are two main reasons that could justify this phenomenon. The first one is the depth of cut a_p, which is 10 μ in all slots of sample 1 and varies from 40 μm to 20 μm on sample 2, indicating that higher a_p generates higher burrs. The second reason is the precision of the machine tools. Sample 1 was machined on a mini-mill with reduced dimensions, which is appropriate for micromilling, being more precise and supplying more rigidity to the system. Sample 2 was machined in a larger machine tool, normally used for conventional machining, with a low spindle speed (5,000 rpm), resulting in less rigidity and less precision to the cutting procedure.

The burrs on sample 1 were considerably less perceptible visually than those of sample 2. For the microslots of sample 2, a_p was higher than in sample 1, therefore, greater volumes of material were dragged by the tool at each pass and more conglomerates of deformed material were deposited at the sides of the slots in the form of burrs. Figure 6.9 shows a comparison between representative slots of sample 1 and sample 2, highlighting that burr formation was substantially more prominent in sample 2.

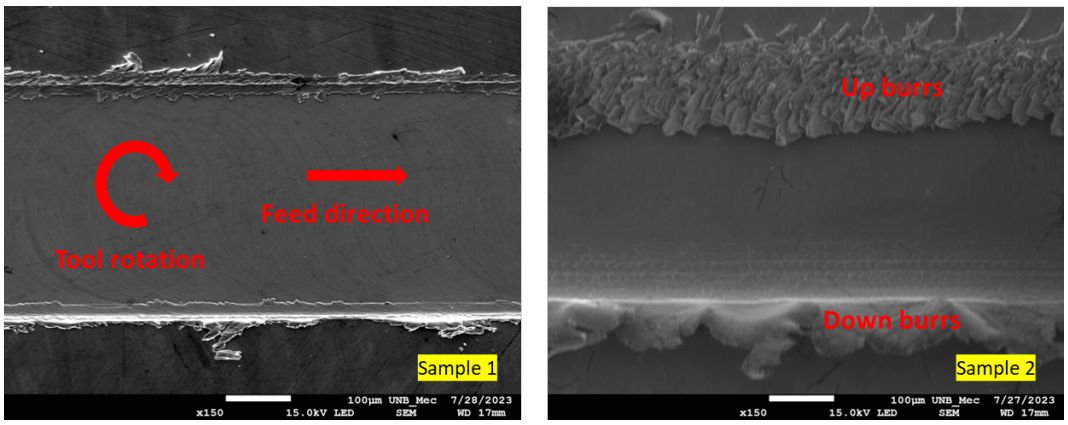

Figure 6.9 – Presence of burrs on representative microslots in both samples.

It was also observed that the burrs on sample 2 presented a tendency to become wider with increase in the machined length, as shown in figure 6.10. This reinforces the idea that tool wear significantly increases burr formation in micromilling. In general, it can be observed that the variation of a_p exerted greater influence than f_z on burr formation.

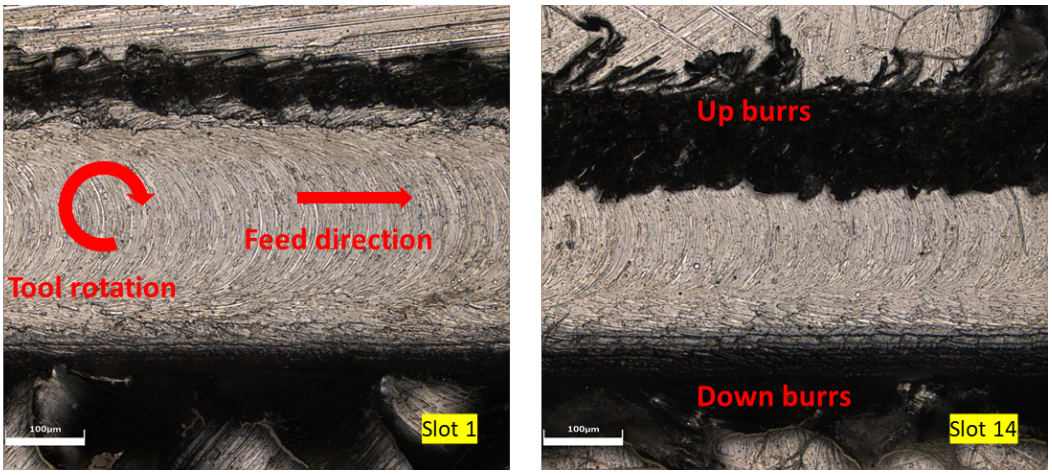

Figure 6.10 – Increase in burrs size with machined length in sample 2.

6.3 Width of the microslots

Measuring the width of the microslots can be considered an indirect measurement of tool wear in micromilling. This is due to the fact that, as the machined length increases, the diameter of the microtool decreases because of wear, and consequently, the width of the slots should decrease in the same proportion. The graphs of width of the microslots on sample 1 and sample 2 are shown in figures 6.11 and 6.12, respectively.

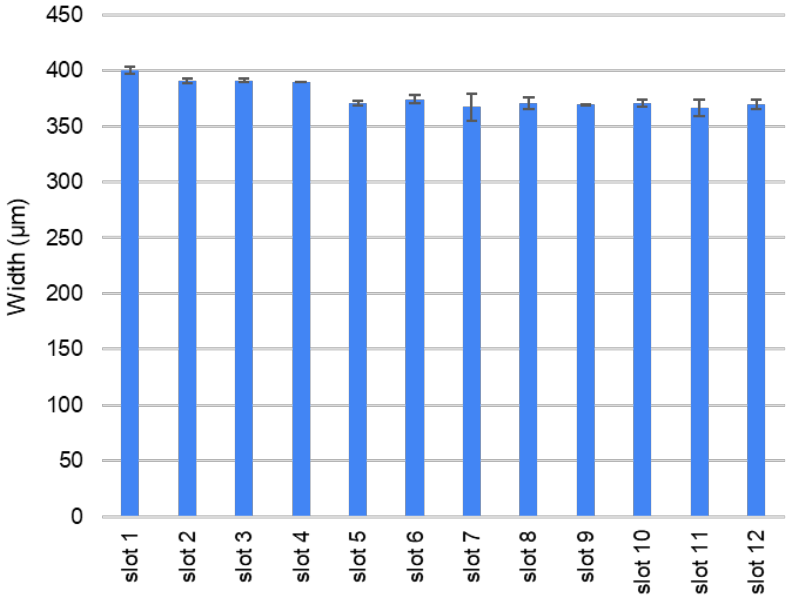

Figure 6.11 – Width of the microslots of sample 1.

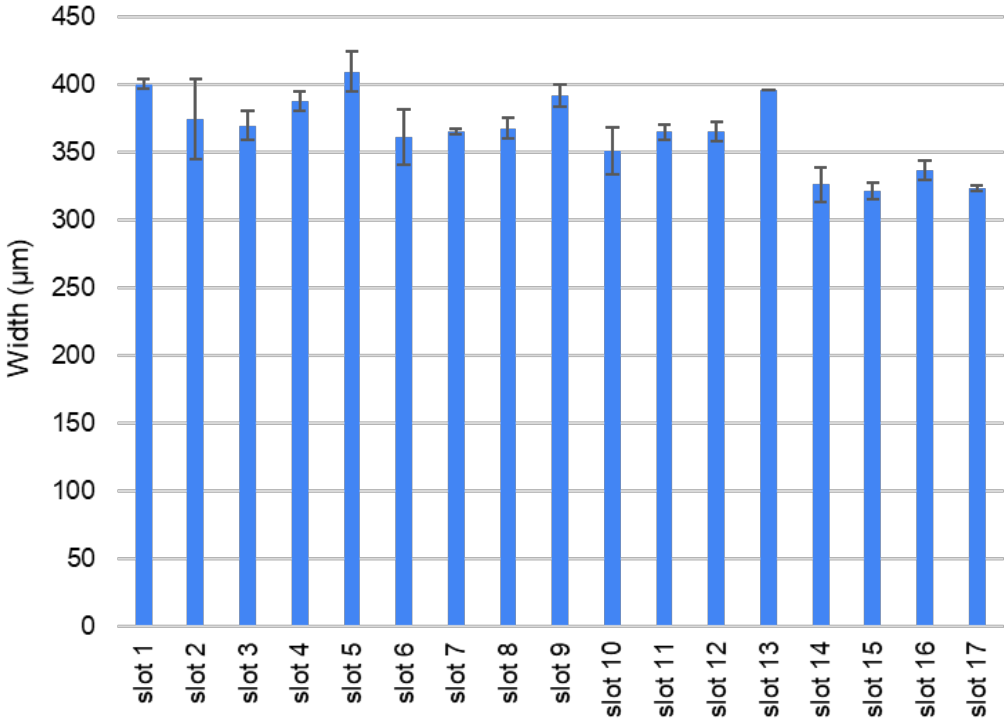

Figure 6.12 – Width of the microslots of sample 2.

As shown in figure 6.11, the width of the slots of sample 1 presented a general tendency to decrease with machined length, with small standard deviations. The smallest registered value of width was that of slot 11, with 366.6 μm. This represents a decrease of 8.35% with respect to the initial value of 400 μm. A similar decrease in tool diameter was observed in the work of Santos (2020). The author observed a diameter reduction of 8.4% when micromilling Ti-6Al-4V. However, the machined length in this author's work was of 1288 mm, which is significantly higher than 180 mm used in the present work, which

highlights the lower machinability of a nickel super-alloy when compared to a titanium alloy.

On the other hand, the width of the microslots of sample 2, figure 6.12, presented more irregularities. Not only are the standard deviations larger, there are also more occurrences of increases in width between two consecutive slots, which is counter-intuitive and is probably resultant of measuring errors. The maximum decrease occurred in slot 15, with 321.2 μm, or 19.7% smaller than the reference of 400 μm. Some factors that can have influenced the greater diameter reduction on sample 2 are the greater machined length and the greater depth of cut (a_p). The values of a_p in sample 2 varied from 40 μm to 10 μm, whereas all the slots of sample 1 had a_p of 10 μm.

It is also possible to notice from figure 6.12 that the variation of f_z affected the width of the microslots. The slots that were machined with the highest f_z, 40 μm, which are slots 1, 5, 9 and 13, are the widest. This indicates that the use of f_z smaller than 40 μm generated worse chip removal, resulting in narrower slots. This phenomenon is a consequence of size effect in micromilling, suggesting that when f_z is too small and too close to the minimum uncut chip thickness, the cutting process is more inefficient.

By comparing the width reduction from slot 1 to slot 12 on both samples, sample 1 presented a reduction of 7.57%, whereas sample 2 presented a reduction of 8.77%. Although the 12 first slots of sample 2 were machined under lubricated condition, they generated more diameter reduction on the cutting tool than the slots of sample 1, which were machined without cutting fluid. This is due to the difference in the depth of cut. Since the slots of sample 2 had higher a_p, they caused more tool wear, despite the use of cutting fluid.

Since the machined length on sample 2 is longer, with 17 microslots, it was expected to present more decrease in tool diameter than sample 1, which has only 12 microslots. However, the decrease in slots width of sample 2 was more than twice as intense as those of sample 1. This significant reduction in width in sample 2, the greater standard deviations and the unexpected occurrences of increase with machined length are owing to the larger burrs in comparison to sample 1. It has been reported that the presence of high burrs in micromilling of Inconel 718 can cause imprecision in tool wear measurement (SILVA; SILVA; OLIVEIRA, 2023). The burrs in sample 2 were considerably higher and wider than those of sample 1, as evidenced in figure 6.13. The presence of large burrs hinders the process of laser scanning, which generates harsh irregularities on the topography obtained by the microscope, figure 6.13 a). When the burrs on the microslots are smaller, the microscope obtains a clearer topography, as shown in figure 6.13 b), and therefore the measurement of the width of the slot is more precise.

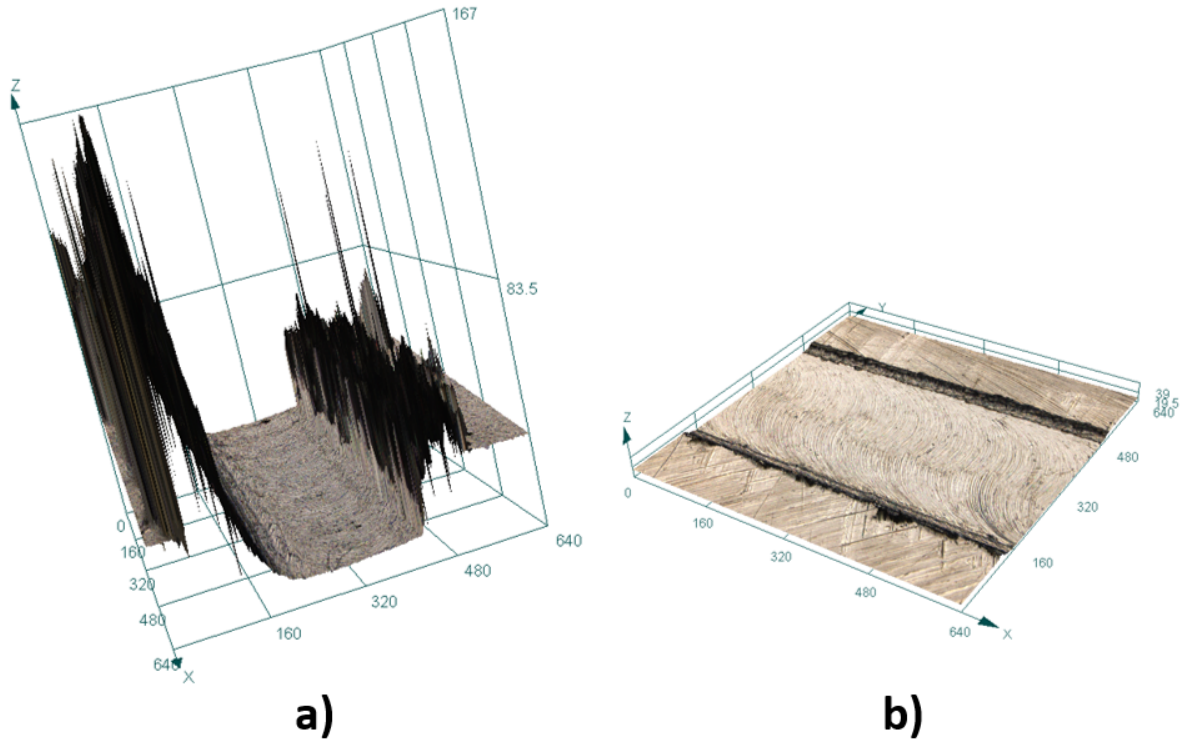

Figure 6.13 – Topography of representative surfaces of slots in a) sample 2 and b) sample 1.

6.4 Comparison with numerical results

6.4.1 Surface quality

Three-dimensional representations of the von Mises stress distribution on the simulated workpieces are shown in figure 6.14. The figures show that the residual stresses on the workpiece machined with the worn tool are higher than those obtained by the sharp tool. The higher residual stresses on the numerical simulations are associated with worse surface quality and worse chip formation. This happens because of size effect, which can be characterized by the non-linear increase in energy per unit volume of material removed, or specific cutting energy, from the decrease in cutting thickness (LIU; MELKOTE, 2007).

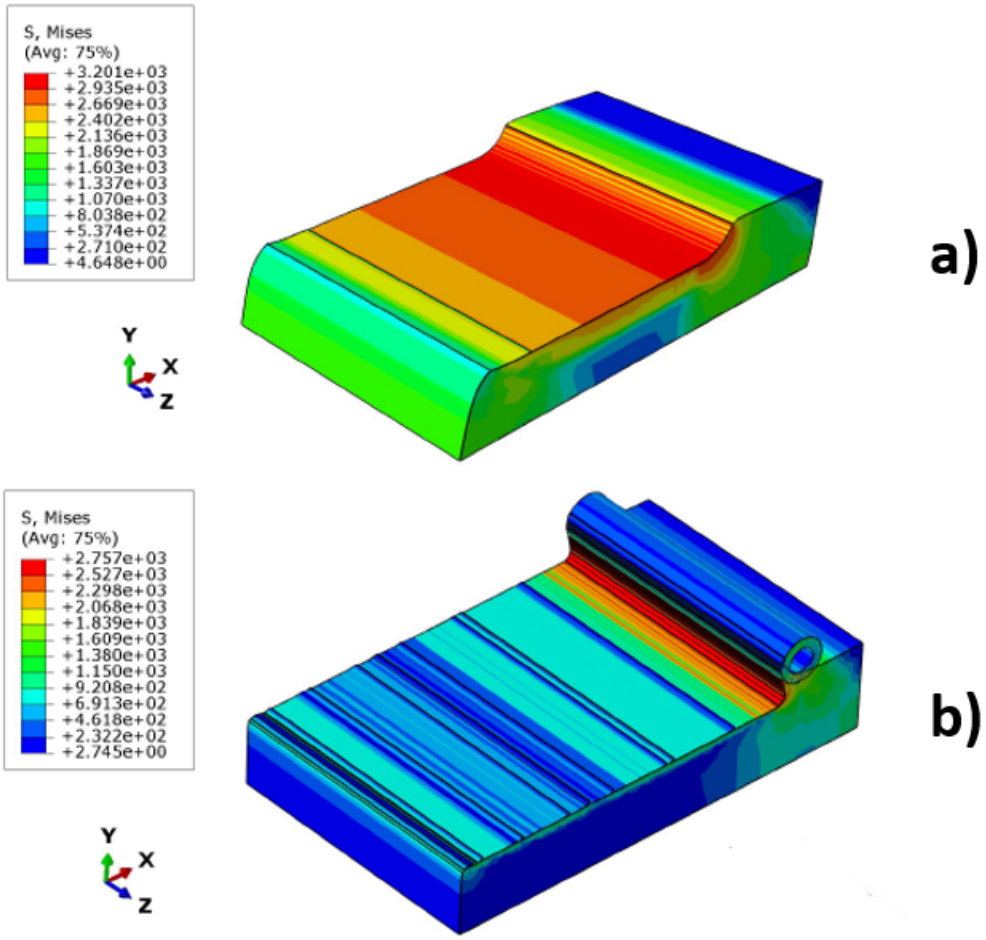

Figure 6.14 – 3D representation of von Mises stress distribution on the simulated workpieces: a) tool edge-radius 5 μm and b) tool edge-radius 1 μm.

The accumulated plastic strain on the simulated workpieces is an indicative of poor surface quality. The maximum values of von Mises stress on the simulations were 3201 MPa for the rounded tool and 2757 MPa for the sharp tool. This indicates that more tool wear results in more deterioration of the machined surface. This computational result matches with the experimental ones. The general conditions of representative slots of each sample are shown in figures 6.15 and 6.16. The images show clearly that the increase in tool wear because of machined length caused deterioration of the slots, with gradually more chip adherence on sample 1 and gradually larger burrs on sample 2. Besides, it can be seen that the burrs on sample 2 are larger than sample 1, mainly because of the higher values of depth of cut.

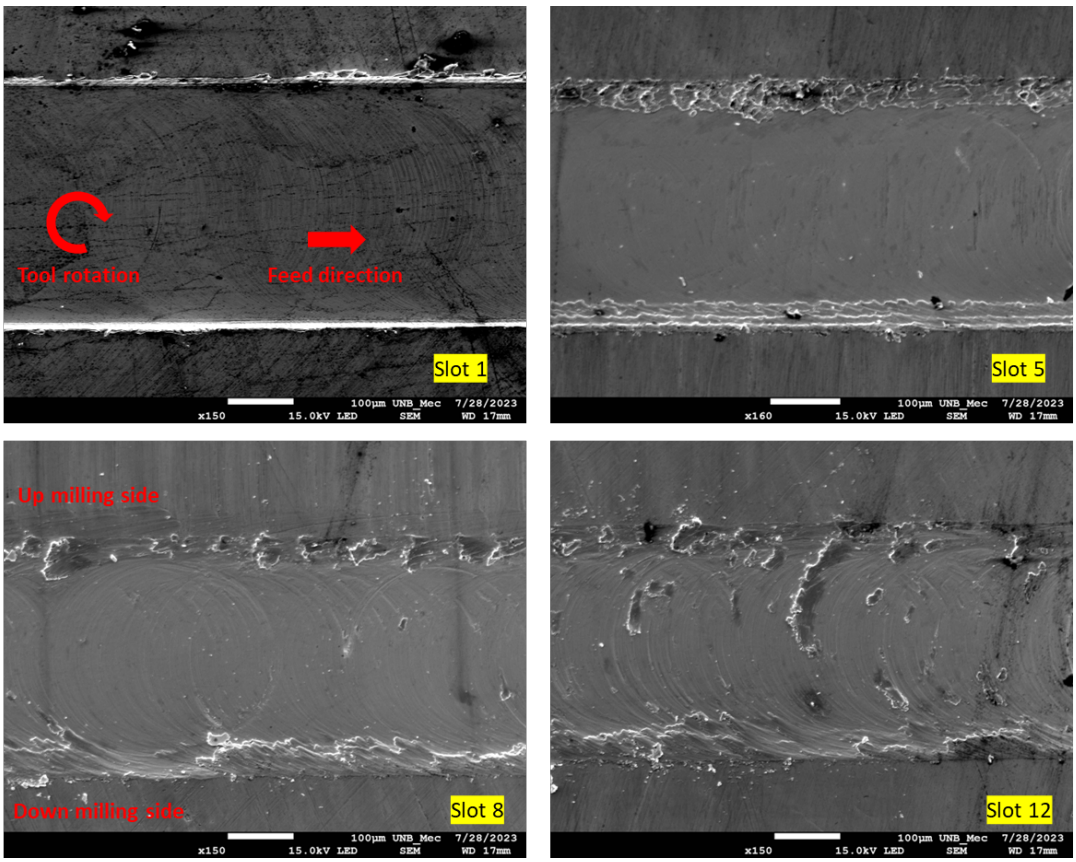

Figure 6.15 – Evolution of slots degradation with machined length on sample 1.

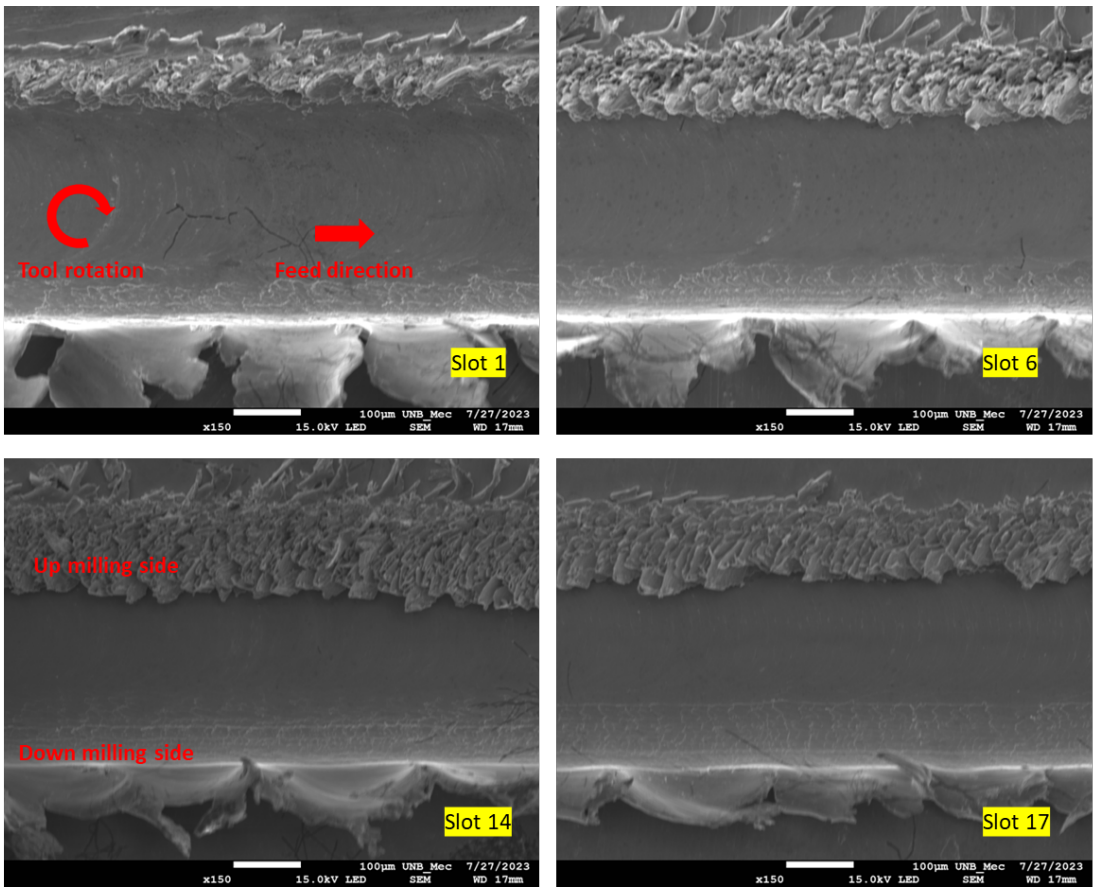

Figure 6.16 – Evolution of slots degradation with machined length on sample 2.

6.4.2 Cutting forces

Figure 6.17 shows the rough signals obtained by the dynamometer for representative slots of sample 1. The signals were then treated to remove noise and were analyzed using the software MATLAB. The forces were measured in the X direction, which is parallel to the feed direction. In general, figure 6.17 shows that the last slots presented higher amplitudes of force than the first slots. The amplitude of forces on slot 1 is roughly 1.5 N and it gradually increases through the next slots, until it reaches roughly 2.5 N on slot 12. This increase in cutting forces through the slots is probably due to the increase on tool wear with machined length.

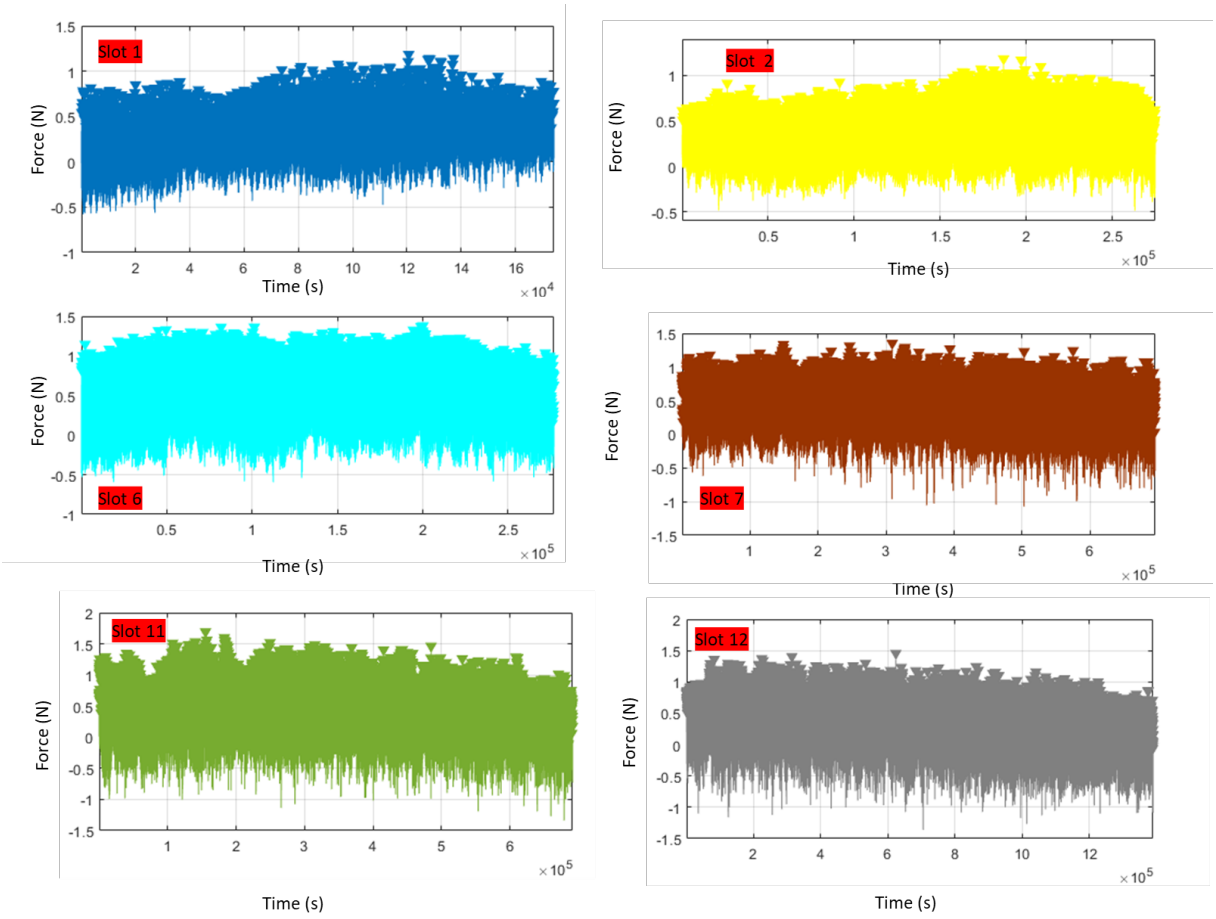

Figure 6.17 – Force rough signals from sample 1.

After the signals were treated, the maximum force and the mean force were determined for each microslot, as shown in figure 6.18. The standard deviations were calculated and used as error bars.

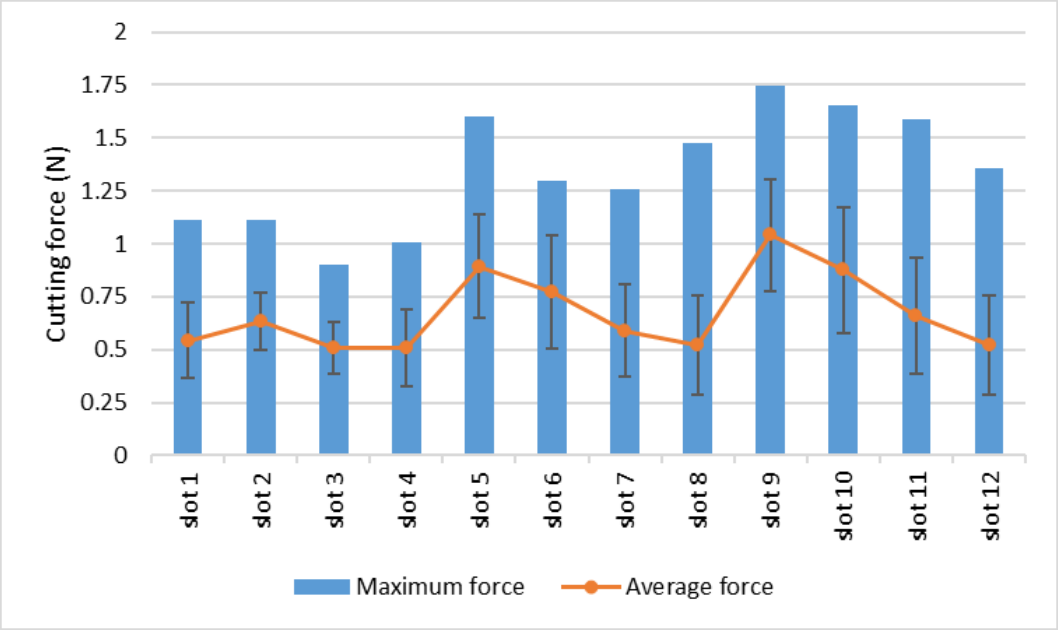

Figure 6.18 – Experimental cutting forces obtained from sample 1.

It can be observed from figure 6.18 that the force presented a high peak on slot 9 (1.04 N) and it decreases gradually in the three consecutive slots, until it reaches 0.52 N in slot 12. A similar behavior occurs on slots 5 (0.77 N) through 8 (0.52 N). This phenomenon evidences the influence of feed per tooth on the cutting forces, because both slots 5 and 9 were manufactured with the highest value of f_z (4 μm), and f_z was gradually reduced in the three consecutive slots, respectively. A similar tendency is observed in slots 1 through 4, even though the average force on slot 2 is higher than slot 1. In general, it can be stated that cutting forces tend to decrease with smaller values of feed per tooth. The same phenomenon was observed in the numerical simulations, as discussed in subsection 4.1.3.

Moreover, figure 6.18 also shows that the mean force in slots 9 through 12 were higher than their counterparts that were fabricated with same f_z. For example, the mean force on slot 10 was higher than on slot 6, which was higher than slot 2, although all these three slots were fabricated with feed of 2.5 μm per tooth. This is due to the fact that the tool was already damaged in the last slots, which evidences the influence of tool wear on the cutting forces. This confirms the numerical results obtained from the FEM simulations. When the tool is damaged by wear, it has larger edge radius, which generates higher forces than a sharper tool (with smaller edge radius), as shown in figures 4.5 and 4.6.

6.4.3 Burrs geometry

In figure 6.19, two workpieces from the numerical simulations were extruded with a depth of 30 μm so as to represent visually the 3D burrs generated in the en of the tool trajectory. The images shows that large amounts of material tend to accumulate at the border of the workpiece, creating exit burrs, as described by Wan, Cheng and Sun (2013). The thickness of the burr is higher when the tool has larger edge radius.

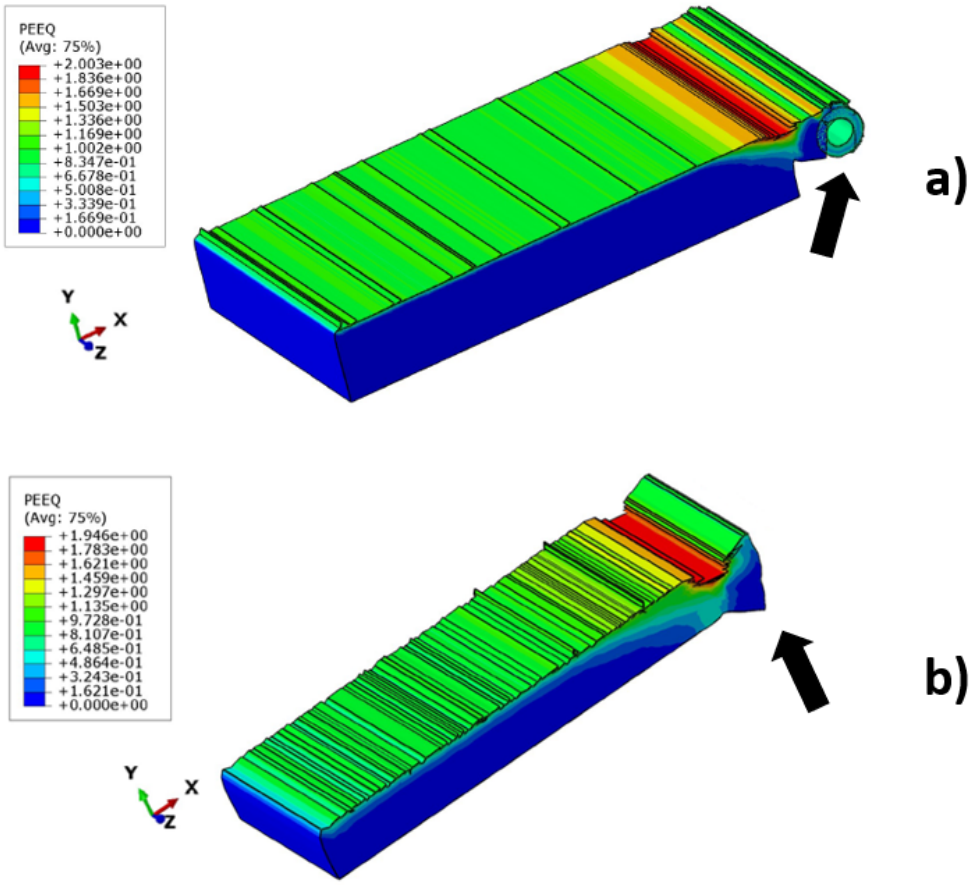

Figure 6.19 – 3D representation of roll-up burrs on the simulated workpieces: a) tool edge-radius 1 μm and b) tool edge-radius 5 μm.

Large burrs were also observed experimentally, especially on the microslots of sample 2. The burrs generated on this sample were larger than those of sample 1, as exemplified in figure 6.20. Figure 6.20 highlights that a large burr was generated at the exit of the slot 1 of sample 2, however this behavior is not seen on slot 1 of sample 1. This phenomenon highlights the influence of feed per tooth on burr formation, since the slots on sample 2 were machined with higher f_z than sample 1.

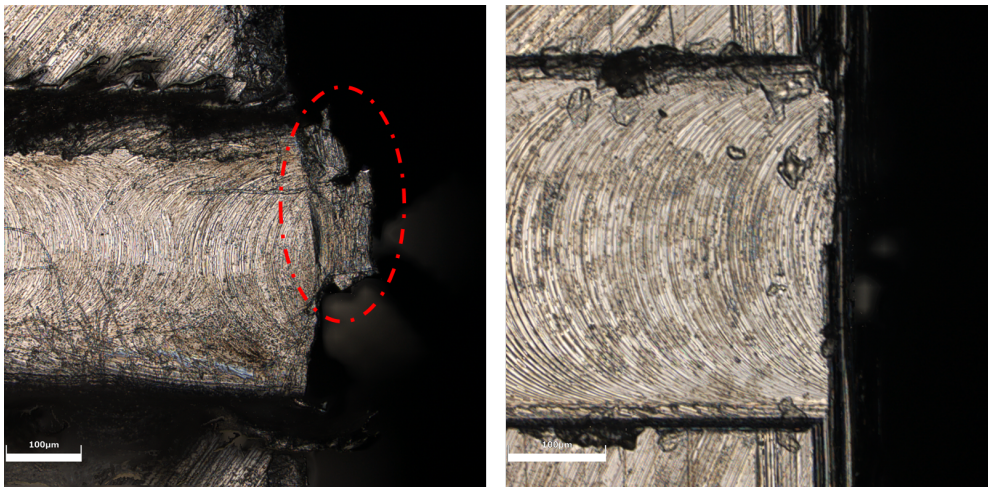

Figure 6.20 – Presence of exit burr on slot 1 of sample 2 (left) and absence of such kind of burrs on sample 1 (right).

6.4.4 Tool wear

The wear of the cutting tool exerts particular influence in micromilled components. Because of their reduced dimensions, microtools tend to wear out rapidly, causing losses in geometrical tolerances of the machined features. Figure 6.21 shows SEM images of the microtool before and after manufacturing 10 slots on sample 1. The images on the right highlight the damage suffered by the tool because of wear, contrasting with the condition of the fresh tool, shown on the left. The presence of white stains on the SEM images of the worn tool indicates the presence of workpiece material adhesion, which directly affects the geometry and the surface quality of the slots.

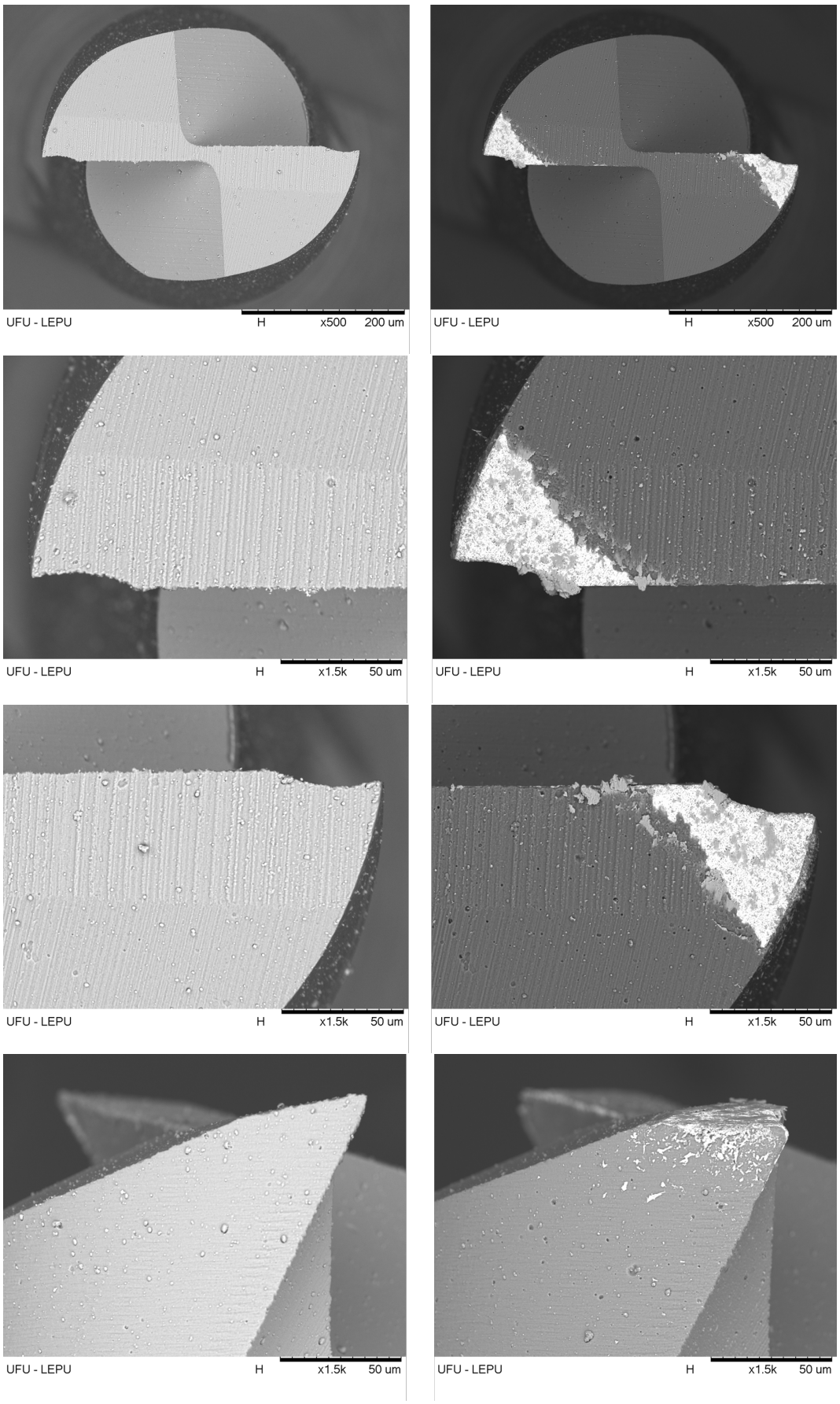

Figure 6.21 – Condition of the micromill before (left) and after (right) a machined length of 150 mm on sample 1.

The white stains on the SEM images indicate the presence of workpiece material adhesion, which directly affects the geometry and the surface quality of the slots. Besides, the interaction between the tool and the workpiece leads to rounding of the tip, increasing the radius of the cutting-edge. These phenomena of rounding of the radius and adhesion of workpiece material during micromilling of Inconel 718 were also reported in the work of Oliveira (2019).

The presence of coating on the cutting tool the can be an important factor to avoid rapid wear in micromilling, as well as the composition of the coating. In the work of Ziberov (2018), the author compared microtools coated with DLC (diamond-like carbon) and with (Al,Ti)N. According to the author, the higher thermal conductivity of DLC enables a more efficient heat distribution during machining, which increases the lifespan of the tool in comparison to the (Al,Ti)N coating. In the work of Santos (2020), the author identified more intense wear evolution in uncoated tools, compared with tools coated with AlCrN, in micromilling of Ti-6Al-4V. In the present work, the use of different coatings could have generated highly different levels of damage on the cutting tools, even for short cutting lengths.

The tool used in the tests of sample 1, shown in figure 6.21, operated under dry condition. Less deterioration of the cutting tool can be achieved if lubrication is used. In the work of Oliveira (2019), the author suggests that wear is higher for dry machining tests than in machining with lubrication. In the tests on sample 2, which occurred under lubrication condition, the tool broke down and therefore could not have been analyzed in the microscope. However, the importance of the application of cutting fluid is reflected on the surface quality of the slots.

Modeling of tool wear in numerical simulations is complex, especially in micromilling, when the radius increase rate is more rapid than in macro machining. Since works about numerical simulations tend to focus on the behavior of the workpiece rather than the tool, it is common in literature to neglect the effects of wear and represent the tool as a rigid body, both in conventional machining and micromachining, which is the case of the present work. Some examples of other works that adopted this approach include those of Lai et al. (2008), Chen et al. (2019), Attanasio et al. (2019), Jing et al. (2020) and Oliveira et al. (2021). Figure 6.22 shows the comparison between the SEM images of the tool used in the micromilling tests of sample 1 and their respective representations as rigid bodies on the numerical simulations, in fresh and worn conditions.

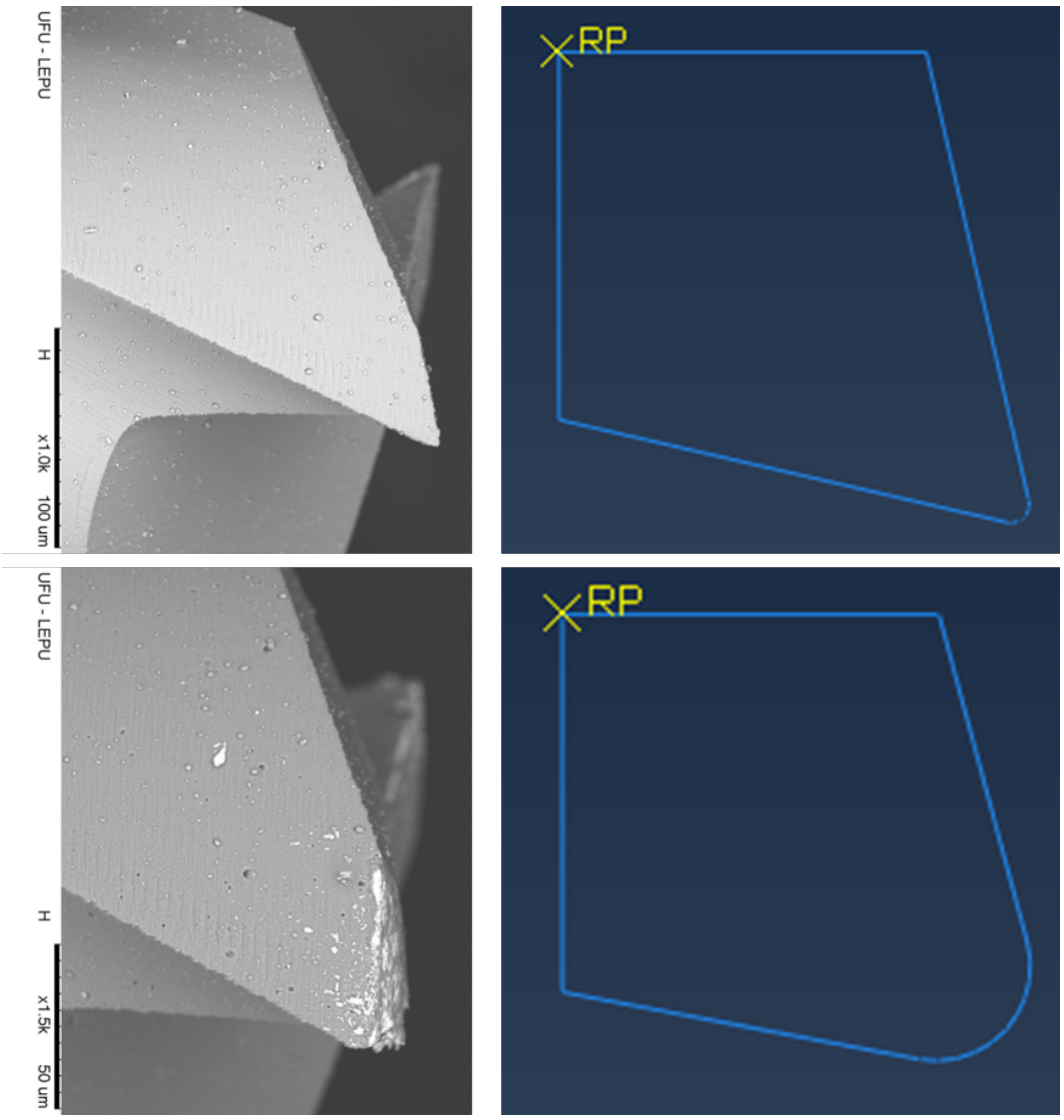

Figure 6.22 – Comparison of SEM images of the microtool and their respective representations on the numerical simulations.

An analytical method to predict crater and flank wear of tungsten carbide tools in turning operations was proposed by Usui, Shirakashi and Kitagawa (1984). The author's approach was then refined and used in more recent works such as those of Özel et al. (2011) and Thepsonthi and Özel (2016). In these two last works, the authors use FEM simulations to calculate the distribution of the rate of volume loss on the tool per unit area per unit time, using a function of the interface temperature, the normal stress and the sliding velocity. Thepsonthi and Özel (2016) observed that the prediction of tool wear using this method changes depending if the workpiece material is modeled using viscoplastic or elasto-viscoplastic approach. The authors predicted higher tool wear using viscoplastic modeling, with an error about 5–10 % over the elasto-viscoplastic model. In the work of Özel et al. (2011), the authors were able to numerically predict less wear in CBN coated tools than in uncoated tools.

6.4.4.1 Tool breakage

It was intended that sample 2 should have 18 microslots, however it only has 17 because the tool abruptly broke down at an attempt to manufacture the eighteenth slot. The tip of the micromill fractured after a very short machined length in slot 18, as observed in figure 6.23. The machining test was interrupted as soon as the tool broke.

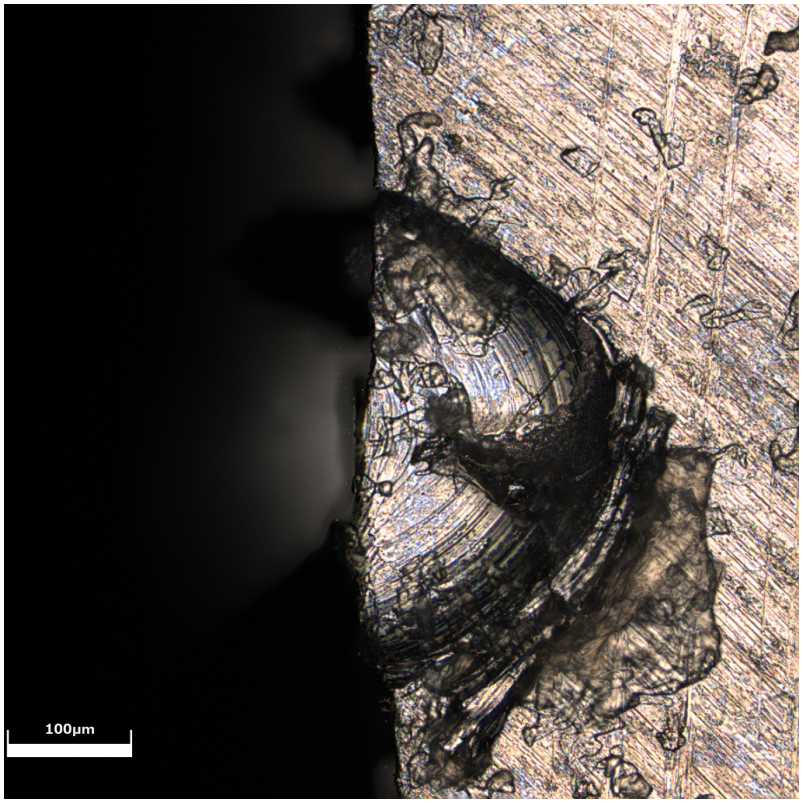

Figure 6.23 – Failed attempt to manufacture slot 18 because of tool breakage.

The breakage of the tool of sample 2 was probably due to excessive wear. Even though most of the machining tests of sample 2 were performed with application of cutting fluid, while the slots of sample 1 were all manufactured under dry machining, the breakage of the tool is still not surprising considering that the length of cut of this micromill was considerably higher than that of sample 1. Besides, the depth of cut was also higher in sample 2 than in sample 1, which considerably increases cutting forces because of the bigger volume of material exerting pressure on the tool.

The fact that the tool broke highlights that the cutting forces increase with tool wear, which is in accordance to what was proved in the numerical simulations. Because of the small dimensions of micromills, it is difficult to predict failure and the breakage often happens abruptly. The coating of the tool can be of crucial importance in avoiding breakage. In their work, Romanus et al. (2014) performed micromilling of sintered ZrO_2 ceramic using a cubic boron nitride (CBN) tools with different coatings. The tool coated with hard carbon broke down after a machined length of only 66 mm, whereas nanograin diamond coated tools survived until 1980 mm.

7 Conclusions

In this work, a numerical and experimental analysis of micromilling of Inconel 718 was performed. FEM simulations of the orthogonal cut of Inconel 718 were performed using Abaqus CAE. In the simulations, two geometries were proposed for the cutting tool: a sharp tool (edge radius 1 μm) and a rounded tool (edge radius 5 μm). The mechanical properties of Inconel 718 were characterized using Johnson-Cook model with isothermal approach. The experimental micromilling trials were performed in two Inconel 718 samples, sample 1 and sample 2. Microslots were machined on both samples using different machining parameters and machine tools. Microscopes were used to generate images of the microslots and to measure their width, surface roughness and burr height. After analyzing the numerical and experimental results, the following conclusions can be drawn:

i. From the numerical simulations:

   - The tool with edge radius 5 μm generates higher residual von Mises stress (11.7%) and higher accumulated plastic strain (42.4%) than the tool with edge radius 1 μm.
   - The use of the rounded tool results in larger burrs and more difficult chip formation than the sharp tool, with a greater layer of uncut material.
   - The minimum uncut chip thickness (MUCT) was found to be between 2.5 μm and 4.0 μm for the tool with edge radius 5 μm and up to 0.5 μm for the tool with edge radius 1 μm, considering the assumptions used in the present work.
   - Accumulated plastic strain on the workpiece is higher when larger values of f_z are used. The increase was found to be 259.2% for the rounded tool (varying f_z from 4.0 μm to 1.0 μ) and 196.8% for the sharp tool (varying f_z from 2.5 μm to 0.5 μm).
   - The rounded tool generates up to three times higher cutting forces than the sharp tool.
   - The presence of hard precipitates on the matrix of the workpiece causes the chips to become more brittle and the cutting forces to become more irregular than in a homogeneous workpiece, evidencing that the elastic effects become more relevant in chip formation when the tool has a larger cutting-edge radius.

- It is not common to simulate tool wear evolution in FEM simulations of machining processes, the tool is often represented as a rigid body. However, the effect of wear can be simulated by changing the edge radius of the rigid tool.

ii. From the micromilling trials:

- Large burrs are common in micromilling of Inconel 718, and they can cause imprecision on indirect tool wear measurement through the geometry of the microslots.
- Increasing the depth of cut (a_p) results in higher burrs in micromilling of Inconel 718. For $a_p = 40$ μm, 30 μm or 20 μm, most down burrs were higher than 100 μm, whereas for $a_p = 10$ μm, all burrs were smaller than 15 μm.
- The machine tool used in sample 2 performed micromilling with less precision than that of sample 1, resulting in more geometrical errors, larger burrs and higher surface roughness.
- The cutting tool used in sample 2 broke down after a machined length of 255 mm, probably because of high tool wear induced by large depth of cut.
- Increasing f_z results in higher cutting forces in micromilling of Inconel 718. For f_z varying from 0.5 μm to 4.0 μm, the average cutting force doubled.
- Machining with lubrication improved the surface quality of the slots by preventing chip adherence, although the formation of large burrs could not be avoided by the use of cutting fluid.

7.1 Suggestions for future works

In order to complement the results obtained in the present work, the following suggestions for future works are proposed:

- Using a more robust FEM model to represent micromilling, for example 3D simulations or models that take into account the evolution of tool wear.
- Simulating micromilling in other materials, different from Inconel 718.
- Evaluating the effect of different lubrication conditions to try to decrease burr heights.

Bibliography

ABENI, A.; CAPPELLINI, C.; ATTANASIO, A. A novel 2D micromilling FEM simulation strategy to optimize the flow stress law of IN625. *Procedia CIRP - 19th Conference on Modeling of Machining Operations*, v. 117, p. 432–437, 2023. DOI: https://doi.org/10.1016/j.procir.2023.03.073. Quoted on page 24.

ALHADEFF, L.; MARSHALL, M.; CURTIS, D.; SLATTER, T. Protocol for tool wear measurement in micro-milling. *Wear*, v. 420-421, p. 54–67, 2019. DOI: https://doi.org/10.1016/j.wear.2018.11.018. Quoted 2 times on pages 8 and 11.

ARAMCHAROEN, A.; MATIVENGA, P. Size effect and tool geometry in micromilling of tool steel. *Precision Engineering*, v. 33, n. 4, p. 402–407, 2009. DOI: https://www.sciencedirect.com/science/article/pii/S0141635908001529?via3Dihub. Quoted 3 times on pages x, 6, and 7.

ASLANTAS, K.; HOPA, H.; PERCIN, M.; UCUN, I.; ÇICEK, A. Cutting performance of nano-crystalline diamond (NCD) coating in micro-milling of Ti6Al4V alloy. *Precision Engineering*, v. 45, p. 55–66, 2016. DOI: https://doi.org/10.1016/j.precisioneng.2016.01.009. Quoted 3 times on pages x, 11, and 12.

ASLANTAS, K.; ÇICEK, A. The effects of cooling/lubrication techniques on cutting performance in micro-milling of Inconel 718 superalloy. *Procedia CIRP*, v. 77, p. 70–73, 2018. DOI: https://www.sciencedirect.com/science/article/pii/S2212827118310680. Quoted 5 times on pages x, 7, 17, 18, and 65.

ATTANASIO, A.; ABENI, A.; ÖZEL, T.; CERETTI, E. Finite element simulation of high speed micro milling in the presence of tool run-out with experimental validations. *The International Journal of Advanced Manufacturing Technology*, v. 100, p. 25–35, 2019. DOI: https://doi.org/10.1007/s00170-018-2678-2. Quoted 4 times on pages xi, 21, 22, and 81.

BRITO, L. C.; GOMES, M. C.; de Oliveira, D.; Bacci da Silva, M.; Viana Duarte, M. A. Vibration features for indirect monitoring of end micromilling process. *Precision Engineering*, v. 79, p. 7–15, 2023. DOI: https://doi.org/10.1016/j.precisioneng.2022.08.012. Quoted on page 65.

BUSHLYA, V.; ZHOU, J.; STAHL, J. Effect of cutting conditions on machinability of superalloy inconel 718 during high speed turning with coated and uncoated pcbn tools. *Procedia CIRP*, v. 3, p. 370–375, 2012. DOI: https://doi.org/10.1016/j.procir.2012.07.064. Quoted on page 16.

CHAE, J.; PARK, S.; FREIHEIT, T. Investigation of micro-cutting operations. *International Journal of Machine Tools and Manufacture*, v. 46, n. 3, p. 313–332, 2006. DOI: https://www.sciencedirect.com/science/article/pii/S0890695505001306. Quoted 2 times on pages 1 and 5.

CHEN, G.; LU, L.; KE, Z.; QIN, X.; REN, C. Influence of constitutive models on finite element simulation of chip formation in orthogonal cutting of Ti-6Al-4V alloy. *Procedia Manufacturing*, v. 33, p. 530–537, 2019. ISSN 2351-9789. DOI: https://doi.org/10.1016/j.promfg.2019.04.066. Quoted 3 times on pages 20, 22, and 81.

CÂMARA, M.; RUBIO, J. C.; ABRÃO, A.; DAVIM, J. State of the art on micromilling of materials, a review. *Journal of Materials Science & Technology*, v. 28, n. 8, p. 673–685, 2012. DOI: https://www.sciencedirect.com/science/article/pii/S1005030212601157. Quoted 3 times on pages 1, 5, and 6.

CÂMARA, M. A. Influência do efeito escala sobre a operação de microfresamento. Belo Horizonte, MG, Brazil, p. 191, 2014. PhD thesis. Quoted on page 7.

DENG, D.; ZHANG, Z.; WAN, W.; MA, Q.; SUN, J. Investigation on burr formation characteristics in micro milling of Ω-shaped reentrant microchannels. *Journal of Manufacturing Processes*, v. 80, p. 754–764, 2022. Doi = https://doi.org/10.1016/j.jmapro.2022.06.012. Quoted on page 25.

ERICE, B.; GALVEZ, F. A coupled elastoplastic-damage constitutive model with lode angle dependent failure criterion. *International Journal of Solids and Structures*, v. 51, n. 1, p. 93–110, 2014. DOI: https://doi.org/10.1016/j.ijsolstr.2013.09.015. Quoted 3 times on pages xiv, 31, and 32.

ERÇETIN, A.; ASLANTAS, K.; ÖZGÜN Özgür. Micro-end milling of biomedical Tz54 magnesium alloy produced through powder metallurgy. *Machining Science and Technology*, Taylor & Francis, v. 24, n. 6, p. 924–947, 2020. DOI: https://doi.org/10.1080/10910344.2020.1771572. Quoted 2 times on pages xi and 36.

FANG, B.; YUAN, Z.; LI, D.; GAO, L. Effect of ultrasonic vibration on finished quality in ultrasonic vibration assisted micromilling of inconel718. *Chinese Journal of Aeronautics*, 2020. DOI: https://doi.org/10.1016/j.cja.2020.09.021. Quoted on page 17.

FEI; CHENG, X.; LIU, Y.; YANG, X.; MENG, F. Micromilling simulation for the hard-to-cut material. *Procedia Engineering*, v. 174, p. 693–699, 2017. DOI: https://doi.org/10.1016/j.cja.2020.09.021. Quoted on page 24.

FENG, Y.; HUNG, T.-P.; LU, Y.-T.; LIN, Y.-F.; HSU, F.-C.; LIN, C.; LU, Y.-C.; LU, X.; LIANG, S. Y. Surface roughness modeling in laser-assisted end milling of inconel 718. *Machining Science and Technology*, v. 23, p. 1–19, 2019. DOI: https://doi.org/10.1080/10910344.2019.1575407. Quoted on page 49.

FILHO, A. F.; SILVA, L. R. R. da; RUZZI, R. de S.; COSTA, E. S.; SALES, W. F.; JACKSON, M. J.; MACHADO Álisson R. Influence of milling direction in the machinability of inconel 718 with submicron grain cemented carbide tools. *The International Journal of Advanced Manufacturing Technology*, v. 105, p. 1343–1355, 2019. DOI: https://doi.org/10.1007/s00170-019-04328-3. Quoted 5 times on pages x, xi, 16, 17, and 42.

FILIZ, S.; CONLEY, C. M.; WASSERMAN, M. B.; OZDOGANLAR, O. B. An experimental investigation of micro-machinability of copper 101 using tungsten carbide micro-endmills. *International Journal of Machine Tools and Manufacture*, v. 47, n. 7, p. 1088–1100, 2007. ISSN 0890-6955. Quoted 2 times on pages 8 and 9.

FILIZ, S.; XIE, L.; WEISS, L. E.; OZDOGANLAR, O. Micromilling of microbarbs for medical implants. *International Journal of Machine Tools and Manufacture*, v. 48, n. 3, p. 459–472, 2008. DOI: https://www.sciencedirect.com/science/article/pii/S0890695507001733. Quoted on page 5.

GILLESPIE, L. K. *Deburring and edge finishing handbook*. New York: Society of Manufacturing Engineers, 1999. Quoted 2 times on pages 13 and 67.

GILLESPIE, L. K. *Hand Deburring: Increasing Shop Productivity*. Dearnorn, Michigan: Society of Manufacturing Engineers, 2003. Quoted on page 14.

GOMES, M. C. Estudo do processo de microfresamento em aço inoxidável ABNT316L produzido por fundição e manufatura aditiva. Uberlândia, MG, Brasil, p. 145, 2022. PhD thesis. Quoted 3 times on pages xii, 58, and 65.

GOMES, M. C.; BRITO, L. C.; Bacci da Silva, M.; Viana Duarte, M. A. Tool wear monitoring in micromilling using support vector machine with vibration and sound sensors. *Precision Engineering*, v. 67, p. 137–151, 2021. DOI: https://doi.org/10.1016/j.precisioneng.2020.09.025. Quoted on page 11.

JAIN, V. K. (Ed.). *Micromanufacturing processes*. Boca Raton, Florida, EUA: CRC Press - Taylor & Francis Group, 2013. Quoted 2 times on pages 1 and 5.

JING, X.; LV, R.; CHEN, Y.; TIAN, Y.; LI, H. Modelling and experimental analysis of the effects of run out, minimum chip thickness and elastic recovery on the cutting force in micro-end-milling. *International Journal of Mechanical Sciences*, v. 176, p. 1055–40, 2020. DOI: https://doi.org/10.1016/j.ijmecsci.2020.105540. Quoted 3 times on pages xi, 23, and 81.

JOHNSON, G. R.; COOK, W. H. Fracture characteristics of three metals subjected to various strains, strain rates, temperatures and pressures. *Engineering Fracture Mechanics*, v. 21, n. 1, p. 31–48, 1985. DOI: https://doi.org/10.1016/0013-7944(85)90052-9. Quoted 2 times on pages 30 and 31.

KHAN, K.; VARGHESE, A.; DIXIT, P.; JOSHI, S. S. Effect of tool path complexity on top burrs in micromilling. *Procedia Manufacturing*, v. 34, p. 432–439, 2019. DOI: https://www.sciencedirect.com/science/article/pii/S2351978919309175. Quoted 2 times on pages 5 and 13.

KIENZLER, A.; DEUCHERT, M.; SCHULZE, V. *Burr Minimization and Removal by Micro Milling Strategies or Micro Peening Processes*. Berlin, Heidelberg: Springer Berlin Heidelberg, 2010. 237–243 p. Quoted on page 14.

LAI, X.; LI, H.; LI, C.; LIN, Z.; NI, J. Modelling and analysis of micro scale milling considering size effect, micro cutter edge radius and minimum chip thickness. *International Journal of Machine Tools and Manufacture*, v. 48, n. 1, p. 1–14, 2008. DOI: https://www.sciencedirect.com/science/article/pii/S089069550700154X. Quoted 3 times on pages x, 8, and 81.

LEE, S.; DORNFELD, D. Precision laser deburring. *Journal of Manufacturing Science and Engineering*, v. 123, 11 2001. Quoted on page 14.

LIANG, X.; LIU, Z.; WANG, B. State-of-the-art of surface integrity induced by tool wear effects in machining process of titanium and nickel alloys: A review. *Measurement*, v. 132, p. 150–181, 2019. DOI: https://doi.org/10.1016/j.measurement.2018.09.045. Quoted on page 31.

LIAO, Y.; LIN, H.; WANG, J. Behaviors of end milling inconel 718 superalloy by cemented carbide tools. *Journal of Materials Processing Technology*, v. 201, n. 1, p. 460–465, 2008. DOI: https://doi.org/10.1016/j.jmatprotec.2007.11.176. Quoted 3 times on pages x, 16, and 66.

LIU, D.; WANG, G.; YU, J.; RONG, Y. K. Molecular dynamics simulation on formation mechanism of grain boundary steps in micro-cutting of polycrystalline copper. *Computational Materials Science*, v. 126, p. 418–425, 2017. DOI: https://doi.org/10.1016/j.commatsci.2016.10.001. Quoted 2 times on pages 8 and 52.

LIU, K.; MELKOTE, S. N. Finite element analysis of the influence of tool edge radius on size effect in orthogonal micro-cutting process. *International Journal of Mechanical Sciences*, v. 49, n. 5, p. 650–660, 2007. ISSN 0020-7403. DOI: https://doi.org/10.1016/j.ijmecsci.2006.09.012. Quoted 3 times on pages 21, 51, and 73.

LIU, Y.; XU, D.; AGMELL, M.; SAOUBI, R. M.; AHADI, A.; STAHL, J.-E.; ZHOU, J. Numerical and experimental investigation of tool geometry effect on residual stresses in orthogonal machining of inconel 718. *Simulation Modelling Practice and Theory*, v. 106, p. 102187, 2021. DOI: https://doi.org/10.1016/j.simpat.2020.102187. Quoted on page 15.

LU, X.; ZHANG, H.; JIA, Z.; FENG, Y.; LIANG, S. Y. Floor surface roughness model considering tool vibration in the process of micro-milling. *The International Journal of Advanced Manufacturing Technology*, v. 94, p. 4415–4425, 2017. DOI: https://doi.org/10.1007/s00170-017-1123-2. Quoted on page 49.

MACHADO, L. Q.; MALCHER, L. Isotropic hardening curve characterization by the resultant profile of ball indentation tests. *Journal of the Brazilian Society of Mechanical Sciences and Engineering*, v. 41, n. 509, 2019. DOI: https://doi.org/10.1007/s40430-019-1976-4. Quoted on page 19.

MALCHER, L.; PIRES, F. A.; SÁ, J. C. de. An assessment of isotropic constitutive models for ductile fracture under high and low stress triaxiality. *International Journal of Plasticity*, v. 30-31, p. 81–115, 2012. ISSN 0749-6419. DOI: https://doi.org/10.1016/j.ijplas.2011.10.005. Quoted on page 49.

MALEKIAN, M.; MOSTOFA, M.; PARK, S.; JUN, M. Modeling of minimum uncut chip thickness in micro machining of aluminum. *Journal of Materials Processing Technology*, v. 212, n. 3, p. 553–559, 2012. DOI: https://www.sciencedirect.com/science/article/pii/S0924013611001622. Quoted on page 7.

MATHAI, G.; MELKOTE, S. Effect of process parameters on the rate of abrasive assisted brush deburring of microgrooves. *International Journal of Machine Tools and Manufacture*, v. 57, p. 46–54, 2012. DOI: https://doi.org/10.1016/j.ijmachtools.2012.02.007. Quoted on page 14.

MATHAI, G.; MELKOTE, S.; ROSEN, D. Material removal during abrasive impregnated brush deburring of micromilled grooves in NiTi foils. *International Journal of Machine Tools and Manufacture*, v. 72, p. 37–49, 2013. DOI: https://doi.org/10.1016/j.ijmachtools.2013.05.009. Quoted on page 14.

MEIJER, A. L.; STANGIER, D.; TILLMANN, W.; BIERMANN, D. Induction of residual compressive stresses in the sub-surface by the adjustment of the micromilling process and the tool´s cutting edge. *CIRP Annals*, v. 71, n. 1, p. 97–100, 2022. DOI: https://doi.org/10.1016/j.cirp.2022.04.065. Quoted on page 50.

NG, C. K.; MELKOTE, S. N.; RAHMAN, M.; Senthil Kumar, A. Experimental study of micro- and nano-scale cutting of aluminum 7075-T6. *International Journal of Machine Tools and Manufacture*, v. 46, n. 9, p. 929–936, 2006. DOI: https://www.sciencedirect.com/science/article/pii/S0890695505002130. Quoted 2 times on pages 1 and 5.

OLIVEIRA, D. D. Efeito escala e integridade superficial no microfresamento da liga de níquel inconel 718. Uberlândia, MG, Brasil, p. 154, 2019. PhD thesis. Quoted 10 times on pages x, xiv, 5, 13, 18, 19, 54, 59, 66, and 81.

OLIVEIRA, D. de; GOMES, M. C.; OLIVEIRA, G. V. de; SANTOS, A. G. dos; SILVA, M. B. da. Experimental and computational contribution to chip geometry evaluation when micromilling inconel 718. *Wear - 23rd International Conference on Wear of Materials*, v. 476, p. 203658, 2021. ISSN 0043-1648. DOI: https://www.sciencedirect.com/science/article/pii/S0043164821000478. Quoted 3 times on pages 47, 49, and 81.

OLIVEIRA, D. de; GOMES, M. C.; SILVA, M. B. da. Influence of cutting fluid application frequency on the surface quality of micromilled slots on inconel 718 alloy. *Procedia Manufacturing - 48th SME North American Manufacturing Research Conference, NAMRC 48*, v. 48, p. 553–558, 2020. ISSN 2351-9789. DOI: https://doi.org/10.1016/j.promfg.2020.05.082. Quoted 2 times on pages 47 and 49.

OLIVEIRA, F. B. de; RODRIGUES, A. R.; COELHO, R. T.; SOUZA, A. F. de. Size effect and minimum chip thickness in micromilling. *International Journal of Machine Tools and Manufacture*, v. 89, p. 39–54, 2015. DOI: https://www.sciencedirect.com/science/article/pii/S0890695514400130. Quoted 2 times on pages 7 and 48.

RAMOS, A. C.; AUTENRIETH, H.; STRAUß, T.; DEUCHERT, M.; HOFFMEISTER, J.; SCHULZE, V. Characterization of the transition from ploughing to cutting in micro machining and evaluation of the minimum thickness of cut. *Journal of Materials Processing Technology*, v. 212, n. 3, p. 594–600, 2012. DOI: https://doi.org/10.1016/j.jmatprotec.2011.07.007. Quoted on page 34.

RAO, U. S.; VIJAYARAGHAVAN, L. Determination of minimum uncut chip thickness in mechanical micro-machining using Johnson-Cook fracture model. *International Journal of Mechatronics and Manufacturing Systems*, v. 6, n. 4, p. 367–380, 2013. DOI: 10.1504/IJMMS.2013.057129. Quoted on page 19.

REED, R. C. *The Superalloys: Fundamentals and Applications*. New York: Cambridge University Press, 2006. Quoted 2 times on pages 15 and 54.

ROMANUS, H.; FERRARIS, E.; BOUQUET, J.; REYNAERTS, D.; LAUWERS, B. Micromilling of sintered zro2 ceramic via cbn and diamond coated tools. *Procedia CIRP - 6th CIRP International Conference on High Performance Cutting, HPC2014*, v. 14, p. 371–376, 2014. DOI: https://doi.org/10.1016/j.procir.2014.03.063. Quoted on page 83.

SAHA, S.; DEB, S.; BANDYOPADHYAY, P. P. Progressive wear based tool failure analysis during dry and mql assisted sustainable micro-milling. *International Journal of Mechanical Sciences*, v. 212, p. 106844, 2021. DOI: https://www.sciencedirect.com/science/article/pii/S002074032100566X. Quoted 2 times on pages 7 and 27.

SANTOS, A. G. dos. Investigação experimental do microfresamento da liga de titânio ti-6al-4v. Uberlândia, MG, Brasil, p. 156, 2020. PhD thesis. Quoted 2 times on pages 71 and 81.

SANTOS, A. G. dos; SILVA, M. B. da; JACKSON, M. J. Tungsten carbide micro-tool wear when micro milling UNS S32205 duplex stainless steel. *Wear*, v. 414-415, p. 109–117, 2018. ISSN 0043-1648. DOI: https://doi.org/10.1016/j.wear.2018.08.007. Quoted 5 times on pages x, 9, 11, 13, and 27.

SILVA, G. de P.; OLIVEIRA, D. de; MALCHER, L. Numerical study of the minimum uncut chip thickness in micro-machining of inconel 718 based on johnson–cook isothermal model. *International Journal of Advanced Manufacturing Technology*, v. 127, p. 2707–2721, 3 2023. DOI: 10.1007/s00170-023-11573-0. Quoted on page 51.

SILVA, G. de P.; SILVA, M. B. da; OLIVEIRA, D. de. Influence of abrasive deburring in indirect tool wear measurement in micromilling of inconel 718. *Journal of the Brazilian Society of Mechanical Sciences and Engineering*, v. 45, n. 262, 2023. DOI: https://doi.org/10.1007/s40430-023-04190-1. Quoted 8 times on pages x, 11, 14, 15, 59, 61, 67, and 72.

SUN, W.; CHEN, Y.-Q.; LUO, G.-A.; ZHANG, M.; ZHANG, H.-Y.; WANG, Y.-R.; HU, P. Organs-on-chips and its applications. *Chinese Journal of Analytical Chemistry*, v. 44, n. 4, p. 533–541, 2016. DOI: https://www.sciencedirect.com/science/article/pii/S1872204016609209. Quoted on page 5.

TAKÁCS, M.; VERÖ, B.; MÉSZÁROS, I. Micromilling of metallic materials. *Journal of Materials Processing Technology*, v. 138, n. 1, p. 152–155, 2003. DOI: https://www.sciencedirect.com/science/article/pii/S09240136. Quoted on page 5.

TENG, X.; HUO, D.; SHYHA, I.; CHEN, W.; WONG, E. An experimental study on tool wear behaviour in micro milling of nano Mg/Ti metal matrix composites. *The International Journal of Advanced Manufacturing Technology*, v. 96, p. 2127–2140, 2018. DOI: https://doi.org/10.1007/s00170-018-1672-z. Quoted on page 10.

THEPSONTHI, T.; ÖZEL, T. 3-D Finite element process simulation of micro-end milling Ti-6Al-4V titanium alloy: Experimental validations on chip flow and tool wear. *Journal of Materials Processing Technology*, v. 221, p. 128–145, 2015. ISSN 0924-0136. DOI: https://doi.org/10.1016/j.jmatprotec.2015.02.019. Quoted 4 times on pages x, 19, 20, and 21.

THEPSONTHI, T.; ÖZEL, T. Simulation of serrated chip formation in micro-milling of titanium alloy Ti-6Al-4V using 2d elasto-viscoplastic finite element modeling. *Production Engineering*, v. 10, p. 575–586, 2016. DOI: https://doi.org/10.1007/s11740-016-0701-8. Quoted 8 times on pages x, xi, 20, 24, 31, 36, 52, and 82.

UCUN İrfan; ASLANTAS, K.; BEDIR, F. The performance of dlc-coated and uncoated ultra-fine carbide tools in micromilling of inconel 718. *Precision Engineering*, v. 41, p. 135–144, 2015. DOI: https://www.sciencedirect.com/science/article/pii/S0141635915000033. Quoted on page 2.

USUI, E.; SHIRAKASHI, T.; KITAGAWA, T. Analytical prediction of cutting tool wear. *Wear*, v. 100, n. 1, p. 129–151, 1984. DOI: https://doi.org/10.1016/0043-1648(84)90010-3. Quoted on page 82.

VAZQUEZ, E.; GOMAR, J.; CIURANA, J.; RODRíGUEZ, C. A. Analyzing effects of cooling and lubrication conditions in micromilling of Ti6Al4V. *Journal of Cleaner Production*, v. 87, p. 906–913, 2015. ISSN 0959-6526. DOI: https://doi.org/10.1016/j.jclepro.2014.10.016. Quoted on page 11.

VENKATESH, V.; SWAIN, N.; SRINIVAS, G.; KUMAR, P.; BARSHILIA, H. C. Review on the machining characteristics and research prospects of conventional microscale machining operations. *Materials and Manufacturing Processes*, v. 32, n. 3, p. 235–262, 2017. DOI: https://doi.org/10.1080/10426914.2016.1151045. Quoted on page 1.

WAN, Y.; CHENG, K.; SUN, S. An innovative method for surface defects prevention in micro milling and its implementation perspectives. *Proceedings of the Institution of Mechanical Engineers, Part J: Journal of Engineering Tribology*, v. 227, n. 12, p. 1347–1355, 2013. DOI: https://doi.org/10.1177/1350650113492507. Quoted on page 77.

WANG, J. S.; SHI, J. S.; GONG, Y. D.; ABBA, G.; CAI, G. Q. A micro milling model considering metal phases and minimum chip thickness. In: *Advances in Machining and Manufacturing Technology IX*. [S.l.]: Trans Tech Publications Ltd, 2008. (Key Engineering Materials, v. 375), p. 505–509. DOI: 10.4028/www.scientific.net/KEM.375-376.505. Quoted 2 times on pages 19 and 27.

WANG, Z.; KOVVURI, V.; ARAUJO, A.; BACCI, M.; HUNG, W.; BUKKAPATNAM, S. Built-up-edge effects on surface deterioration in micromilling processes. *Journal of Manufacturing Processes*, v. 24, p. 321–327, 2016. DOI: https://doi.org/10.1016/j.jmapro.2016.03.016. Quoted 3 times on pages x, 12, and 13.

YADAV, R.; CHAKLADAR, N.; PAUL, S. Micro-milling of ti-6al-4 v with controlled burr formation. *International Journal of Mechanical Sciences*, v. 231, p. 107582, 2022. DOI: https://doi.org/10.1016/j.ijmecsci.2022.107582. Quoted on page 26.

YUAN, Y.; JING, X.; EHMANN, K. F.; CAO, J.; LI, H.; ZHANG, D. Modeling of cutting forces in micro end-milling. *Journal of Manufacturing Processes*, v. 31, p. 844–858, 2018. DOI: https://doi.org/10.1016/j.jmapro.2018.01.012. Quoted on page 22.

ZHANG, Z.; MEN, X.; PAN, Y.; WANG, Z.; SHI, Q.; FU, X. Research on simulation of sicp/al finite element cutting based on cohesive model. *Materials Today Communications*, v. 32, p. 1038–48, 2022. DOI: https://doi.org/10.1016/j.mtcomm.2022.103848. Quoted on page 23.

ZIBEROV, M. Aplicação da microusinagem (miniaturização) nas artes plásticas – a obra de mykola syadristy. *Manufatura em Foco*, v. 5, n. 30, p. 22–23, 2017. DOI: https://www.manufaturaemfoco.com.br/aplicacao-da-microusinagem-miniaturizacao-nas-artes-plasticas-a-obra-de-mykola-syadristy/. Quoted on page 1.

ZIBEROV, M. *Microfresamento da Liga Ti-6Al-4V com Microferramentas com Diferentes Revestimentos e Aplicação de MQL*. 2018. 132 p. Tese (Doutorado) — Universidade Federal de Uberlândia, Uberlândia, MG, Brasil. Quoted 2 times on pages 65 and 81.

ZIBEROV, M.; de Oliveira, D.; da Silva, M. B.; HUNG, W. N. Wear of tialn and dlc coated microtools in micromilling of Ti-6Al-4V alloy. *Journal of Manufacturing Processes*, v. 56, p. 337–349, 2020. ISSN 1526-6125. DOI: https://doi.org/10.1016/j.jmapro.2020.04.082. Quoted 5 times on pages x, 9, 10, 11, and 27.

ÖZEL, T.; OLLEAK, A.; THEPSONTHI, T. Micro milling of titanium alloy Ti-6Al-4V: 3-D finite element modeling for prediction of chip flow and burr formation. *Production Engineering*, v. 11, p. 435–444, 2017. DOI: https://doi.org/10.1007/s11740-017-0761-4. Quoted 3 times on pages xi, 25, and 26.

ÖZEL, T.; THEPSONTHI, T.; ULUTAN, D.; KAFTANOğLU, B. Experiments and finite element simulations on micro-milling of ti–6al–4v alloy with uncoated and cbn coated micro-tools. *Cirp Annals-manufacturing Technology - CIRP ANN-MANUF TECHNOL*, v. 60, p. 85–88, 12 2011. Quoted on page 82.